*Ford Motor Company*
AERONUTRONIC DIVISION

*Ford Motor Company*
AERONUTRONIC DIVISION

RESEARCH LABORATORY

TECHNICAL REPORT

# RESEARCH ON THEORETICAL STUDIES OF THE STATISTICAL CHARACTERISTICS OF SUNLIT CLOUDS (U)

## VOLUME ONE OF TWO

Prepared for:  Advanced Research Projects Agency
The Pentagon
Washington 25, D. C.

Under Contract with the Office of Naval Research

Contract No.  NOnr 3606(00)
ARPA Order No.  237-61
Amend. 1  6-16-61

Prepared by:  E. Bauer
D. C. Garwood
J. A. Jamieson
M. H. Johnson
P. J. Wyatt

14 October 1962

ABSTRACT

The work presented in this report falls into two classes,
namely on the reflectivity of solar infrared from high altitude clouds,
and on the effect of the energy reflected from these clouds on the
statistical performance criteria of a satellite-borne missile detection
system.  The scattering of infrared from clouds of spherical water drop-
lets has been treated by Mie theory.  For wavelengths in the range
2.5 - 10 micron, and for large angle scattering ( $\geqslant$ 60 - 90°) the
effective reflectivity is due to single rather than to multiple scattering
by water droplets, as a result of the relatively large absorption and
the forward peak in the differential scattering cross section.  The
effective diffuse reflectivity under these conditions is of the order of
1 - 2 percent.  For actual situations, some discussion has been given of
atmospheric transmission losses as well as of meteorological data on the
distribution of high altitude clouds.  Comparison with experiment is made
in a (classified) appendix, and the results are found to be consistent
with the limited experimental data.  The statistical problem consists of
the detection of rare high radiance signals in a background having
occasional high radiance levels.  The detection criterion thus involves
maximizing peak rather than mean signal-to-noise ratios.  An analysis
in terms of likelihood ratios is developed, and it is shown that the
Neyman-Pearson criterion provides a usable partial maximization of sig-
nal detection probability.  In practical cases, the Neyman-Pearson
criterion is equivalent to setting up a single threshold.  Limited numeri-
cal applications are made for single and correlated detector elements.

CONTENTS

iii

ILLUSTRATIONS

ILLUSTRATIONS (continued)

TABLES

## ACKNOWLEDGEMENT

SECTION 1

INTRODUCTION

1.1 THE PROBLEM

A primary factor in IR surveillance from satellites for the purpose of detecting rocket boosters is the infrared background in which the booster must be detected. This report deals with the infrared background in the 2.7 micron band arising from clouds illuminated by the sun. It is known that sunlit clouds are the major sources of background radiance.

The problem of the sunlit cloud background can be separated into two parts. The first part is the determination of the reflected solar flux from an illuminated cloud taking properly into account the infrared absorption in the atmosphere itself. The second part is the specification of the statistical character of the background in terms of cloud frequency distributions for height, size, and for irregularities. Here it is essential to consider various kinds of detection and data processing systems because different statistical properties of the background determine the performance of the different systems.

In the present report a fairly complete treatment of the first part of the problem is presented. The second part is also treated with an attempt to achieve some generality. However, the treatment is far from complete and should only be regarded as an initial attempt.

1-1

## 1.2 OUTLINE OF PRESENT WORK

Because of the unsatisfactory state of our knowledge of the reflectivity of clouds in the infrared -- theoretical estimates differ by almost two orders of magnitude, a thorough study of infrared reflection from clouds is made in Sections 2 and 3. The problem of Mie scattering from water droplets having a distribution of radii is treated in Section 2, where it is shown that in the near infrared the effective cloud reflection mechanism for large scattering angles ($\theta \gtrsim 60°$) is single scattering, while the effective cloud reflectivity for these large scattering angles is of order 1 - 2%. Thus the problem of the scattering of infrared from clouds of water droplets has been here solved with sufficient accuracy for most practical purposes.*

The results of Section 2 are applied in Section 3 to the case of a real atmosphere, where transmission losses and scattering efficiencies are combined to provide a series of isoradiance plots assuming uniform tropospheric cloud cover. Some discussion is given of the possible effects of large ice crystals (Appendix 3A), while the results for cloud reflectance are compared with the limited experimental data in Appendix 3B, and are found to be consistent with these data.

----

*For definiteness the numerical analysis is limited to the 2.7 micron band. The same scattering analysis with somewhat different numerical coefficients applies for a $2.7 \mu \lesssim \lambda \lesssim 10$ micron, but at lower wavelengths the problem is essentially different because the absorptivity of the droplets is reduced to such an extent that multiple scattering has to be taken into account. At longer wavelengths it is essentially a matter of grey body radiation.

The treatment of the statistical aspects of the background in Section 4 begins with a general discussion of criteria for performance based on statistical decision theory. Conceptual difficulties with elemental costs and with a priori probabilities which are essential concepts in this formulation are pointed out. It is ultimately made plausible in Section 4.2 that a simple criterion based on likelihood ratios has some degree of validity. The likelihood ratio test is applied to various assumed radiance distributions in Section 4.4 where it is shown that non-Gaussian bimodal distributions have an entirely different effect depending on whether the system is evaluated by likelihood ratio or r.m.s. noise criteria. In such bimodal distributions, the large background radiances, although infrequent, have a large effect on performance which is not reflected in the r.m.s. noise criterion. It is also shown by an example in Section 4.2 how the frequency distribution for radiance is related to the height distribution of the clouds through the calculation of cloud reflectivity given in Sections 2 and 3. In Sections 4.3 and 4.4, an attempt is made to apply the likelihood ratio test to a comparison of single sensors with multiple sensors with correlation, leading to a rather obvious result that correlation does enhance system performance if the spatial extent of a cloud is larger than the spatial extent of the target. Finally, in Section 4.6 some remarks are made about optimum linear filters.

In Appendix 4A an attempt is made to study two-dimensional autocorrelation functions and Wiener spectra on the surface of a sphere. It was found that the Wiener-Khinchine theorem does not hold under these conditions.

SECTION 2

SCATTERING OF INFRARED FROM ASSEMBLIES OF WATER DROPLETS

2.1 PHYSICAL PROPERTIES OF HIGH ALTITUDE CLOUDS

A high altitude cloud is an assembly of water droplets or ice crystals, or a mixture of the two at an altitude of approximately 20,000 feet or more. Such a cloud may move relatively slowly under the influence of horizontal winds, as in the case of cirrus clouds or orographic disturbances, or comparatively rapidly ($10-10^3$ cm/sec) as a result of internal convection as in the case of cumulus clouds.[2.1]

As yet there is rather little detailed experimental data on high altitude cloud properties. Measurements of low altitude clouds indicate water droplets with a mean radius of the order of 5 micron with perhaps 0.1-1 gm $H_2O/m^3$. At higher altitudes one may perhaps expect a somewhat lower water content. The droplet size distribution may be represented as[2.2]

$$n(r) \, dr = N_o \, r^n \, e^{-ar} \, dr \qquad (2.1)$$

where $n(r)$ is the number of particles per cc with radius $r - (r + dr)$. The mode radius of this distribution is $r_c = n/a$. Deirmendjian[2.2] uses $n = 6$, $a = 1.5$ micron$^{-1}$, so that $r_c = 4$ micron. Here this distribution

is examined in detail. Cases with smaller and larger droplet size, $r_c$ = 2, 8 micron, and with the same mean width of the frequency distribution as for n = 6, a = 1.5 $micron^{-1}$, are also investigated, as are models with $r_c$ = 4 micron but with narrower and wider standard deviations. All the particle size distributions are shown in Figure 2.1 and Table 2.1. In general we shall deal with thick clouds--this to be defined precisely later--and thus the actual number of particles per cc or the liquid water content of the cloud do not affect the scattering directly.

A cloud rises due to the buoyant forces present when the temperature within it is higher than the ambient temperature. As the cloud rises, its temperature drops as a result of both its adiabatic expansion and of turbulent mixing with the surrounding atmosphere. Thus, under certain conditions, there will be ice crystals in clouds. For instance, cirrus clouds are largely or entirely ice, while cumulus clouds may also contain some ice crystals.[*]

There are wide variations in the shape and size of ice crystals, ranging from frozen water droplets, which may be almost spherical and of the same mass as the water drops, all the way to prisms and hexagonal cylinders up to 500 micron in their longest dimension.[2.1] The shape, size, number density and motion of these ice crystals are complicated and incompletely understood functions of the ambient conditions, and it is difficult to make any definitive statement about them, particularly with respect to the frequency with which high altitude clouds of ice crystals may occur. In this study, clouds will be treated as assemblies of water droplets. In other words, effects arising from the specular reflection

---

[*] It should be pointed out that water droplets of 1-10 micron radius freeze at -35 to $-40^{\circ}C$ because of surface tension effects. See Ref. 3.3.
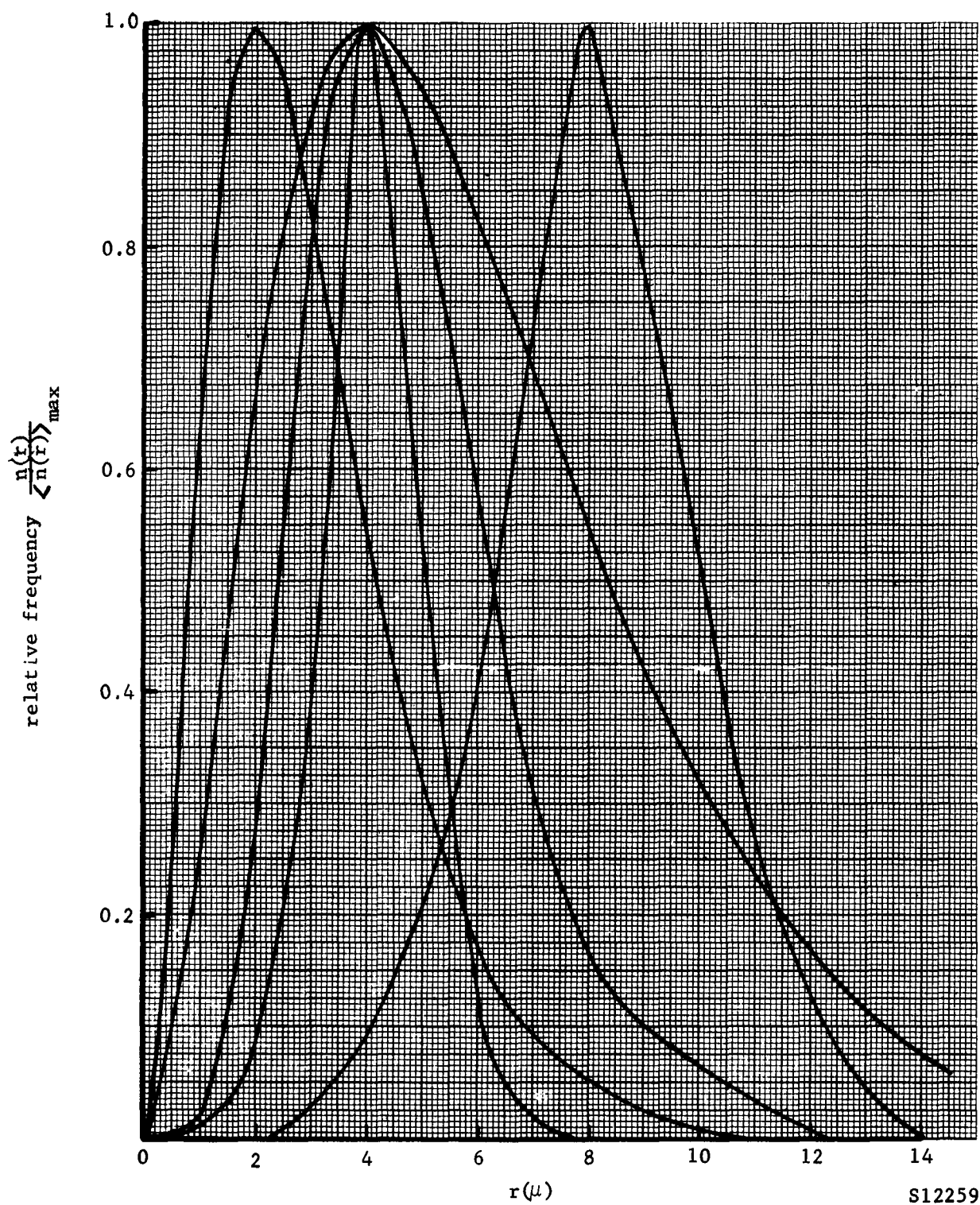
FIG 2.1  ASSUMED PARTICLE SIZE DISTRIBUTIONS

S12259

2-3

TABLE 2.1

SCATTERING OF INFRARED FROM VARIOUS DISTRIBUTIONS OF PARTICLES

| | | | | | |
|---|---|---|---|---|---|
| Particle Mode Radius $r_c$ = n/a (micron) | 2 | 4 | 4 | 4 | 8 |
| Width of Distribution | Regular | Narrow | Regular | Wide | Regular |
| n | 2 | 24 | 6 | 2 | 24 |
| a (micron$^{-1}$) | 1 | 6 | 1.5 | 0.5 | 3 |
| Mean Mass per Particle (gm) | $2.5 \times 10^{-10}$ | $3.40 \times 10^{-10}$ | $6.25 \times 10^{-10}$ | $2.01 \times 10^{-9}$ | $2.72 \times 10^{-9}$ |
| Density of Water (gm/m$^3$) for 100 particles/cc | .0251 | .0340 | .0625 | .2011 | .2723 |
| $\sigma_{abs}$ ($10^{-6}$ cm$^2$) | .234 | .358 | .562 | 1.247 | 2.009 |
| $\sigma_{scatt}$ ($10^{-6}$ cm$^2$) | .735 | 1.349 | 1.466 | 2.151 | 3.064 |
| $\sigma_{abs} / \sigma_{scatt}$ | 0.318 | 0.265 | 0.383 | 0.580 | 0.656 |
| $x_c$ = $2 \pi r_c / \lambda$ | 4.65 | 9.3 | 9.3 | 9.3 | 18.6 |

2-4

of light from ice crystals such as haloes, sun dogs, etc.,[2.4] will not be taken into account. Some of these effects are discussed in Appendix 3A.

The refractive index of water in the infrared has been tabulated by Centeno.[2.5] The results in the 2.7 micron band are shown in Figure 2.2. There is no information on the temperature variation of the refractive index of water, or on the refractive index of ice in this frequency range. The most noticeable feature is the fact that water absorbs significantly only for $\lambda \gtrsim 2.7$ micron. The physical reason for this is that this is the wavelength corresponding to the highest molecular vibration frequency of the $H_2O$ molecule, or to the maximum frequency of the spectrum of "lattice vibrations" of water.

## 2.2 SCATTERING OF INFRARED BY A SINGLE DROP

The scattering of electromagnetic radiation of wavelength $\lambda$ from a sphere of radius r is characterized by the parameter

$$x = \text{perimeter/wavelength} = 2 \pi r / \lambda \ . \qquad (2.2)$$

If $x \gg 1$, we are in the "geometrical optics" region, while Rayleigh scattering holds for $x \ll 1$. However, for $x \gtrsim 1$, which is the case in the visible and near infrared for the particle sizes under consideration, the difficult "Mie Scattering" analysis applies.[2.6,2.7] To solve the problem in this regime it is necessary to solve Maxwell's equations for a plane incident wave and spherical outgoing scattered wave subject to the appropriate boundary conditions on the scattering sphere. The resulting expressions giving the angular distribution and total scattering cross section are given in Ref. 2.6, p. 630 ff, and Ref. 2.7, p. 114 ff. In the notation of the latter reference, the results are
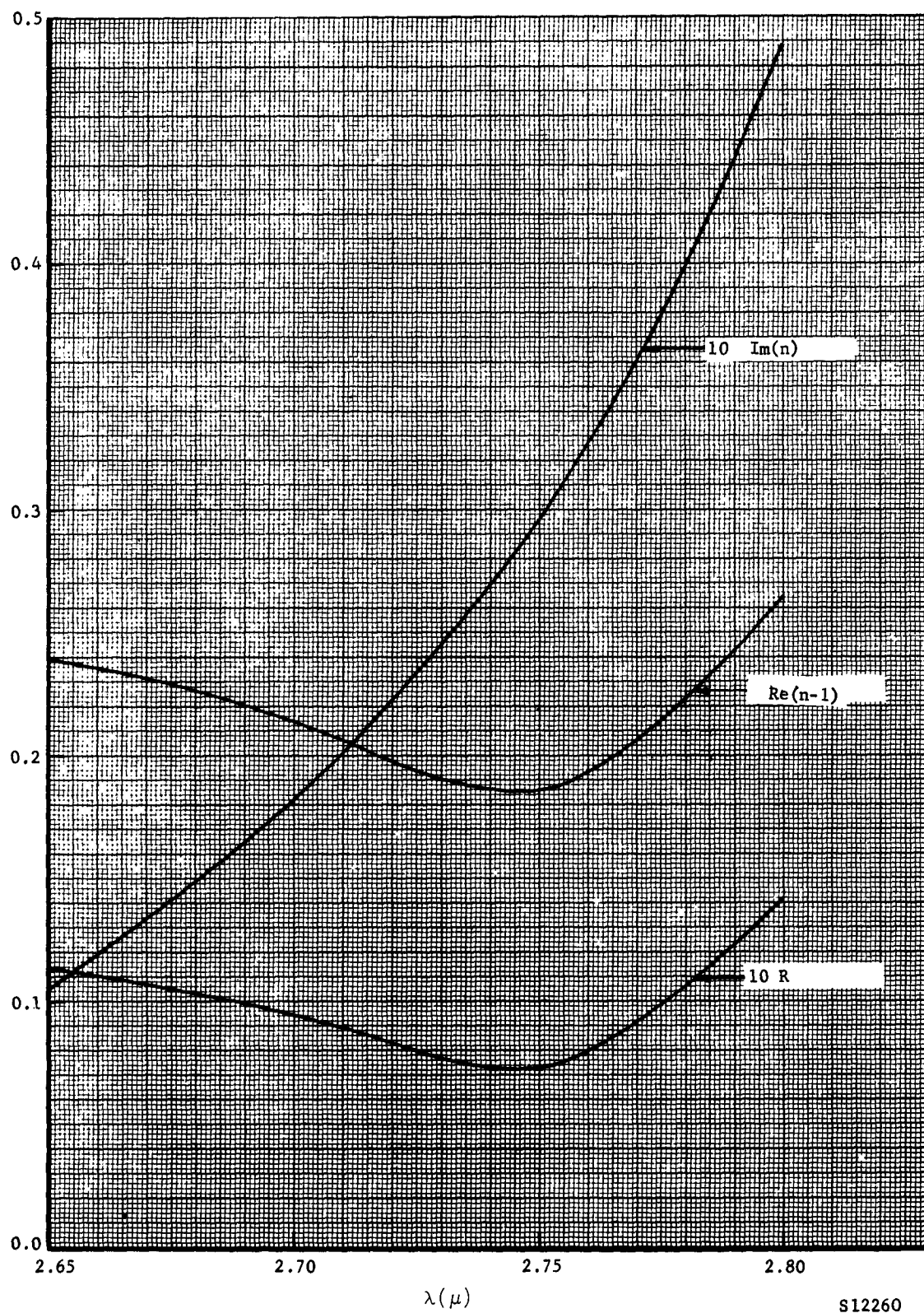
FIGURE 2.2  REFRACTIVE INDEX OF WATER FROM 2.65-2.80 $\mu$ [REF. 2.5]

$$i \ (\theta) = \left| S_1 \ (\theta) \right|^2 \ ; \ i \ (\theta) = \left| S_2 \ (\theta) \right|^2 \tag{2.3a}$$

$$S_1 \ (\theta) = \sum_{n=1}^{\infty} \frac{2n+1}{n(n+1)} \left[ \frac{a_n \ P_n^1(\cos\theta)}{\sin\theta} + b_n(d/d\theta) \ P_n^1(\cos\theta) \right] \tag{2.3b}$$

$$S_2 \ (\theta) = \sum_{n=1}^{\infty} \frac{(2n+1)}{n(n+1)} \left[ \frac{b_n \ P_n^1(\cos\theta)}{\sin\theta} + a_n(d/d\theta) P_n^1(\cos\theta) \right] \tag{2.3c}$$

$$a_n = \frac{\psi_n'(y) \ \psi_n(x) - m \ \psi_n(y) \ \psi_n'(x)}{\psi_n'(y) \ \zeta_n(x) - m \ \psi_n(y) \ \zeta_n'(x)} \tag{2.3d}$$

$$b_n = \frac{m \ \psi_n'(y) \ \psi_n(x) - \psi_n(y) \ \psi_n'(x)}{m \ \psi_n'(y) \ \zeta_n(x) - \psi_n(y) \ \zeta_n'(x)} \tag{2.3e}$$

$$\psi_n(z) = (\pi z/2)^{1/2} \ J_{n+1/2}(z) \tag{2.3f}$$

$$\chi_n(z) = -(\pi z/2)^{1/2} \ N_{n+1/2}(z) \tag{2.3g}$$

$$\zeta_n(z) = (\pi z/2)^{1/2} \ H_{n+1/2}^{(2)}(z) \tag{2.3h}$$

$$y = m \ x \tag{2.3i}$$

$$m = n' - in'' \ \text{(note the minus sign!)} \tag{2.3j}$$

2-7

$$\sigma_{scatt} = (2\pi r^2/x^2) \sum_{n=1}^{\infty} (2n+1) \left\{ |a_n|^2 + |b_n|^2 \right\} \qquad (2.4a)$$

$$\sigma_{ext} = (2\pi r^2/x^2) \sum_{n=1}^{\infty} (2n+1) \; Re(a_n + b_n) \qquad (2.4b)$$

where $i_{\parallel}(\theta)$ and $i_{\perp}(\theta)$ are the intensities of radiation scattered through angle $\theta$ with polarization parallel and perpendicular to the plane of observation, which is the plane defined by the incident and scattered rays. $P_n^{\prime}(\cos\theta)$ are associated Legendre polynomials, $J_{\nu}(z)$, $N_{\nu}(z)$ and $H^{(2)}_{\nu}(z)$ are respectively Bessel functions of first and second kind and Hankel functions of the second kind

$$H^{(2)}_{\nu}(z) = J_{\nu}(z) - i \, N_{\nu}(z) \qquad (2.5)$$

m is the complex refractive index of the scatterer defined here with a negative imaginary part. $\sigma_{scatt}$ is the total scattering cross section and

$$\sigma_{ext} = \sigma_{scatt} + \sigma_{abs} \qquad (2.6)$$

is the extinction scattering cross section; $\sigma_{abs}$ is the absorption cross section.

These expressions have to be evaluated numerically, using a high speed computer. For the present purpose the computations were carried out on the Aeronutronic IBM 709 computer using a program locally called CLOUD. This program computes the differential scattered intensity per particle averaged over the particle size distribution (2.1) in units

2-8

of $(2\pi R/\lambda)^2$, where R = distance from scatterer to observer. It applies for x > 0.1. The intensity shown in Figure 2.3 has been averaged over the scattered intensities for polarizations parallel and perpendicular to the plane of scattering

$$i_{av}(\theta) = 1/2 \left[ i_{//} (\theta) + i_{\perp} (\theta) \right] \qquad (2.7)$$

The program automatically computes the angular distributions $i_{av}$, $i_{\perp}$, i and the total and scattering cross sections. The results of Figure 2.3 and Table 2.1 give the results over the 2.7 micron band; in other words, for the scattering cross section of Table 2.1, for example

$$\sigma_{scatt} = (1/3) \left[ \sigma_{scatt} (2.675) + \sigma_{scatt} (2.725) + \sigma_{scatt} (2.775) \right]$$

$$(2.8)$$

where the complex refractive indices shown in Figure 2.2 show a number of interesting characteristics.

(1) The effect of averaging over a particular size distribution is to smooth out the rapid variations in the angular scattering distribution. For illustrations see Reference 2.2.

(2) The angular distribution is always heavily peaked in the forward direction* and the ratio of forward to backward scattering is very insensitive to the details of the distribution. This may be under stood because the refractive index (n' - in") is not very different from

---

*   For Deirmendjian's distribution[2.2]--that is, n = 6, a = 1.5 micron$^{-1}$ in Equation (2.1)--90% of single scattered radiation goes into angles of less than $36°$, while the scattering through angles of greater than $90°$ is essentially isotropic.
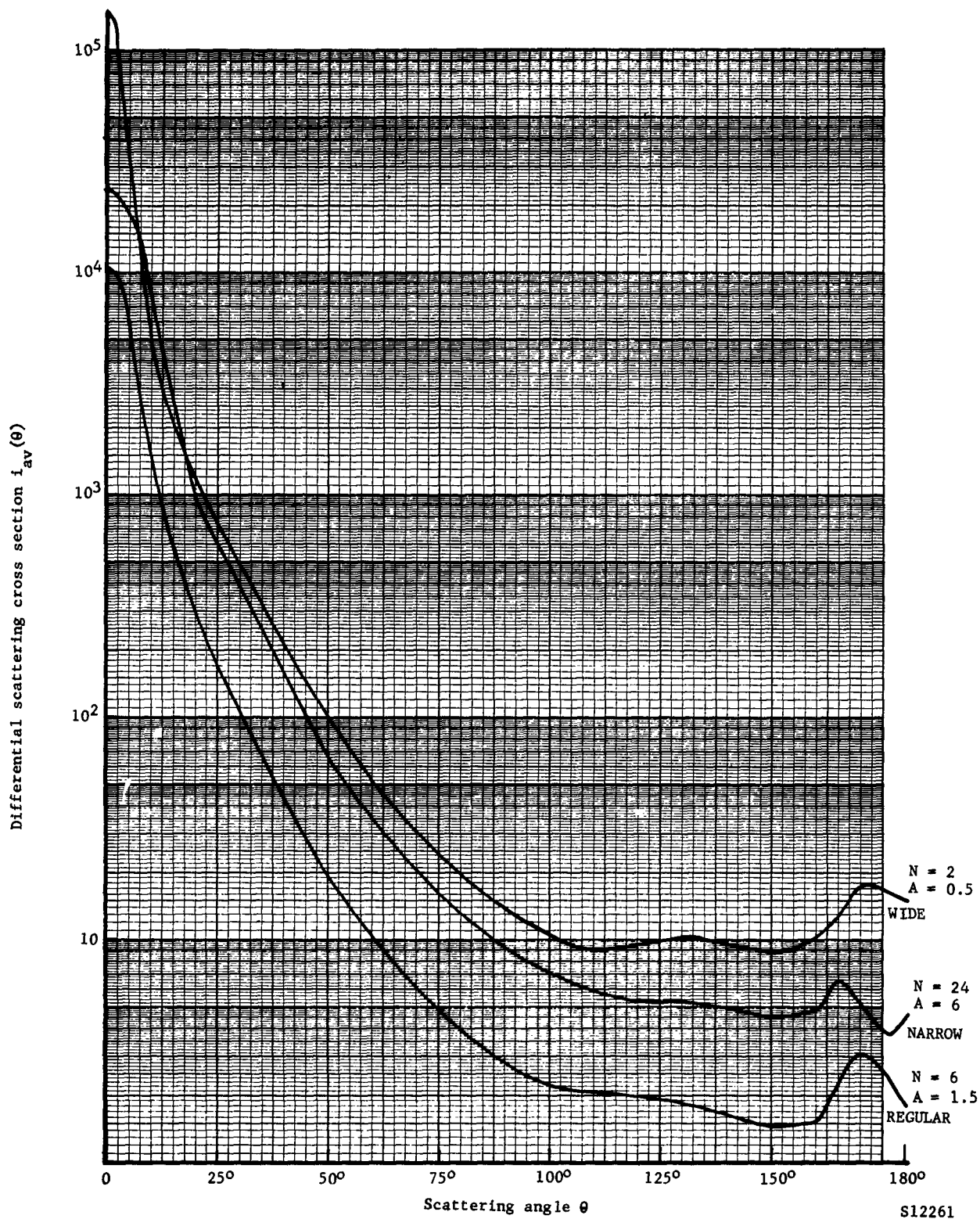
FIGURE 2.3   DIFFERENTIAL SCATTERING CROSS SECTION FOR A SPHERICAL WATER DROPLET
AVERAGED OVER PARTICLE SIZE DISTRIBUTIONS OF EQUATION (2.1).

(a)   EFFECT OF BARYING THE DISTRIBUTION WIDTH FOR CONSTANT DISTRIBUTION
MODE RADIUS, $r_c$ = 4 MICRON
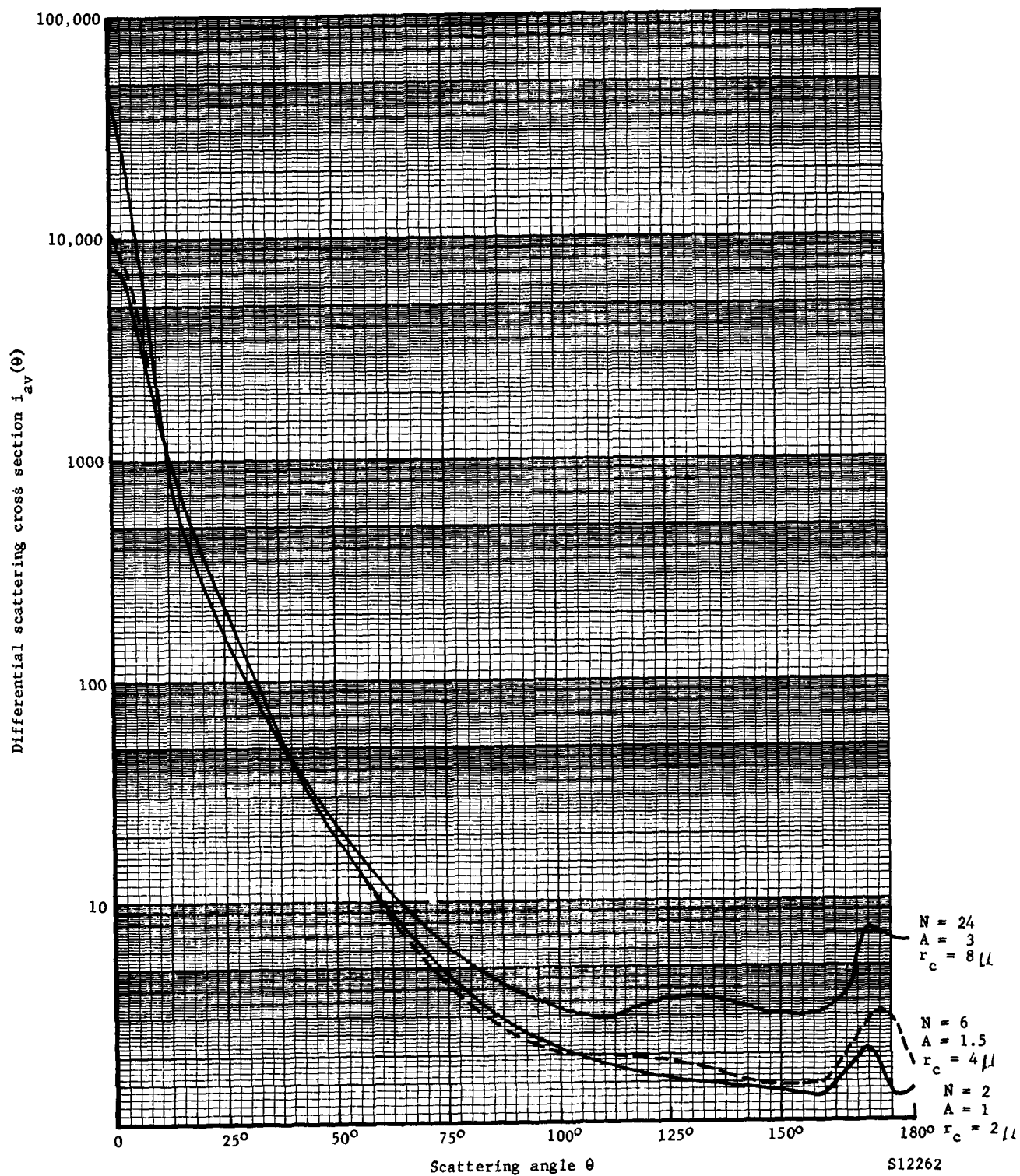
2-10 a

FIGURE 2.3   DIFFERENTIAL SCATTERING CROSS SECTION FOR A SPHERICAL WATER DROPLET
AVERAGED OVER PARTICLE SIZE DISTRIBUTIONS OF EQUATION (2.1).

(b)   EFFECT OF VARYING THE DISTRIBUTION MODE RADIUS $r_c$ AT CONSTANT
DISTRIBUTION WIDTH

2-10 b

one, so that the reflectivity R for an infinite plane slab

$$R = \frac{(n' - 1)^2 + n''^2}{(n' + 1)^2 + n''^2} \qquad (2.9)$$

is quite small, actually of the order 1 percent (see Figure 2.2). In fact, the relative amount of energy scattered through angles greater than $\pi/2 - J(\pi/2)/J(0)$ where

$$J(\theta) = \int_0^{2\pi} d\phi \int_\theta^\pi \sin\theta \ d\theta \ i_{av}(\theta) \qquad (2.10)$$

is also of the order of 1 percent.

(3) The different particle size distributions do show some difference in their behavior at intermediate angles ($10° \lesssim \theta \lesssim 120°$), but even these differences are not very large. This is certainly a consequence of the smoothing effect of the particle size distribution.

(4) The total or extinction cross section $\sigma_{ext}$ of Equation (2.6) increases with increasing $r_c$, but not strictly proportionally to $r_c^2$. This effect again is due partly to the effect of the size distribution, and partly to the oscillatory behavior of $\sigma_{ext}(x)$ (cf. Ref. 2.6, p. 659, Figure 13.14).

(5) It is noteworthy that $\sigma_{abs}/\sigma_{scatt}$ increases with increasing $r_c$, even though, of course, no change in refractive index occurs. This may be understood qualitatively as follows. In the geometrical optics region defined by $x = 2\pi r/\lambda \gg 1$, for a sphere of radius r is proportional to the surface area; that is, $\sigma_{scatt} \propto r^2$. On the other hand, the absorption cross section is proportional both to

2-11

the scattering cross section and to the path length within the absorber, which again is proportional to the radius, so that $\sigma_{abs} \propto r^3$. It is clear from this why one might expect $\sigma_{abs}/\sigma_{scatt}$ to increase with increasing $r_c$ or $x_c$.

(6) The small maximum in $i_{av}(\theta)$ at $\theta = 170°$ is a residual rainbow[2.2, 2.4] that is essentially a refraction phenomenon arising from internal reflection combined with scattering. Increasing the absorption will reduce the importance of this phenomenon.

(7) The insensitivity of the results to the particle size distribution leads one to suspect a similar insensitivity to wavelength in the 2 micron - 15 micron region, since the refractive index changes comparatively little.

To sum up the results of the Mie scattering calculation, most of the scattering from a single drop is in the forward direction, and the scattering is essentially isotropic for scattering angles $\theta \gtrsim 90°$. The result that the effective large angle reflectivity is of the order of 1 percent seems to be quite unambiguous; any statement to the contrary is dubious. Finally $\sigma_{abs}/\sigma_{scatt} \sim 0.3$, which represents a very significant degree of absorption for the multiple scattering problem.

## 2.3 SCATTERING BY AN ASSEMBLY OF DROPS

### a. Introduction

It is required to calculate the spectral radiance of a cloud of water droplets under conditions of given (solar) illumination. That is, a flux of radiation $F_o$ watt/cm$^2$ in the relevant frequency band[*]is incident on the cloud, and we ask for the spectral radiance H of the cloud,

---

[*] In the frequency band 2.65 - 2.80 micron, $F_o = 5.7 \times 10^{-4}$ watt/cm$^2$. (See Ref. 2.8).

which is the power sent into unit solid angle from unit surface area.
Thus H is measured in watt/cm$^2$ sterad. Explicitly, if the illuminated
surface area of the cloud is $S_{ill}$, the radiance may be expressed in
terms of the differential scattering cross section per unit area, $Q_c(i,\theta)$
of the cloud as

$$H(\theta, \phi) \, S_{ill} = F_o \, S_{ill} \, Q_c(i, \theta) \qquad (2.11)$$

The aim here is to evaluate $Q_c(i,\theta)$.

In this section it is first shown that multiple scattering is
unimportant except for very small angle scattering. Then a general
treatment of the reflection from a planar cloud is given. In appendices
we give a model to make quantitative estimates of the effect of multiple
scattering, and also a discussion of the scattering from spherical clouds.
The discussion of spherical clouds has been relegated to an appendix
first, because it is not as important as the case of planar clouds, and
secondly, because it has not proved possible to give a numerical solution
of the same degree of generality as for planar clouds.

It should be noted that the results of the present section
have rather wide applicability since the scattering cross section $i_{av}(\theta)$
is essentially independent of the drop size distribution over a fairly
wide range, and since, in addition, the result for a large cloud is in-
dependent of the number density of droplets.

b.  Single vs. Multiple Scattering

The possible effect of multiple scattering presents considerable
difficulties in the case of a large cloud. The general problem of radia-
tive transfer with partial absorption and an anisotropic angular distri-
bution has not been solved.[2.9,2.10] However, in the present situation
of predominantly forward scattering with non-zero absorption, the effect
of scattering of orders higher than single scattering has been shown to
be small except for very small scattering angles. (See Ref. 2.9b).

This result can be understood qualitatively as follows:  Most
of the scattering is in the forward direction.  For Deirmendjian's
distribution,[2.2] 90 percent of the single scattered energy goes into
$\theta < 36^{\circ}$, while the scattering is essentially isotropic for $\theta > 90^{\circ}$.
Also, $\sigma_{abs}/\sigma_{scatt} \sim 0.3$ (cf. Table 2.1), so that in three collisions
the total intensity is down to 1/e times the original intensity due to
absorption.  By this time, however 90 percent of the remaining energy
would be scattered into angles less than $\sqrt{3} \cdot 36^{\circ} = 65^{\circ}$.  Thus,
multiple scattering will be unimportant for scattering through angles
greater than 60 to $90^{\circ}$.

This same result has been obtained by Goldstein[2.9b] by an
explicit numerical evaluation.  Goldstein compares first and second
order scattering with absorption by using some representative  Mie
scattering results of Dermendjian.[2.2]  In this way he finds that single
scattering far outweighs double scattering except for scattering through
very small angles.[*]

The predominance of single over multiple scattering makes the
calculation of the reflection of near infrared radiation from clouds
possible.  This result has a number of interesting consequences:

(1)  The absorptivity of water droplets is very high throughout
the region $\lambda = 2.5 - 10$ micron and above.  Thus, the present analysis
applies throughout this frequency range with appropriate quantitative
modifications.

---

[*]  It should be pointed out that while the expansion in different orders
of scattering can be written down formally, yet for anisotropic angu-
lar  distributions at least the real importance of the different
orders of scattering is very hard to estimate except by explicit
numerical evaluation.

(2) In the visible region the absorptivity of water is very low. Thus, in this region, a large cloud may be represented at least roughly as a diffuse Lambert's Law reflector, because of the large amount of multiple scattering. However, the justification of this procedure is by no means trivial, and in particular we do not know how to treat the region 1 micron $< \lambda <$ 2.5 micron.

(3) In the far IR ($\gtrsim$ 10 micron) a cloud acts as a grey body emitter.

(4) It follows that, except possibly in the visible, the description of a cloud as a Lambertial diffuse reflector is a very poor one on physical grounds. Of course, it may turn out under certain conditions that the concept of "diffuse reflectivity" may be useful for an empirical description of cloud reflection if the effective diffuse reflectivity coefficient does not vary very much with scattering angle in the appropriate region.

(5) For low altitude clouds there will be a significant degree of attenuation due to the absorption of water vapor in the cloud in the 2.7 micron band. This mechanism is not effective above 30 Kft, where the effective extinction of the beam within the cloud is due entirely to absorption by the droplets rather than by scattering. Thus if there are N scatterers per unit volume, the effective extinction distance within the cloud, $\beta^{-1}$, is given by the relation

$$\beta = N \sigma_{abs} \qquad (2.12)$$

(6) The extinction distance $\beta^{-1}$ enables a precise distinction to be made between small and large clouds. If the characteristic distance scale of a cloud is denoted by L, then for $L \gg \beta^{-1}$, one is dealing with a small cloud composed of $NL^3$ droplets all scattering independently. Thus, the total scattering cross section of a small cloud is given as

2-15

$$Q_{scatt}^{(small)} \sim NL^3 \, \sigma_{scatt} \qquad (2.13)$$

On the other hand, for a large cloud defined in terms of $L \gg \beta^{-1}$, the effective cloud volume seen is not $L^2$ but $L^2/\beta$, since the incident beam only penetrates $\beta^{-1}$ into the cloud. Thus, for a large cloud

$$Q_{(scatt)}^{(large)} \sim N \, \frac{L^2}{\beta} \, \sigma_{scatt} = L^2 \, \frac{\sigma_{scatt}}{\sigma_{abs}} \qquad (2.14)$$

In other words, for a large cloud the total scattering cross section is independent of the number of scatterers per cc or of the scattering cross section per scatterer $\sigma_{scatt}$. Of course, the angular distribution does depend on

$$\frac{[\partial\sigma/\partial\pi]_\theta}{\sigma_{abs}} \quad .$$

c.  **A Planar Cloud**

Consider the single scattering from a large slab of material containing N scatterers per unit volume and having a flat top surface with an illuminated area $S_{ill}$, which is the (xy)-plane $z = 0$ of our system of coordinates (see Figure 2.4). The angles of incidence and exit are respectively i and e measured from the local normal, and z increases going into the scattering medium.

A volume of element $dV_A$ has a total scattering cross section $N \, dV_A \, \sigma_{scatt}$, and the total amount of single scattered radiation sent into unit solid angle in the direction ($\theta$, $\phi$) is

$$H^{(1)}(\theta) \, S_{ill} = F_o N \int dV_A \, e^{-\beta(r_{IA} + r_{AE})} [\partial\sigma/\partial\pi]_\theta \qquad (2.15a)$$

2-16

FROM SUN

TO DETECTOR

I    X    Z    Y    E

i   e

A  $\theta$
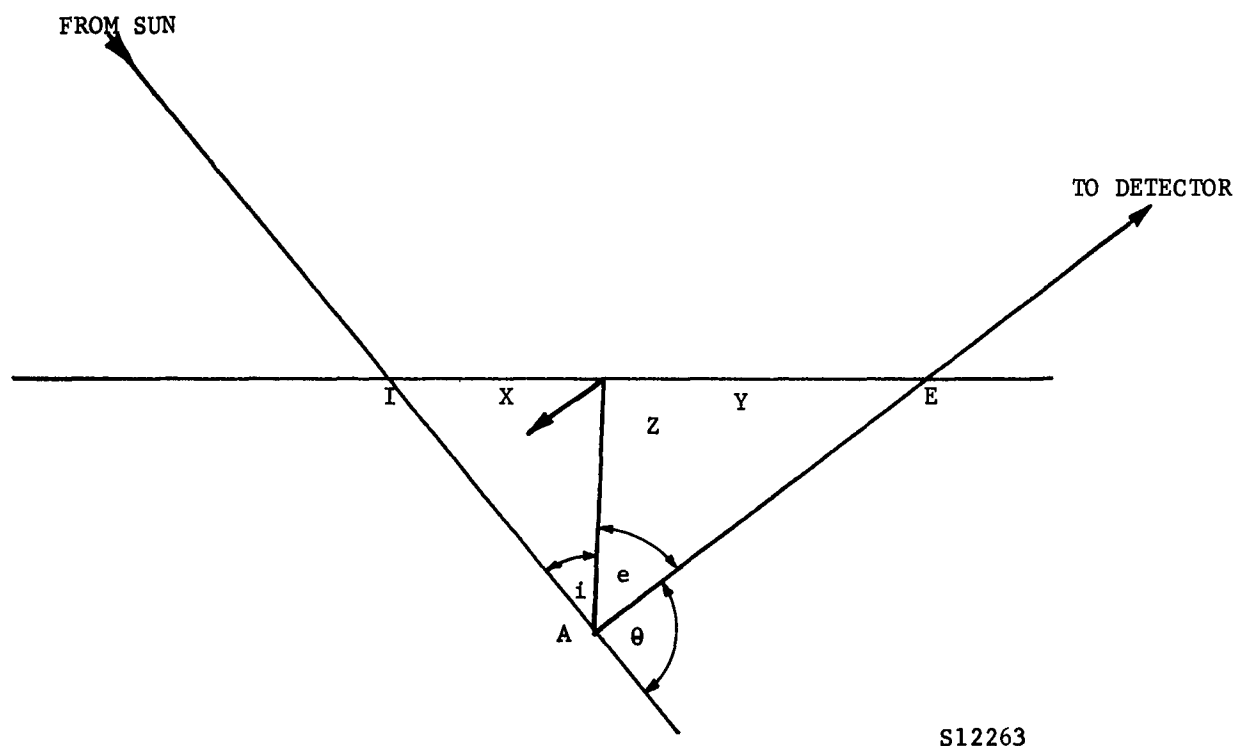
S12263

FIGURE 2.4.  GEOMETRY FOR SCATTERING FROM A LARGE PLANAR CLOUD

$$\left[\partial\sigma/\partial n\right]_\theta = \sigma_{scatt}\, i_{av}(\theta)/J(0) \qquad (2.15b)$$

where $J(0) = 745$ for Deirmendjian's distribution of droplet sizes ($n = 6$, $a = 1.5$ micron$^{-1}$) in Equation (2.1). This quantity is defined in Equation (2.10). All the quantities entering here have been defined either in the text of in Figure 2.4. The factor $e^{-\beta\,(r_{IA} + r_{AE})}$ gives the effective extinction of the ray which is scattered through an angle $\theta$ at the point A. The effective extinction is, of course, due to absorption (see Equation (2.12) and the discussion immediately preceding it).

The integration over $dV_A$ is carried out extending $\iint dx\,dy$ over $S_{ill}$ and letting z go from 0 to $\infty$. This gives the result

$$H^{(1)}(\theta) = F_o N \left[\partial\sigma/\partial n\right]_\theta \int_0^\infty dz\, e^{-\beta f(i.e)\, z} = \frac{F_o N \left[\partial\sigma/\partial n\right]_\theta}{f(i,e)}$$

$$(2.16a)$$

$$f(i,e) = 1/\cos i + 1/\cos e \qquad (2.16b)$$

Finally, using Equation (2.12) for $\beta$, one gets the result

$$H^{(1)}(\theta) = \frac{F_o\left[\partial\sigma/\partial n\right]_\theta}{\sigma_{abs}f(i,e)} = F_o \left(\sigma_{scatt}/\sigma_{abs}\right)\frac{i_{av}(\theta)}{J(0)\, f(i,e)} \qquad (2.17)$$

This result may be understood physically. For a large cloud the absolute magnitude of the single scattered energy is proportional to the incident flux $F_o$ and to the illuminated surface area $S_{ill}$, but does not depend on the absolute magnitude of the scattering cross section per

2-18

scatterer $\sigma_{scatt}$ or on the number of scatterers per cc, N. The angular distribution depends on the differential scattering cross section from each scatterer, modified by the extinction within the cloud, which gives rise to an "albedo" factor ( $\sigma_{scatt}/\sigma_{abs}$) and to a geometrical factor $[f(i,e)]^{-1}$. See item (6) of Section 2.2.

The differential scattering cross section per unit illuminated surface area, $Q_c(i, \theta)$ of Equation (2.11), is plotted in Figure 2.5 for various valuesof i in the important case of coplanar scattering when the incident ray, the local normal, and the exit ray all lie in the same plane, so that

$$i + e + \theta = \pi \qquad (2.18a)$$

$$f(i, e) = 1/\cos i - 1/\cos(\theta + i) \qquad (2.18b)$$

It is possible to write down the result (2.17, 2.11) in terms of Lambert's Law diffuse scattering with an effective diffuse reflection coefficient $\eta = \eta(i, \theta)$. The appropriate expressions are

$$Q_c(i, \theta) = [\eta(i, \theta) / \pi] \cos i \cos e \qquad (2.19a)$$

$$\eta(i, \theta) = \frac{[\partial \sigma / \partial \pi]_\theta}{\cos i \cos e \ \sigma_{abs} \ f(i, e)} \qquad (2.19b)$$
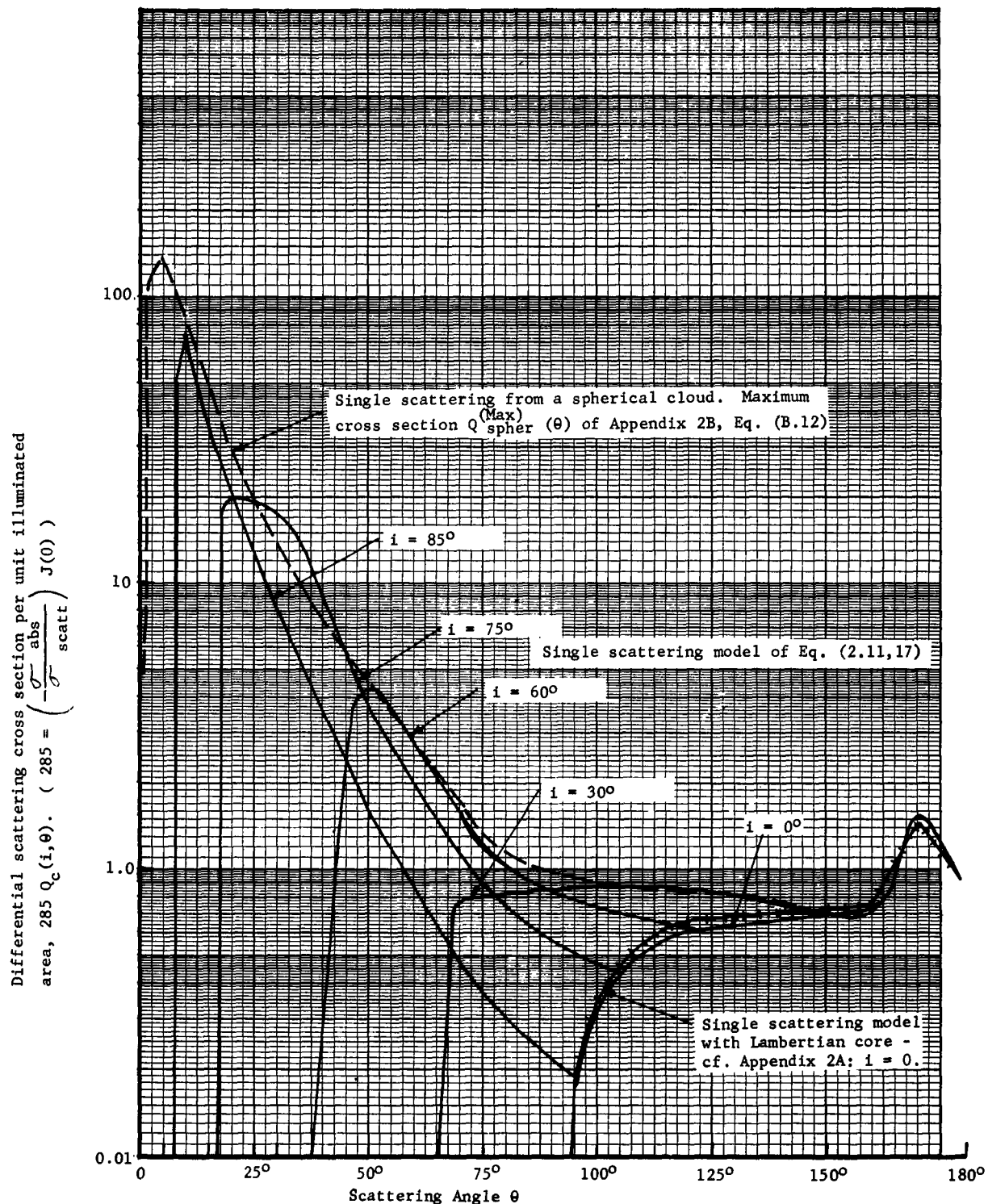
FIGURE 2.5   SCATTERING FROM A LARGE PLANAR CLOUD

NOTE:   For the calculations presented here, it has been assumed
        that the incident ray, the reflected ray, and the local
        normal - AI, AE, AK of Figure 2.4 - all lie in the same
        plane.

2-20

Some typical numerical values of $\eta$ (i, $\theta$) are given here:[*]

$$i = e = 0 \quad, \theta = 180^\circ; \quad \eta = .0099 \qquad (2.20a)$$

$$i = e = 5^\circ, \theta = 170^\circ; \quad \eta = .017 \qquad (2.20b)$$

$$i = e = 45^\circ, \theta = 90^\circ; \quad \eta = .024 \qquad (2.20c)$$

$$i = e = 60^\circ, 0 = 60^\circ; \quad \eta = .060 \qquad (2.20d)$$

$$i = 0, e = \theta = 90^\circ; \quad \eta = .033 \qquad (2.20e)$$

In view of the single scattering mechanism, the concept of a "diffuse reflectivity" is rather unphysical. Also, the angular variation of the numerical values of $\eta$ (i, $\theta$) indicates that it is not a very useful concept for quantitative discussion.

---

[*] These values, like the results of Figure 2.5, refer to the coplanar case, so that they give maximum values for the scattering cross section or reflectivity.

REFERENCE LIST FOR SECTION 2

2.1     B. J. Mason, "The Physics of Clouds", Oxford (1957).

2.2     D. Deirmendjian, "Scattering and Polarization of Polydispersed
        Suspensions with Partial Absorption", Rand Corporation, RM-3228-PR
        (June 1962).  See also earlier publications by the same author
        referenced therein.

2.3     F. H. Ludlam & B. J. Mason,"The Physics of Clouds", Handbuch der
        Physik, 48, Springer, Berlin (1957).

2.4     M. Minnaert, "The Nature of Light and Color in the Open Air",
        Dover, New York (1954).

2.5     M. Centeno, "Refractive Index of Liquid Water in the Near Infrared",
        J. Opt. Soc. America 31, 244 (1941).

2.6     M. Born & E. Wolf, "Principles of Optics", Pergamon, New York (1959).

2.7     H. C. van de Hulst, "Light Scattering by Small Particles", Wiley,
        New York (1957).

2.8     F. S. Johnson, Editor, "Satellite Environment Handbook", p. 79,
        Stanford (1961).

2.9a    J. S. Goldstein, "The Infrared Reflectivity of a Planetary
        Atmosphere", Astrophys. J., 132, 473 (1960).

2.9b    "Numerical Solutions of the Auxiliary Equation for an Inhomogeneous
        Planetary Atmosphere", talk presented at the 11th International
        Astrophysical Symposium, Liege, July 1962.

2.10    V. R. Stull & G. N. Plass, "Emissivity of Dispersed Carbon Particles",
        J. Opt. Soc. America 50, 121 (1960).

APPENDIX 2A

A MODEL TO ESTIMATE THE EFFECT OF MULTIPLE SCATTERING


A phenomenological way to estimate the importance of multiple scattering is to regard the cloud as made up of a single scattering layer one extinction depth thick and a diffuse core with effective diffuse reflectivity $\eta$ *. The coefficient $\eta$ * is obtained by matching the radiance given by this model, H*($\theta$), with that for the single scattering model for a given value $\theta$* of $\theta$.

Instead of Equation (2.16a) we have

$$H*(\theta) = F_o N [\partial\sigma/\partial\pi]_\theta \int_0^{\beta^{-1}} dz\ e^{-\beta\ f(i,e)\ z} + F_o(\eta */\pi)\ \cos i\ \cos e$$

(2A.1a)

$$= H(\theta)\left[1 - e^{-f(i,e)}\right] + F_o(\eta */\pi)\ \cos i\ \cos e$$

where

$$\eta * = \frac{e^{-f(i,e)}[\partial\sigma/\partial\pi]_{\theta*}}{f(i,e)\ \cos i\ \cos e\ \sigma_{abs}}$$

(2A.1b)

$$i + e + \theta* = \pi$$

Clearly the choice of $\theta$* is not unique. $\theta* = \pi$ for backward scattering gives $i = e = 0$, $f(i,e) = 2$, $\eta * = .0099\ e^{-2} = .00134$. The function $Q_c*(i,\theta)$ is shown in Figure 2.5 for $i = 0$, for comparison with $Q_c$.

It should be noted that the fact that $Q_c^*$ is similar to $Q_c$ does not by itself prove that multiple scattering is unimportant, but merely demonstrates the self-consistency of the present way of introducing multiple scattering in terms of a diffuse core underlying a single scattering layer.

APPENDIX 2B

SCATTERING FROM A SPHERICAL CLOUD

It has not been possible to carry through the analysis of
Section 2, Paragraph 2.3c for scattering from a planar cloud to the
case of a spherical cloud. The reason for this is that we have not
succeeded in evaluating the volume integral of Equation (2.15a) for
spherical geometry. In the present appendix are given the formulation
of the problem and an approximate estimate of the cross section.

Consider the scattering of electromagnetic radiation through
an angle $\theta$ by a sphere of radius a. In particular, a typical ray is
shown in Figure 2B.1. The ray is incident on the sphere whose center
is at the origin 0 at a point I whose spherical polar coordinates are
(a, $\gamma'$, $\delta'$), is scattered at a point A(a-z, $\gamma$, $\delta$), and leaves the
sphere at a point E(a, $\gamma''$, $\delta''$). The angles IOA, AOE are denoted by
$\epsilon'$, $\epsilon''$ and the angles OÎA, OÊA are denoted by i, e in analogy with
the planar case.*

_____

*
   It should be noted that i and e are constant for the planar case of
   scattering through a constant angle $\theta$, so that one gets different
   scattering curves for different values of i, as are shown in Figure 2.5.
   This is not the case for spherical geometry, where i,e vary for all
   the different rays corresponding to scattering through an angle $\theta$, so
   that there is a unique angular scattering curve. However, this
   feature complicates the evaluation of the integrals.
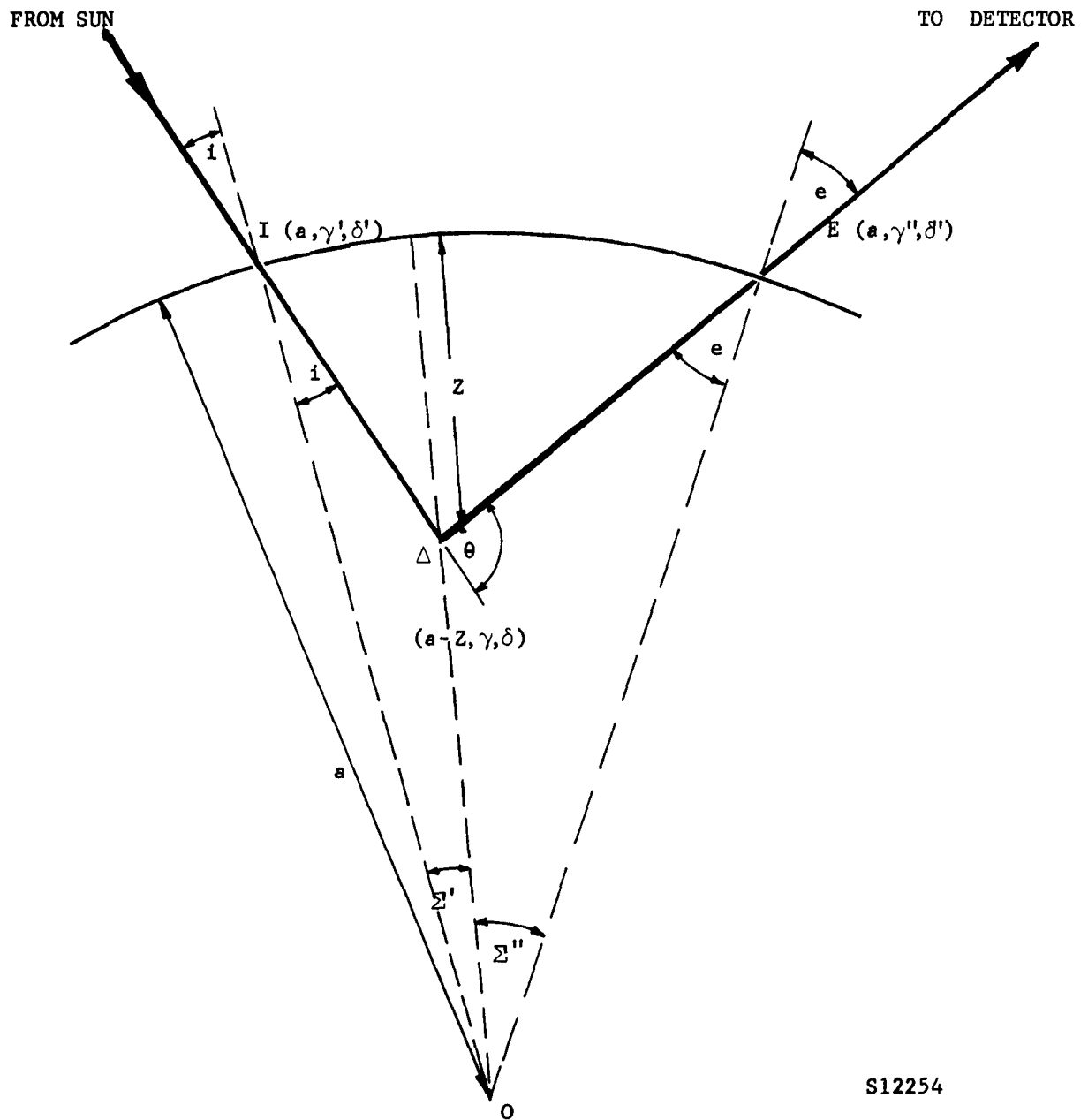
FIGURE 2B.1.  GEOMETRY FOR SCATTERING BY A SPHERICAL CLOUD.

        IAE DENOTES THE PATH OF A TYPICAL RAY SCATTERED THROUGH AN ANGLE
$\theta$ : NOTE THAT IN GENERAL THE FOUR POINTS I,A,O,E, DO NOT ALL LIE IN A PLANE.

The triangle rule for (IOA) gives the exact result

$$\epsilon' = \arcsin \left[ \frac{\sin i}{1 - z/a} \right] - i \qquad (2B.1)$$

For large clouds defined in analogy in the discussion of Equation (2.14) by

$$a \gg \beta^{-1}, \text{ ie } a \gg z , \qquad (2B.2)$$

we may work to the lowest order in a/z. Then Equation (2B.1) gives

$$\epsilon' = (z/a) \tan i + 0(z/a)^2 \qquad (2B.3a)$$

$$r_{IA} = z/\cos i + 0(z^2/a) , \qquad (2B.3b)$$

and to this order the volume element is

$$d_{VA} = dz \; dS \left[ 1 + 0(z/a) \right] . \qquad (2B.4)$$

Here dS is an appropriately defined surface element:

$$dS = a^2 \; g( \gamma , \delta ) \; d \cos \gamma \; d \delta \qquad (2B.5a)$$

$$= a^2 \; g'( \gamma', \delta') \; d \cos \gamma' \; d \delta' , \qquad (2B.5b)$$

where g, g' may be functions of the appropriate angles but are independent of z to the lowest order in (z/a). Thus, to this order the radiance of the cloud due to scattering through an angle θ is

$$\left[\partial W/\partial x\right]_\theta = F_o\, N \left[\partial \sigma/\partial x\right]_\theta \int dV_A\, e^{-\beta\,(r_{IA} + r_{AE})} \qquad (2B.6a)$$

$$= F_o\, N \left[\partial \sigma/\partial x\right]_\theta \int dV_A\, e^{-\beta z\, f(i,e)} \left[1 + O(z/a)\right] \qquad (2B.6b)$$

$$= \frac{F_o\, N}{\beta} \left[\partial \sigma/\partial x\right]_\theta \int \frac{dS}{f(i,e)} \qquad (2B.6c)$$

where

$$f(i,e) = 1/\cos i + 1/\cos e \qquad (2.16b)$$

Thus far it has not proved possible to evaluate the integral $\int dS/f(i,e)$ exactly. In general one may put

$$\int \frac{dS}{f(i,e)} = S_{ill}^{(\theta)} \left\langle 1/f(i,e) \right\rangle_{av} \qquad (2B.7a)$$

$$S_{ill}^{(\theta)} = a^2 \int_{-\pi/2}^{\pi/2} \cos\psi\, d\psi \int_{\frac{\pi}{2}-\theta}^{\frac{\pi}{2}} d\omega = 2\theta \qquad (2B.7b)$$

where the coordinates ( $\psi$ , $\omega$ ) are defined in Section 3.3, and in particular in Figure 3.1 .

An upper bound to $\left\langle 1/f(i,e) \right\rangle_{av}$ may be set as follows. First of all, consider coplanar scattering; i.e., I, A, O, and E all in the same plane, and

$$i + e + \theta = \pi - \varepsilon' - \varepsilon'' = \pi \left[1 - O(z/a)\right] \simeq \pi \qquad (2B.8)$$

In this case for constant scattering angle $\theta$,

$$f(i,e) = 1/\cos i = 1/\cos(\theta + i) \qquad (2B.9)$$

and as $i$ varies,

$$f(\theta) = 2/\sin(1/2\theta) \leqslant f(i,e) \leqslant \infty \quad (i = \pi/2) \ . \qquad (2B.10)$$

Thus we have an upper bound on $\left\langle 1/f(i,e) \right\rangle_{av}$

$$\left\langle 1/f(i,e) \right\rangle_{av} \leqslant 1/f(\theta) \ . \qquad (2B.11)$$

Thus an upper bound for the scattering cross section per unit illuminated area, $Q_{spher}(\theta)$, is given by the expression

$$Q_{spher}(\theta) = \frac{[\partial\sigma/\partial\mathcal{R}]_\theta}{F_o \, S_{ill}(\theta)} \leqslant \frac{(1/\sigma_{abs})[\partial\sigma/\partial\mathcal{R}]_\theta}{f(\theta)} = Q_{spher}^{(Max)}(\theta)$$

$$(2B.12)$$

The function $Q_{spher}^{(Max)}(\theta)$ is shown in Figure 2.5.

In general the representation of a planar cloud is significantly more useful than that of a spherical cloud. However, under certain conditions of oblique viewing the effect of the edges of clouds may be important, and here the model of a spherical cloud may prove of interest. In any case, the analysis can certainly be extended, although numerical techniques may be necessary to evaluate $\left\langle 1/f(i,e) \right\rangle_{av}$.

SECTION 3

SCATTERING OF SOLAR INFRARED FROM CLOUDS

3.1 METEOROLOGICAL DATA

Natural clouds are made up of assemblies of water droplets or ice crystals. In either case, the water content is in the range $0.1 - 1$ gm/m$^3$ at the higher altitudes, and up to $10$ gm/m$^3$ at sea level. For water clouds, observed droplets range in size from $2 - 30$ micron radius, with mode radii $4 - 8$ microns. In the case of ice crystals, the particles may be of roughly the same size, or there may be significantly fewer particles up to $500$ microns in their largest dimension. The shape of the ice crystals may be hexagonal, prismatic, or complex, and the crystals may possibly be aligned by convection currents within a cumulus cloud, or (less probably) by wind shear in the case of cirrus or stratus clouds.

Cumulus clouds in general cool by adiabatic expansion accompanying their rise, rather than by thermal exchange with the ambient atmosphere. These clouds undergo constant convective stirring, which leads to the characteristic anvil or mushroom shape of thunderheads. It should be mentioned that $1 - 10$ micron droplets freeze at $-35^\circ C$ to $-40^\circ C$ on account of surface tension effects, so that the question of under what conditions clouds are made up of ice crystals rather than water droplets does not necessarily have a simple answer.

3-1

Below the tropopause (30-40 Kft) there is a great deal of local atmospheric structure and, hence, various types of clouds. In general, there is a relatively high probability (10% for the continental U.S.A.) of more or less uniform cloud cover at the tropopause. At the present there is not much quantitative data on higher clouds except for Tiros satellite pictures, which have not yet been processed completely. Tropical thunderstorms associated with hurricanes or typhoons form cumulus systems up to several hundred miles across which have been known to "burst through" the tropopause and rise to a significant height. At higher latitudes there is not much statistical information, but one might infer that for a cloud to rise a height h above the tropopause the linear dimension of the cloud has to be at least of the order h.

There are known several rare and not very dense types of very high altitude clouds. These are "noctilucent" clouds at up to 30 Km (90-100 Kft) altitude, which are very thin and composed of ice crystals, and "nacreous" or "mother-of-pearl" clouds at 20-30 Km which are inferred to be composed of spherical particles of rather uniform size on account of their color.

In summary, it must be stressed that the present discussion clearly does not do justice to the large amount of meteorological work of observing and classifying cloud data. Up to the present, most experimental work deals with rather low altitude clouds (less than 10 Km or 30 Kft) as far as observation and sampling go. New information from satellites, balloons and high altitude jet airplanes is beginning to supplement these data. Unquestionably, in 3 to 5 years there will be available much more information on high altitude clouds than exists at present.

## 3.2  TRANSMISSION LOSSES

### a.  Introduction

The attenuation of solar infrared in the 2.7 micron atmospheric absorption band, which is here interpreted as $3675 \pm 100$ cm$^{-1}$, is to be examined for heights above 10 Km.  The absorption in this band is due both to $CO_2$ and to $H_2O$.  The $CO_2$ in the upper atmosphere is well known to be mixed uniformly with air (.03% by volume).  The amount of $CO_2$ at S.T.P. in a vertical one-way path to infinity is 240 atm-cm (cf. Ref. 3.1, ch. VIII), and at a pressure of $(p/p_o)$ atmospheres, the residual amount is 240 $(p/p_o)$ atm-cm.

The amount of water vapor and its distribution are not so firmly established.  Here the latest compilation of Gutnick[3.5] is used. The results are shown in Table 3.1.  It should be noted that Gutnick's estimates only extend up to 34 Km, and it is quite possible that there is a significant amount of water at higher altitudes.  For instance, if the density of water vapor from 34-50 Km is 0.2 gm/m$^3$, the amounts of precipitable water at all altitudes in Table 3.1 have to be increased by .0032 gm/cm$^2$.  This is simply a measure of the experimental uncertainty of this quantity.[*]

------------------------------------------------

[*]It should be pointed out that it is not completely clear whether the water vapor concentration is a single function of height[3.5], or whether in fact there are large variations, by factors up to 100 - 1000 between a "wet" and a "dry" atmosphere[3.6].  The present concensus favors the uniform distribution.

TABLE 3.1 '

ATMOSPHERIC WATER VAPOR CONCENTRATION AT HIGH ALTITUDES

| Altitude h (Km) | Atmospheric Density $\rho$ (Kg/m$^3$) | Mixing Ratio m (gm/Kg air) | Water Density $\rho$m (gm/m$^3$) | Precipitable Water (gm/cm$^2$) from 34 Km Down* |
|---|---|---|---|---|
| 10 | $4.135 \times 10^{-1}$ | .038 | $1.571 \times 10^{-2}$ | .00678 |
| 12 | $3.119 \times 10^{-1}$ | .017 | $.530 \times 10^{-2}$ | .00468 |
| 14 | $2.279 \times 10^{-1}$ | .010 | $.228 \times 10^{-2}$ | .00392 |
| 16 | $1.665 \times 10^{-1}$ | .0095 | $.158 \times 10^{-2}$ | .00353 |
| 18 | $1.217 \times 10^{-1}$ | .012 | $.146 \times 10^{-2}$ | .00323 |
| 20 | $8.891 \times 10^{-2}$ | .018 | $.160 \times 10^{-2}$ | .00292 |
| 22 | $6.500 \times 10^{-2}$ | .027 | $.176 \times 10^{-2}$ | .00259 |
| 24 | $4.752 \times 10^{-2}$ | .039 | $.185 \times 10^{-2}$ | .00223 |
| 26 | $3.436 \times 10^{-2}$ | .060 | $.206 \times 10^{-2}$ | .00184 |
| 28 | $2.436 \times 10^{-2}$ | .088 | $.217 \times 10^{-2}$ | .00141 |
| 30 | $1.786 \times 10^{-2}$ | .125 | $.223 \times 10^{-2}$ | .00097 |
| 32 | $1.304 \times 10^{-2}$ | .180 | $.235 \times 10^{-2}$ | .00051 |
| 34 | $9.602 \times 10^{-3}$ | .290 | $.279 \times 10^{-2}$ | 0 |

*(1) Precipitable water from height $h_o$ to $h_1$ = $\int_{h_o}^{h_1} (\rho m)_h \, dh.$

(2) If ($\rho$ m) $\approx 2 \times 10^{-3}$ gm/m$^3$ from 34 - 50 Km altitude, the additional amount of precipitable water is .0032 gm/cm$^2$ below 34 Km.

The transmissivity for a vertical one-way path from infinity down to the reference altitude h is given in Table 3.2. The transmissivity factors used there have been obtained from the calculations of Plass, Stull, and Wyatt[3.7]. It should be mentioned that the transmissivity calculations apply to constant pressure; we have used values corresponding to $\frac{1}{2}$ p(h), where p(h) is the atmospheric pressure corresponding to the reference altitude. This is clearly not completely satisfactory from a quantitative standpoint, but provides an estimate, which is all that is called for in the present application.

b. <u>Slant Path Transmission</u>

The fact that the densities of $CO_2$ and $H_2O$ are functions only of altitude (rather than of geographic location) implies that for a slant path from a point A to infinity, inclined at an angle $\gamma$ to the vertical, the effective absorbing path length is given by the relation

$$\text{Slant Path Length (Angle } \gamma \text{)} = \text{(Vertical Path Length )} / \cos\gamma \quad (3.1)$$

This condition holds for an appropriate range of $\gamma$ : in particular, if $R_o$ = radius of the earth, $h_o$ = maximum height at which there is significant attenuation ($h_o \sim 100 - 150$ Kft), then (3.1) holds, provided

$$\left( \frac{\pi}{2} - \gamma \right) \gg h_o / R_o , \quad (3.2)$$

or, since $h_o / R_o \sim 20$ minutes of arc, Eq. (3.1) holds for $0 \leqslant \gamma < 89°$.

If the vertical one-way transmissivity from point A to infinity is t, then, provided Eq. (3.1) holds,

$$\text{Slant Path Transmission Loss} = t^{(\cos\gamma)^{-n}} ; \quad 0 < n \leqslant 1 \quad (3.3)$$

3-5

## TABLE 3.2

VERTICAL TRANSMISSION LOSS IN THE 2.7 MICRON BAND FOR A VERTICAL ONE-WAY PATH FROM INFINITY DOWN TO THE REFERENCE ALTITUDE

| Altitude h (Km) | Temperature T(h) (°K) | Pressure ½P(h) (atm) | Amount of CO₂ (atm-cm) | Amount of Water Vapor (pr-cm) (a) | (b) | $t_{CO_2}$ | $t_{H_2O}$ (a) | (b) | $t_{CO_2} \times t_{H_2O}$ (b) |
|---|---|---|---|---|---|---|---|---|---|
| 0 | 288 | 0.5 | 240 | | | .01 | | | |
| 10 | 223 | 0.1 | 62.8 | .0068 | .0100 | .46 | .68 | .64 | .29 |
| 15 | 217 | 0.05 | 28.7 | .0037 | .0069 | .68 | .81 | .75 | .51 |
| 20 | 217 | 0.02 | 13.1 | .0029 | .0061 | .85 | .88 | .84 | .71 |
| 25 | 217 | 0.01 | 5.98 | .0020 | .0052 | .92 | .93 | .89 | .82 |
| 30 | 231 | 0.005 | 2.81 | .00097 | .0042 | >.95 | >.95 | >.93 | >.88 |

Notes:

(1) All data on transmissivities come from Ref. 3.7. All values except sea level correspond to T = 200°K.

(2) The amount of water vapor below 10 Km is highly variable. Model (a) corresponds to assuming no water vapor above 34 Km, while model (b) corresponds to assuming a uniform water vapor density from 34 - 50 Km. See Table 3.1.

(3) Transmissivity factors are obtained from the following tabulated values, all averaged over 100 cm⁻¹ intervals -

$$t = \tfrac{1}{2} (\ (t \ (3600) + t (3700) \ )$$

(4) Interpolation for the amount of absorbing material is carried out as indicated in Ref. 3.7, Vol. I, Section 5-2.

where$^{3.8}$

        n = 1 for the "weak line approximation"

        n = ½ for the "strong line approximation with no overlap"  (3.4)

        n < ½ for the "strong line approximation with overlap"

The overall problem is a very complicated one$^{3.8}$. In the calculations
of isoradiance plots in Section 3.3, we use n = 1; i.e., the "weak line
approximation."

## 3.3 REFLECTION OF SOLAR INFRARED FROM A UNIFORM CLOUD COVER

    a.  <u>Introduction</u>

        In Section 3.3 we discuss a uniform tropospheric cloud background.
In practice there would be large black areas due to the absence of
clouds at the tropopause and occasional bright spots arising from high
altititude clouds.

        For definiteness we consider a satellite D at a height
$(r-a) = (\rho - 1)a$ above the surface of the earth, whose radius is a.
For a numerical example, we take the satellite height to be 2000 miles,
so that $\rho$ = 1.5. Let the sun S be at an angle of elevation ، relative
to the satellite. The question is now the following. The satellite
scans the portion of the surface of the earth that it can observe with a
very narrow beam. Under these conditions, how much radiation in the
2.7 micron band does the satellite receive as a function of its direction
of view, of the elevation angle, of the normal one-way transmissivity
factor t of Section 3.2, and of the scattering law $i_{av}(\theta)$ of Section 2
and Table 3.3?

3-7

## TABLE 3.3

## THE SCATTERING FUNCTION $i_{av}(\theta)$[*]

| Scattering Angle $\theta$ (degrees) | $i_{av}(\theta)$ |
|:---:|:---:|
| 0 | 10,448 |
| 5 | 5,970.2 |
| 10 | 1,599.4 |
| 15 | 559.9 |
| 20 | 297.8 |
| 30 | 107.6 |
| 40 | 44.07 |
| 50 | 20.10 |
| 60 | 10.21 |
| 70 | 5.929 |
| 80 | 4.091 |
| 90 | 2.659 |
| 100 | 2.171 |
| 120 | 2.078 |
| 140 | 1.984 |
| 160 | 1.891 |
| 180 | 1.798 |

---

[*]This function differs from the exact result of Section 2 in that the "rainbow" maximum at $\theta = 170^{\circ}$ has been smoothed out.

The numerical calculations have been carried out for $t = 0.1$ and 0.5 and for $\alpha = 0°$, $45°$, $90°$, $120°$, and the calculation has been programmed so that a different scattering law $i_{av}(\theta)$ may be inserted readily in the form of a table if it is desired to repeat the calculation for different values of the parameters.

b. <u>Geometrical Considerations</u>

The geocentric coordinate system used here is a slight modification of that of Zirker, Whipple and Davis[3.10]. All the coordinates that arise are shown in Figure 3.2, where $\overrightarrow{DO}$ defines the z-axis and DOS the (zy)-plane, so that

$$D = (0, 0, a\rho) \tag{3.5a}$$

$$S = \lim_{\phi \to \infty} \phi (0, \sin\alpha, \cos\alpha) \tag{3.5b}$$

The geocentric angles are a latitude $\psi$ and a longitude $\omega$. The latitude $\psi = 0$ defines the equatorial (yz)-plane, and the latitude $\psi = \pi/2$ defines the positive x-axis. The longitude $\omega = 0$ defines the positive z-axis, and point A on the surface of the earth has the coordinates

$$A = a(\sin\psi, \cos\psi \sin\omega, \cos\psi \cos\omega) \tag{3.6}$$

and the surface element on the sphere is

$$dS = a^2 \cos\psi \, d\psi \, d\omega . \tag{3.7}$$

The vector $\overrightarrow{AD}$ has magnitude $b$, and is given as

$$\overrightarrow{AD} = a(-\sin\psi, -\cos\psi \sin\omega, \rho - \cos\psi \cos\omega) \tag{3.8a}$$

$$|\overrightarrow{AD}|^2 / a^2 = b^2 = 1 + \rho^2 - 2\rho \cos\psi \cos\omega \tag{3.8b}$$

FIG. 3.2.   LIMITING VALUES OF $\omega$.

The viewed illuminated portion of the earth is characterized by
$|\omega| \leq \delta = \text{arc cos}(1/\rho)$ because of the condition $O^A D \geq {}^A_c D = \pi/2$.   See
Eq. (3.12).

In terms of these geocentric angles ($\psi$, $\omega$), the local angles of incidence, exit, and scattering at the point A are given by the following relations:

$$\cos i = (\overrightarrow{E_{OA}}, \overrightarrow{E_{AS}}) = \cos \psi \cos(\alpha - \omega) \tag{3.9a}$$

$$\cos e = (\overrightarrow{E_{OA}}, \overrightarrow{E_{AD}}) = (1/D)(\rho \cos \psi \cos \omega - 1) \tag{3.9b}$$

$$\cos \beta = (\overrightarrow{E_{AS}}, \overrightarrow{E_{AD}}) = (1/D) \left[ \rho \cos \alpha - \cos \psi \cos(\alpha - \omega) \right] \tag{3.9c}$$

where $\overrightarrow{E_{OA}}$ is the unit vector parallel to $\overrightarrow{OA}$, and so on. The angle $\beta = \pi - \theta$, where $\theta$ is the scattering angle of Section 2.

In principle, this specifies the problem. However, it is more convenient to express the results in terms of the angles of view of the satellite, here chosen as ($\xi$, $\eta$) and sketched in Fig. 3.1. By referring to Fig. 3.1, one sees that

$$\cos \widehat{COA} = (\overrightarrow{E_{OA}}, \overrightarrow{E_{OC}}) = \cos \psi \cos \omega \tag{3.10a}$$

$$CA = a \sin \widehat{COA} = a(1-\cos^2 \psi \cos^2 \omega)^{\frac{1}{2}} \tag{3.10b}$$

$$AB = a \sin \psi , \tag{3.10c}$$

and thus

$$\sin \xi = AB/AC = \sin \psi / (1-\cos^2 \psi \cos^2 \omega)^{\frac{1}{2}} \tag{3.11a}$$

$$\sin \eta = AC/AD = (1-\cos^2 \psi \cos^2 \omega)^{\frac{1}{2}}/D. \tag{3.11b}$$
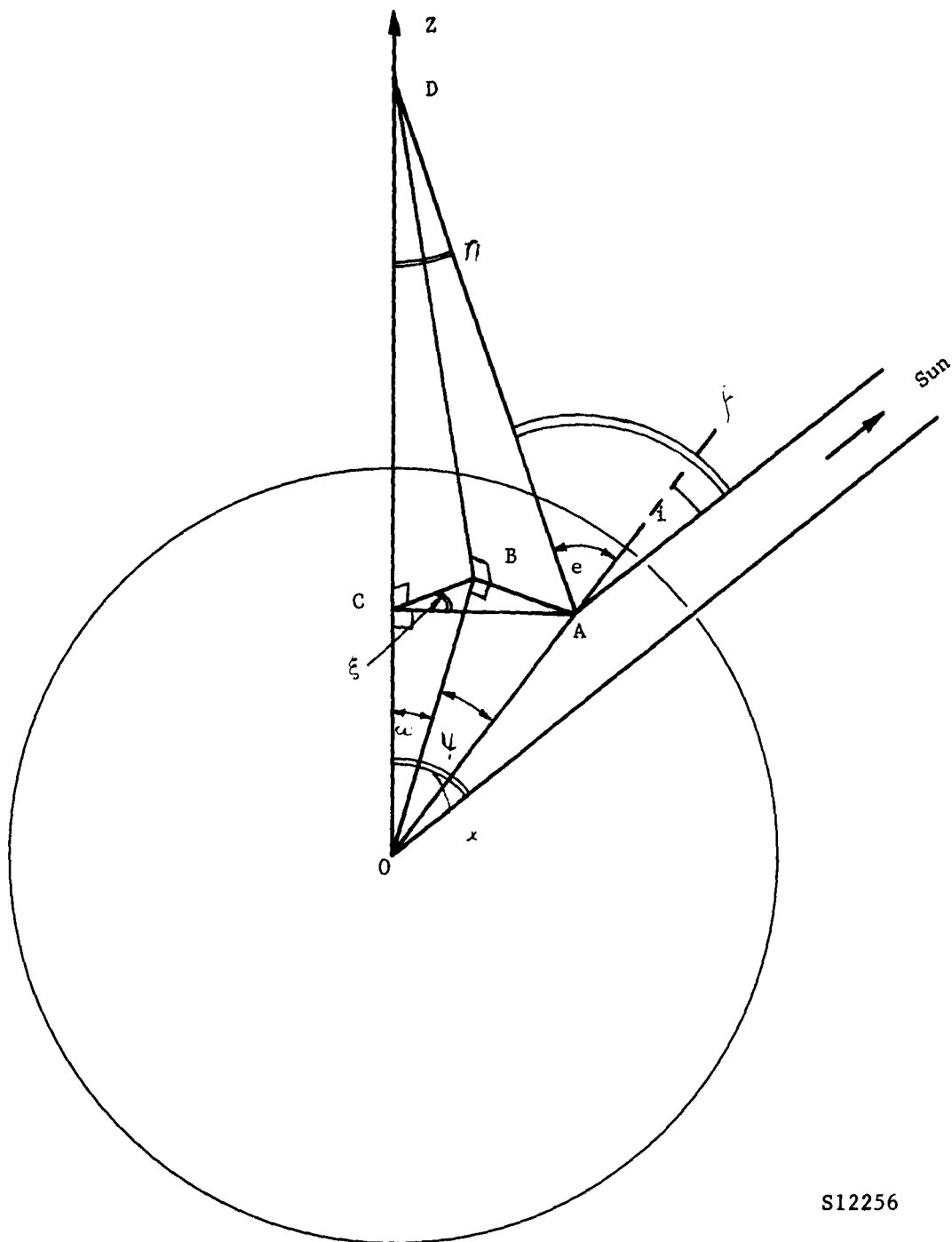
FIG. 3.1.  GEOMETRY FOR SCATTERING OF SOLAR RADIATION FROM A POINT A ON THE SURFACE
OF THE EARTH TO THE DETECTOR D.

$\alpha$ is the elevation angle, $(\psi, \omega)$ are the latitude and longitude of A, i, e, $\theta =$
$\pi - \beta$ are the angles of incidence, exit and scattering for the ray SAD under
consideration here.  $(\iota, \eta_i)$ are the angles of view of A from the satellite.

3-12

There is one further matter to be discussed, namely the limiting values of the angles ( $\psi, \omega$ ). First consider $\omega$ , and see Fig. 3.2. The limiting ray $\overrightarrow{DA}_c$ corresponds to $D\widehat{A}_c0 = \pi/2$ , and thus for $0 \leqslant \alpha \leqslant \pi$ ,

$$\text{Min} \ ( \delta , |\alpha - \tfrac{\pi}{2} | ) \leqslant \omega \leqslant \delta = \text{arc cos} \ (1/\rho ). \quad (3.12)$$

For the limit on $\psi$ , see Fig. 3.3, where the limiting ray $\overrightarrow{DA}_d$ is shown.

$$\cos D\widehat{O}A_d = 1/\rho = (\overrightarrow{E}_{DO}, \overrightarrow{E}_{OAd}) = \cos \psi \cos \omega \quad (3.13)$$

so that for each $\omega$ which satisfies (3.12), we have the limits on $\psi$ -

$$|\psi| \leqslant \text{arc cos}(1/\rho \cos \omega ) \quad (3.14)$$

c. **Isoradiance Plots**

The earth is taken to be covered by a uniform layer of thick flat-topped clouds at an altitude corresponding to a vertical one-way transmissivity, t, measured from the cloud top altitude to infinity. One calculates the spectral radiance H(A) at a variable point A on the layer

$$H(A) = F_o \left[ \frac{\sigma_{scatt}}{\sigma_{abs}} \right] \frac{i_{av}(\theta)}{J(0) \ f(i,e)} \ t^{f(i,e)} \quad (3.15)$$

The point A is characterized by geocentric latitude and longitude $\psi, \omega$ respectively and for a given set of angles ( $\psi, \omega$ ) the angles of incidence, exit and scattering i,e, $\theta = \pi - \beta$ are given by Eq. (3.9). The term $t^{f(i,e)}$ gives the fractional energy loss on a slant path: sun-cloud point A - detector under the "weak line approximation" of Eq. (3.3, 3.4). In general, this factor is

$$t^{f_n (i,e)} = t^{1[(\cos i)^n + 1/(\cos e)^n]} , \ 0 < n \leqslant 1. \quad (3.16)$$

S12258

FIG. 3.3.  LIMITING VALUES OF LATITUDE $\psi$ .

For a given value of $\omega$ , the viewed illuminated portion of the earth is
characterized by $O^A D \gg O^A_d D = \pi/2$, and thus $|\psi| \leq$ arc cos(1/$\rho$ cos $\omega$).  See
Eq. (3.12-14).

3-14

$F_o$ = .000568 watt/cm$^2$ is the solar radiance in the 2.7 micron band[3.10], while the remaining terms just give the angular scattering cross section per unit area, $Q_c(i,\theta)$ of Eq. (2.11, 16, 17) and Fig. 2.5.

The scattering function $i_{av}(\theta)$ used here is given in Table 3.3. It differs slightly from the accurate form of Section 2.2, Fig. 2.3, in that the "rainbow" maximum at $\theta = 170°$ has been smoothed out. This was done because this maximum complicates the plotting significantly, and its effect is a factor of two at most, which is not particularly significant for a first look at the isoradiance contours.

The computational problem is the following. For a given cloud point characterized by the geocentric latitude and longitude ($\psi, \omega$), the satellite viewing angles ( $\xi$ , $\eta$ ) are determined from Eq. (3.11) and the angles (i,e, $\beta = \pi - \theta$) are obtained from Eq. (3.9). The function $i_{av}(\theta)$ is obtained by a "table look-up" routine and H(A) calculated from Eq. (3.15). This part of the problem is carried out on a high-speed digital computer for a range of points A. From these data isoradiance contours are obtained as a function of the satellite look angles ( $\xi$ , $\eta$ ) by manual cross plotting. The isoradiance plots for a range of transmissivity factors t and elevation angles $\alpha$ are given in Fig. 3.4.

Fig. 3.4  Isoradiance Plots

The lines drawn are contours of equal brightness as a function of the satellite view angles ( $\xi_s$ , $\eta$ ).  They are calculated from Eq. (3.15) for various elevation angles $\alpha$ and transmission factors t.  The numbers listed give log H, where H is measured in watt/cm$^2$ sterad, increasing up to the value of the central maximum on a given plot.  Graphs are shown for $\alpha$ = 0, 45°, 90°, 120° and for t = 0.1, 05.

3-15a
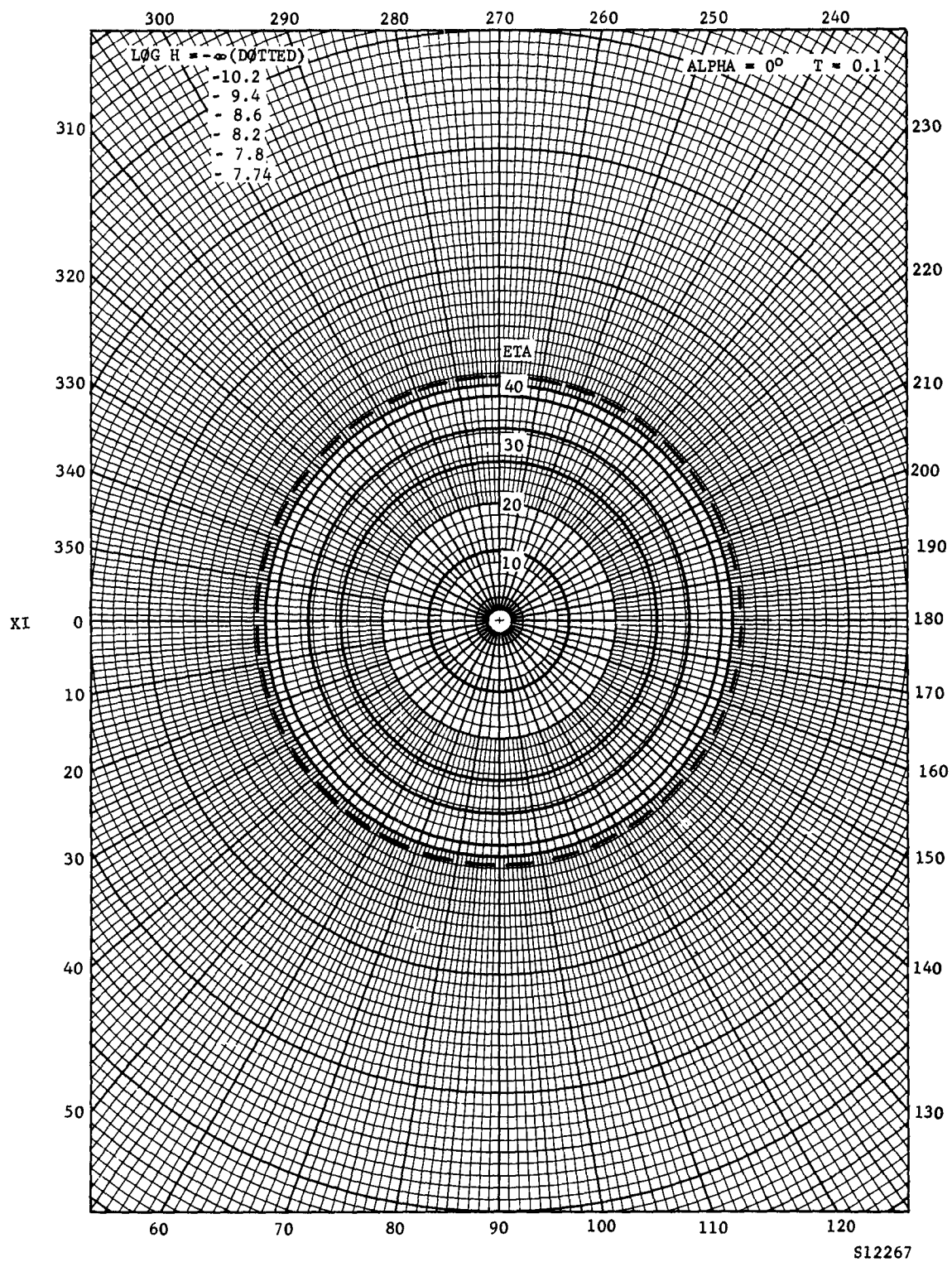
FIGURE 3.4   ISORADIANCE PLOTS

3-16
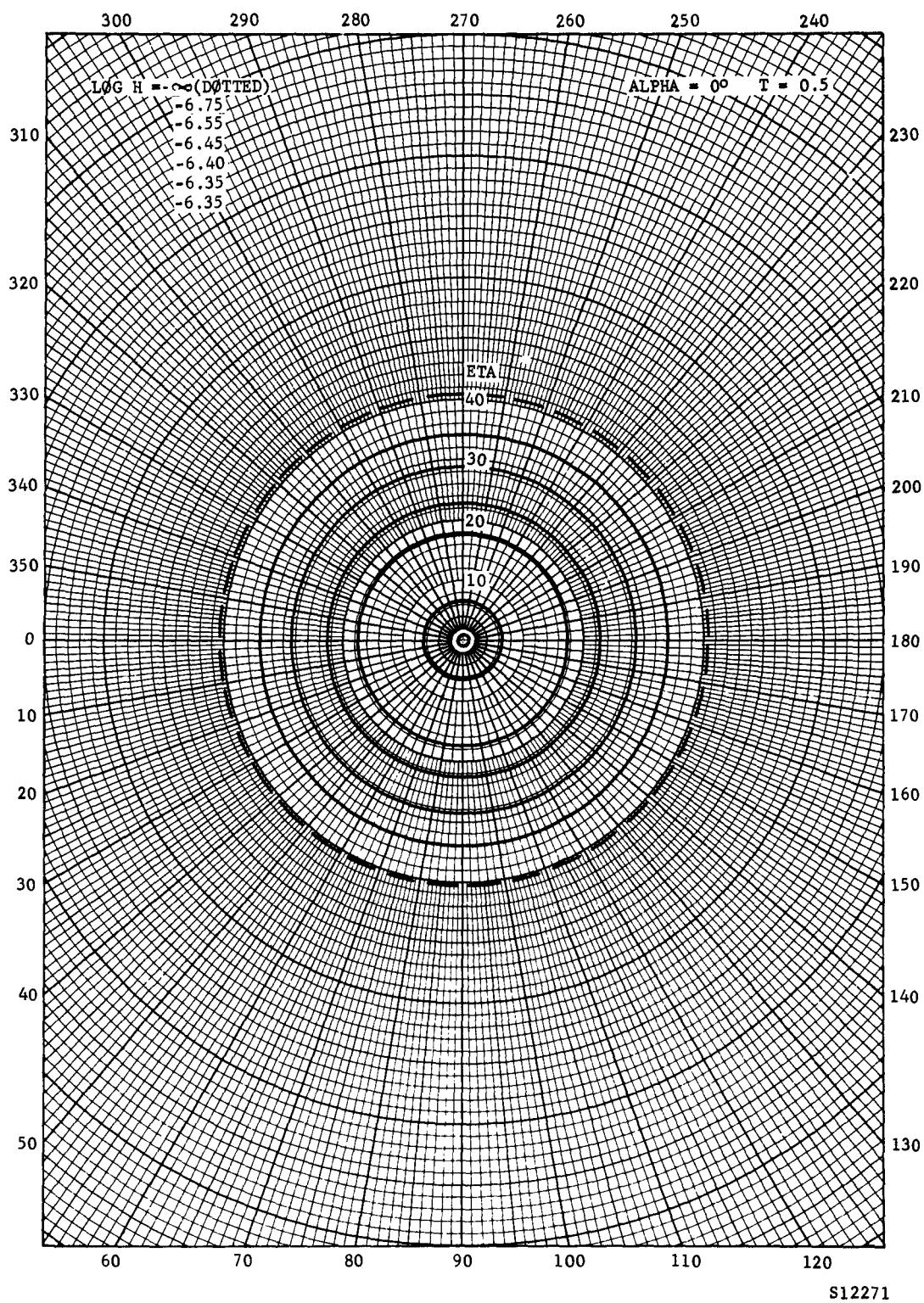
FIGURE 3.4 (Continued) ISORADIANCE PLOTS
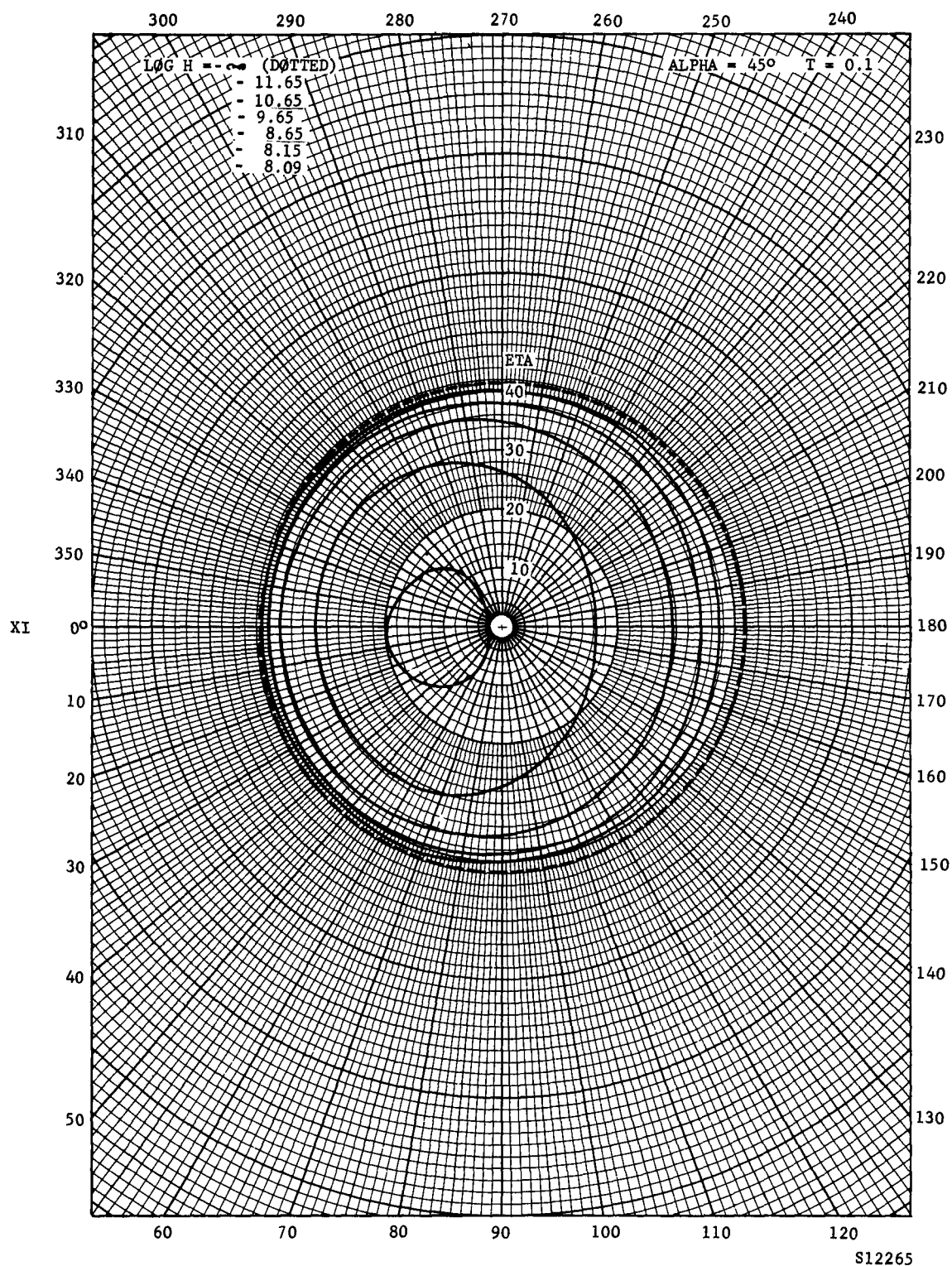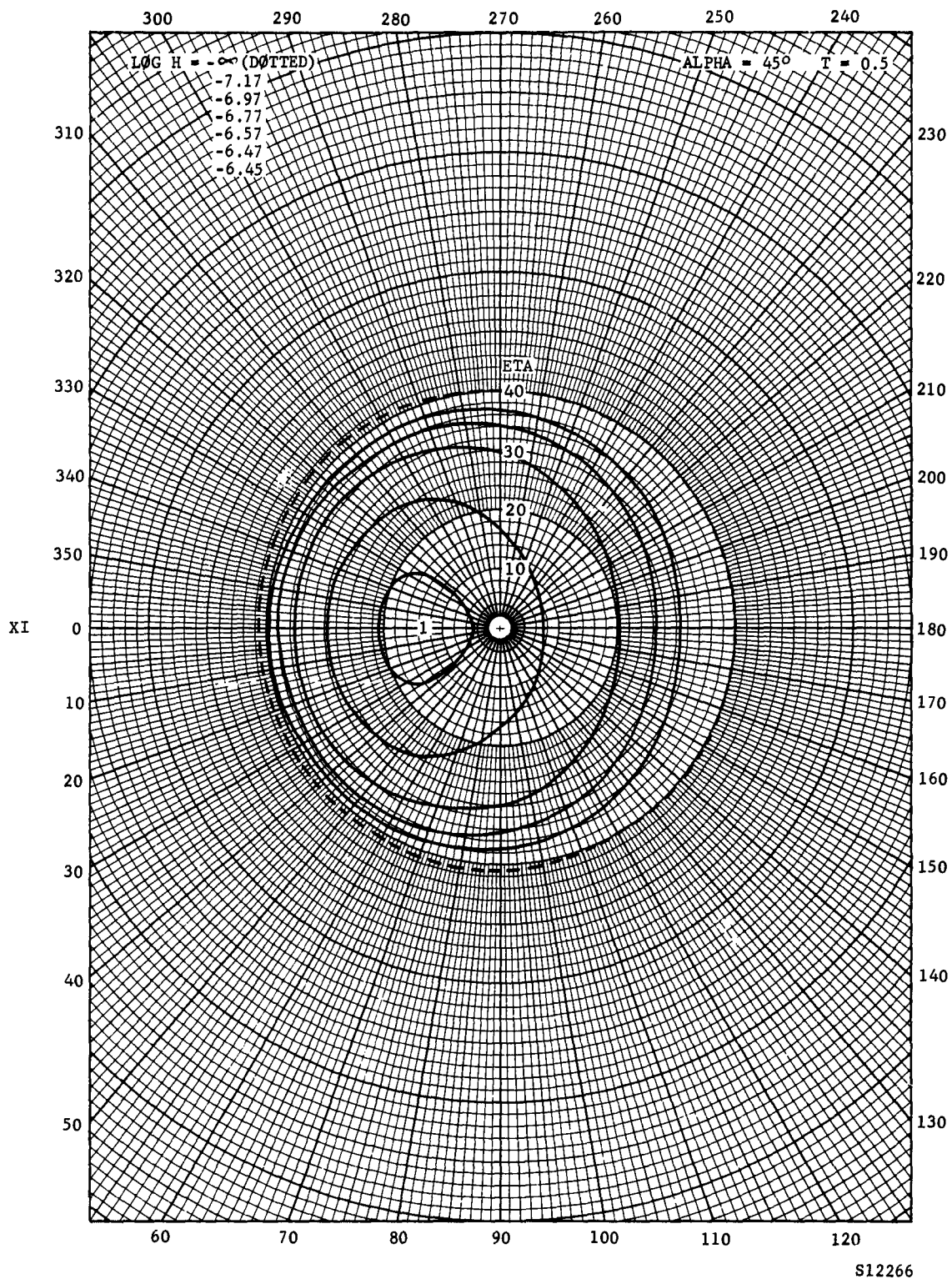
3-17

FIGURE 3.4 (Continued) ISORDIANCE PLOTS

S12265

3-18

FIGURE 3.4 (Continued) ISORDIANCE PLOTS

3-19

FIGURE 3.4  (Continued)  ISORDIANCE PLOTS

3-20

FIGURE 3.4 (Continued) ISORDIANCE PLOTS

3-21

S12272

FIGURE 3.4 (Continued) ISORDIANCE PLOTS

3-22

FIGURE 3 4 (Continued) ISORDIANCE PLOTS

3-23
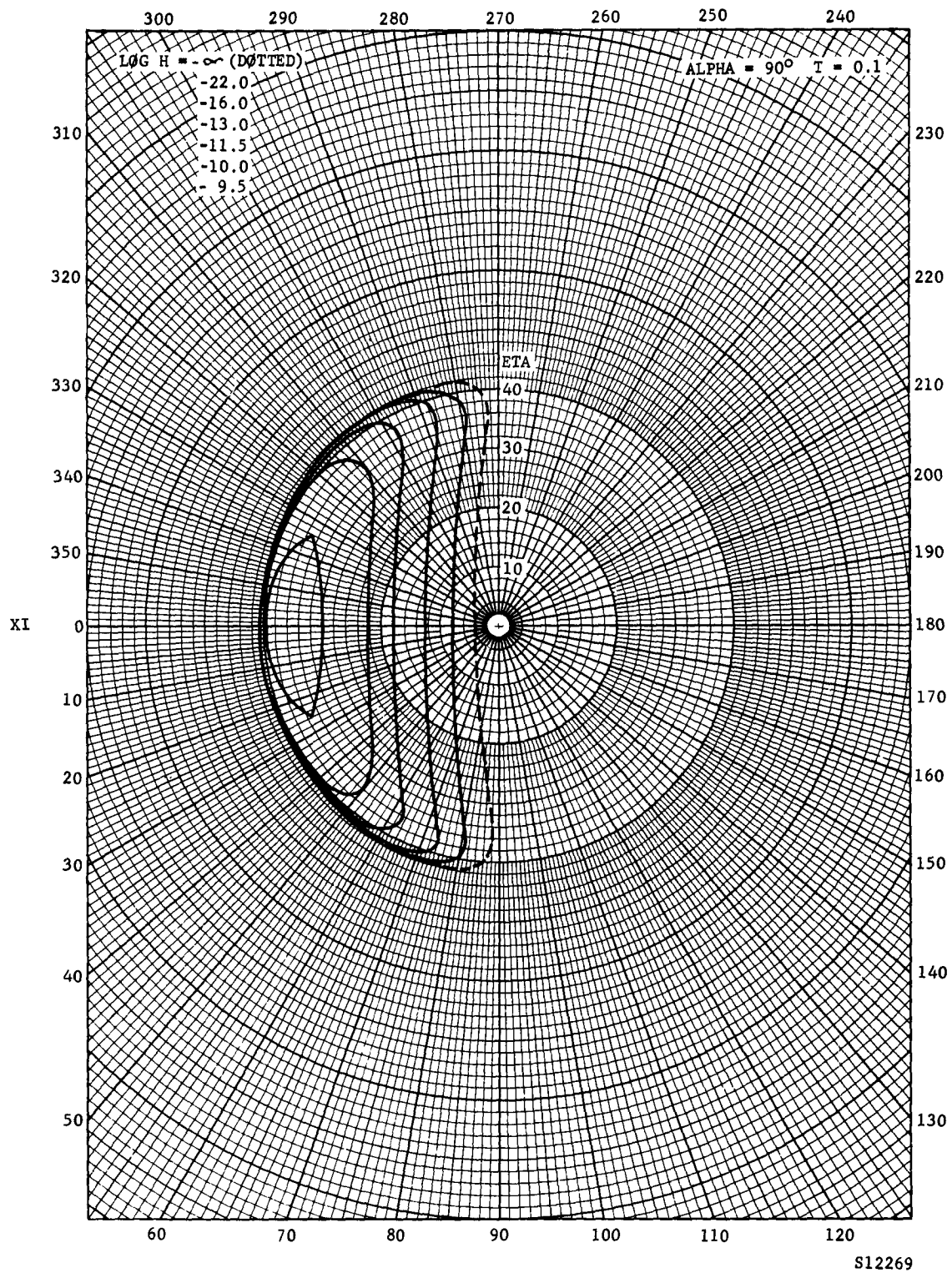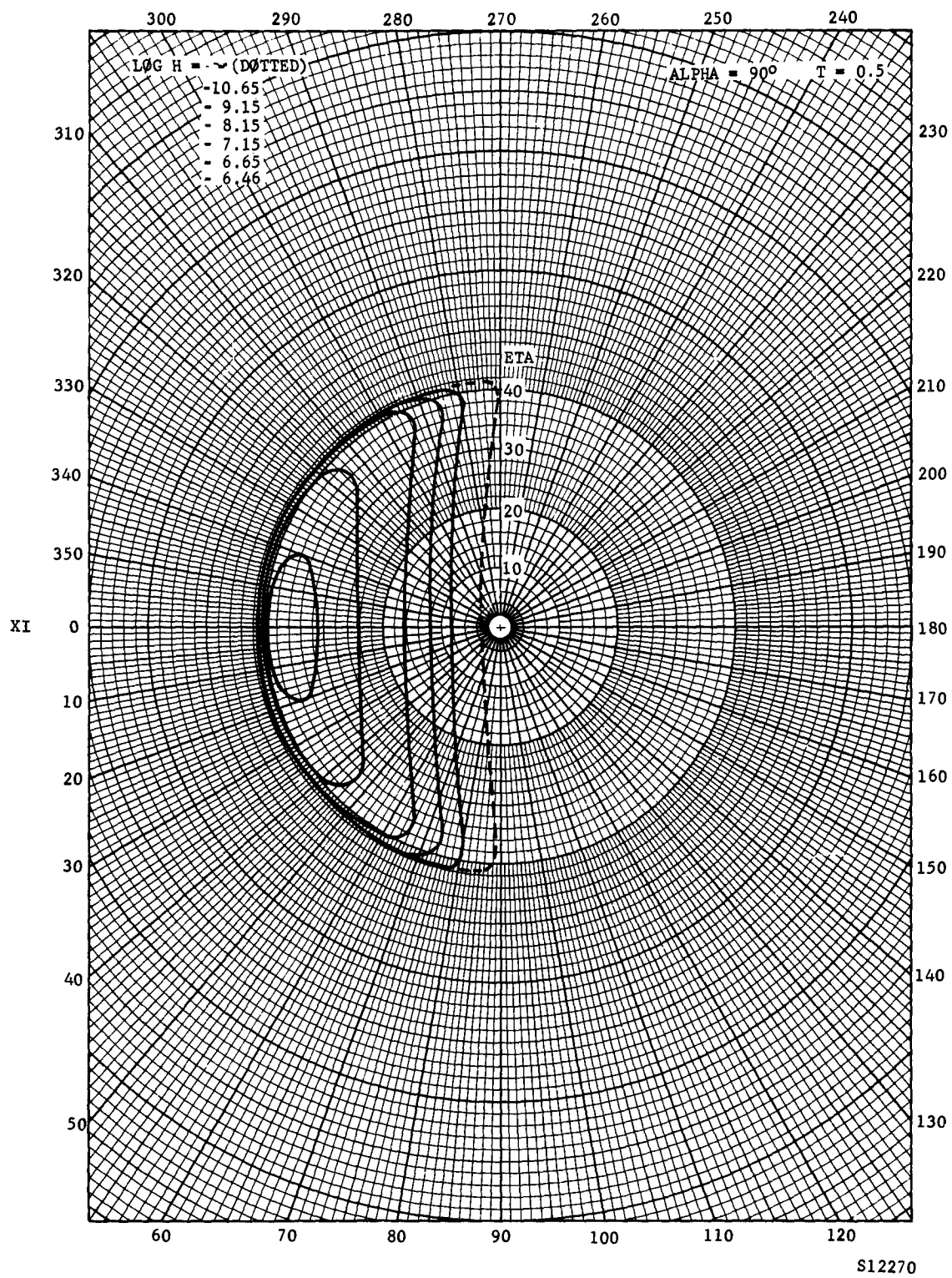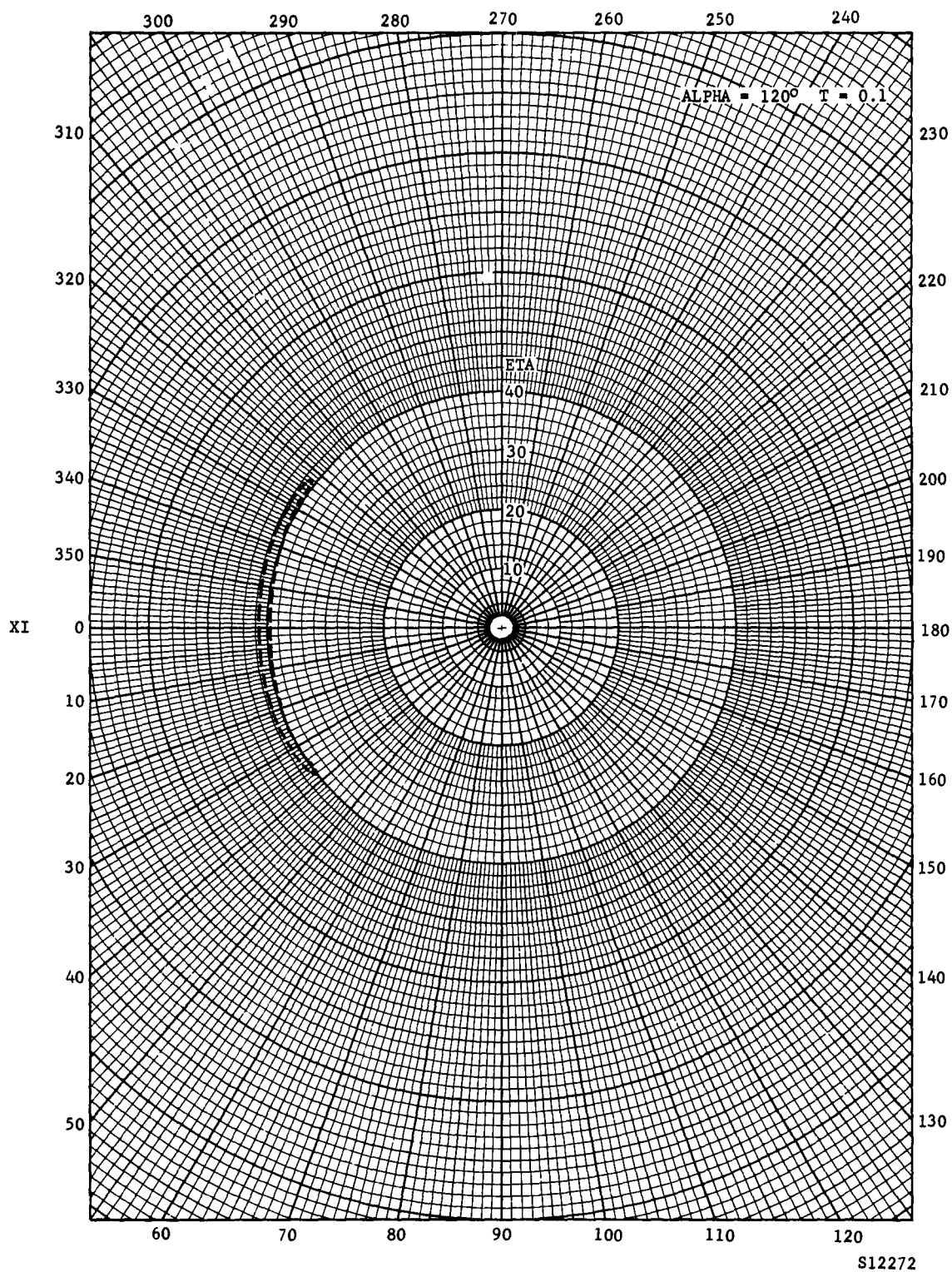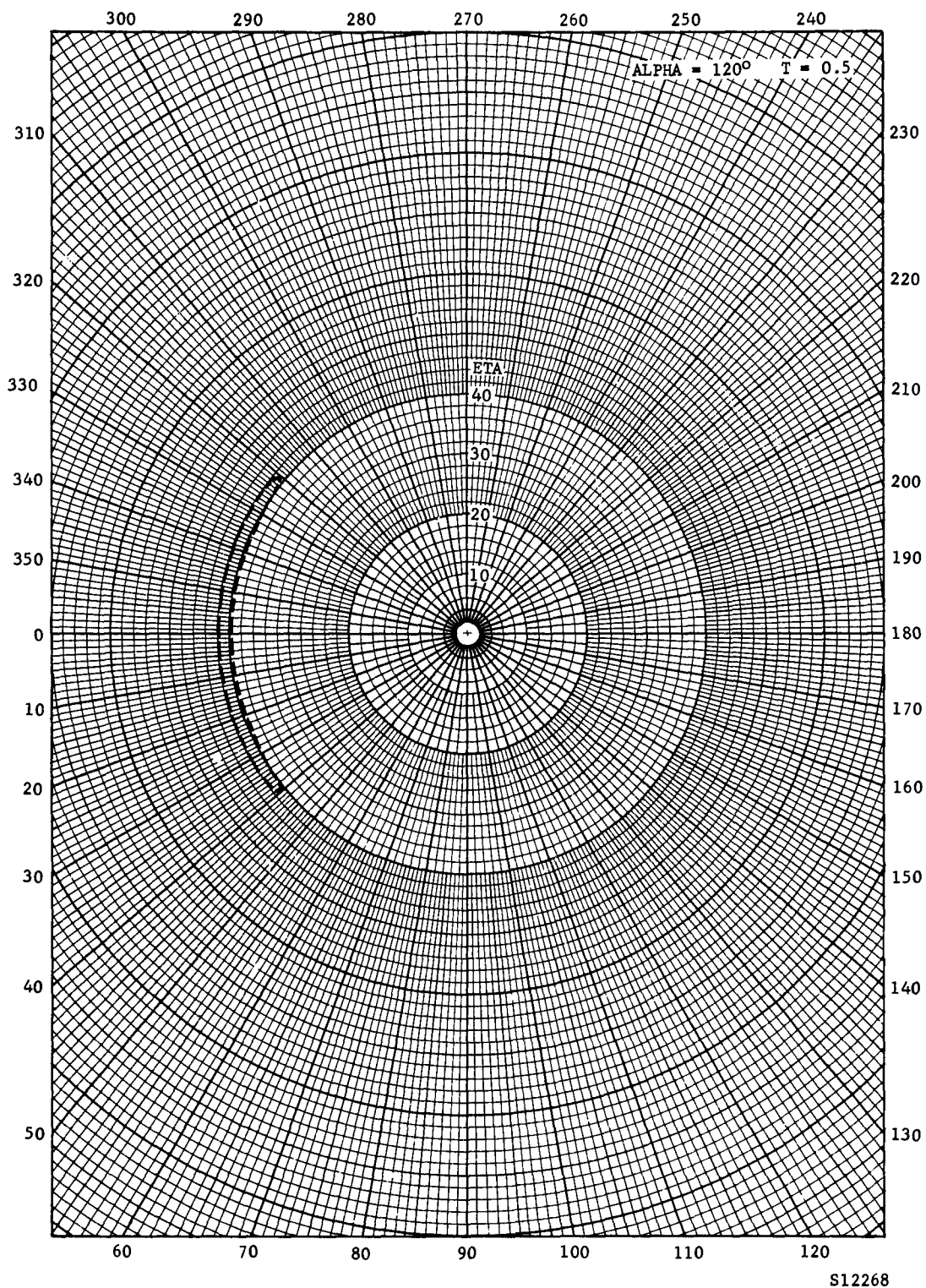
d.  Effect of Inhomogeneities

Apart from the obvious effect of holes in the cloud cover at the tropopause on the isoradiance curves of Fig. 3.4, irregularities and detailed structure in the top of the cloud cover can produce certain changes.  Casual observation from jet airplanes shows that sometimes the cloud cover looks extremely uniform, sometimes it has a very regular structure, and sometimes it is quite irregular, with convective humps above the general level of the surface and with occasional wisps of ice crystals from cirrus.  Of course, by looking from airplanes one cannot give a quantitative measure of the scale of irregularities.  The question arises, how much and in what ways will these phenomena affect the general level of the radiance of the cloud cover?

First of all, the relevant measure of "flatness" of the cloud tops is given in terms of the extinction length

$$\beta^{-1} = N \; \sigma_{abs}$$

For Deirmendjian's distribution of Section 2 (cf. Ref. 2.2, Table 2.1) with N = 100 particles/cc, the extinction distance is of the order of 200 meters.

Consider next regular modulations of the cloud top.  If the cloud top is made us of closely packed circular cylinders of spheres, elementary geometrical considerations show that if the sun local normal angle is less than $60^{\circ}$, the effect of <u>shadowing</u> will be to cut the overall radiance by less than a factor of two.  The effect of <u>modulation</u> clearly depends on the frequency response of the detector system as well as on the precise direction of the scan, but no detailed examination seems called for at this point.

3-24

The effect of large irregularities will clearly be to distort the picture significantly, but any estimate of the magnitude and characteristics of these distortions involves so much detailed input information that once again no further investigation seems appropriate in the present context.

Finally, it is clear that the overall effect of inhomogeneities depends on the resolving power of the detecting system.

APPENDIX 3A

SPECULAR REFLECTION FROM ICE CRYSTALS


At present there exists essentially no experimental information on the actual composition of high altitude clouds , but it seems at least plausible to suppose that they contain a certain fraction of ice crystals. It may well be that the reflection properties of natural clouds of ice crystals do not differ very much from those of clouds of water droplets, but this point is certainly not established. The purpose of this appendix is to outline some characteristic differences between water droplets and ice crystals, mainly to provide a starting point for more detailed future work.

The problems to be mentioned are the composition as far as crystal size under given conditions is concerned, the motion of the crystals with reference to possible alignment effects, and the diffraction pattern produced by crystals of given size.

b. Composition and Structure of Clouds

It is established that the size and crystal structure of ice crystals depends significantly on the conditions under which a cloud is produced.

(1) Current work by B. J. Mason's group at Imperial College, London,[3.11] has established both experimentally and theoretically that cloud droplets of less than 20 $\mu$ radius cannot capture smaller droplets to grow by coalescence. On the other hand, in a supercooled mixture of water droplets and ice crystals, the crystals grow at the expense of the droplets as a result of a vapor pressure gradient.

(2)  Artificial ice fogs produced in winter by seeding the moist air near Old Faithful geyser in Yellowstone National Park[3.12] appear to show an overall angular scattering distribution rather similar to that predicted by Mie theory calculations like Deirmendjian's[3.13] and the present ones (cf. Section 2).  However, there are also some very striking specular effects.

(3)  As against this, certain other measurements on natural ice fogs off the West Coast of Alaska dealt essentially with frozen water droplets[3.14].

(4)  Extensive measurements by Weickmann & Aufm Kampe[3.2] have discovered prismatic single crystals up to several hundred microns in length and with a length-breadth ratio of the order of 1 - 5, and hexagonal plates of the same maximum dimension and perhaps 50 microns thick.

In summary, there does not appear at present to be sufficient experimental evidence to enable us to make any categorical statements about the size and shape of ice crystals.  In particular, there seems to be no justification in favor of using results for low altitude ice fogs to infer the behavior of high altitude cirrus clouds.  Such factors as the absolute humidity, density, temperature and temperature gradient and availability and type of condensation nuclei are simply not understood adequately as far as their detailed effect on cloud composition and structure is concerned.

b.  Motion and Alignment of Ice Crystals

The terminal fall speed of a sphere of radius a and density $\rho$ in a medium of density $\rho_m$ and viscosity $\eta_m$ is

$$v_{term} = (2/9) \, g \, a^2 \, (\rho - \rho_m)/ \eta_m .$$
(A.1)

For air, $\eta_m = 10^{-4}$ gm/cm sec, so that for water droplets of radius $a = 1$, 10, 100 microns the terminal speed $v_{term}$ is respectively $10^{-2}$, 1, $10^2$ cm/sec. In other words, for crystals of dimensions 1 - 500 microns, possible convective flow speeds in clouds, which may go up to $10^3$ cm/sec, are adequate to maintain the particles in suspension.

Ice crystals may be aligned either by non-uniform flow fields such as wind shear (especially for needle-shaped particles), or by aerodynamic forces, which are particularly important for disks and other flattened objects (L/D $>$ 1). The effect of wind shear can readily be shown to be unimportant. In laminar flow, wind shears $\partial u / \partial y$ are of the order .03 (cm/sec)/cm$^{3.15}$, and thus for a crystal of dimensions $10^2 \times 10^2 \times 10$ (in micron), the force $A \eta_m \partial u / \partial y$ is of order $10^{-10}$ dyn, as against the gravitational force mg $\sim 10^{-4}$ dyn. Thus, unless velocity gradients in turbulent flows are $10^4$ - $10^6$ times larger than these observed values, the effect of wind shears will be negligible.

As far as the overal aerodynamic motion of objects of various shapes under the action of viscosity and gravity is concerned, qualitatively this is a very complex "phugoid" motion. Two examples of this are shown in Fig. 3A.1. Whether the motion is damped or autorotating depends on parameters such as the wing loading, Reynold's number, ratio of the moments of inertia, etc. The overall aerodynamic problem is a very difficult one[3.16, 17, 18].

c. Diffraction Pattern

As a measure of the importance of diffraction effects, consider the Fraunhofer diffraction from a circular aperture of radius a. The angle $\theta_1$ of the first zero in the diffraction pattern produced by light of wavelength $\lambda$ is given by the relation

$$\sin \theta_1 = 0.61 \, (\lambda / a). \qquad\qquad (A.2)$$
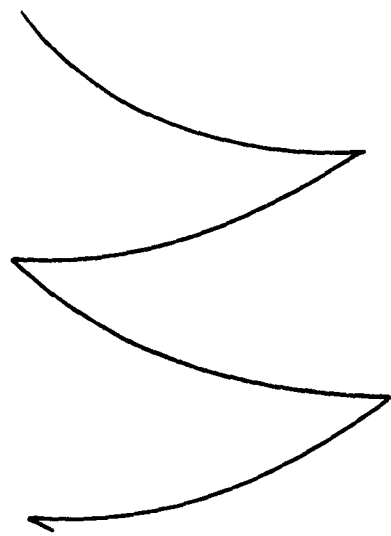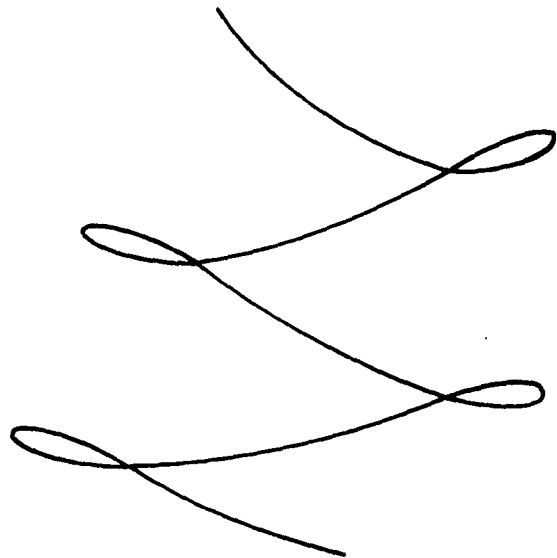
(a)  DAMPED MOTION                    (b)  AUTOROTATING MOTION

S12255

FIGURE 3A.1.  POSSIBLE PHUGOID MOTIONS OF ICE CRYSTALS

Clearly this angle $\theta_1$ gives a measure of the effective width of the diffraction pattern. For $(\lambda/a) \gtrsim 1$, $\theta_1$ is so large that the structure of the scattering object is unimportant: in this situation treating the crystal as a sphere will clearly be a good approximation. On the other hand, diffraction effects are clearly unimportant for $(\lambda/a) \ll 1$, so that the specular reflection will be important in this region. In this geometrical optics case it is necessary to understand the orientation and motion of the crystals, as well as their shape and size, in considerable detail. This sort of information is simply not available at present.

d. The Energy Reflected Specularly from a Cloud of Ice Crystals

Let the flux of solar radiation be $F_o$ watt/cm$^2$ in the relevant frequency range. Under conditions of specular reflection, a fraction

$$q = \frac{\sigma_{scatt}}{\sigma_{scatt} + \sigma_{abs}} \tag{A.3}$$

of this energy goes into a solid angle $\delta\omega$ about the direction of specular reflection, where

$$\delta\omega = \delta\omega_{diffraction} + \delta\omega_{motion} \tag{A.4a}$$

$$\delta\omega_{diffraction} \sim \theta_1^2 \tag{A.4b}$$

$$\delta\omega_{motion} \sim \langle \theta_2^2 \rangle_{av} \tag{A.4c}$$

where $\theta_2$ is the mean change in orientation of the crystal under the action of aerodynamic forces.

For a single crystal of area $A = \pi a^2$, the energy radiated per unit solid angle within a cone $\delta\omega$ about the direction of specular reflection is

$$\left[ \partial W_1 / \partial \Omega \right] = F_o A q / \delta\omega .$$  (A.5)

Now if there are N crystals per cc, the extinction distance is of the order

$$\beta^{-1} \sim (NA)^{-1}$$  (A.6)

Thus for a large cloud the total energy radiated specularly per unit of illuminated surface area and per unit solid angle within a mean solid angle $\delta\omega$ about the direction of specular reflection is

(A.7)

$$H_{spec} = \frac{\left[ \partial W_1 / \partial \Omega \right] \; N \; S_{ill}}{S_{ill}} \sim F_o q / \delta\omega \; (\text{watt/cm}^2 \; \text{sterad}),$$

where $q \sim 0.7$ while $\delta\omega$ is of course not known in general.

The result (A.7) should be compared with the result (2.17) of the Mie scattering analysis

$$H(\theta) = F_o \frac{\sigma_{scatt}}{\sigma_{abs}} \frac{i_{av}(\theta)}{J(0) \; f(i,e)}$$  (2.17)

For scattering angles greater than $60^\circ$ or so, $i_{av}(\theta)/f(i,e) \sim 1$, and thus

$$H(\theta) \sim F_o/300 \quad (\text{watt/cm}^2 \; \text{sterad}) \; \text{for} \; \theta \gtrsim 60^\circ\text{-}90^\circ.$$  (A.8)

It is clear that at least for scattering angles greater than $60^\circ - 90^\circ$, at the appropriate angle the effect of specular reflection will predominate over Mie scattering. The relative magnitude and thus the lower limit to scattering angles for which this is true depends on $\delta\omega$ , but for $\delta\omega \sim 1$, $\theta \gtrsim 60 - 90^\circ$, $H_{spec} \sim 200 \, H(\theta)$.

REFERENCE LIST FOR SECTION 3

3.1   cf. "Handbook of Geophysics for Air Force Designers", Air Force
      Cambridge Research Center, 2nd Edition (1959).

3.2   cf. B. J. Mason, "The Physics of Clouds", Oxford (1957).

3.3   F. H. Ludlam & B. J. Mason, "The Physics of Clouds", Handbuch
      der Physik, 48, Springer, Berlin (1957).

3.4   Landold-Börnstein, "Physikalisch-Chemische Tabellen", 6th Edition,
      Springer, Berlin, 3, p. 586 ff. (1952).

3.5   M. Gutnick (1962), cf. J. N. Howard & J. S. Garing, "The Transmission
      of the Atmosphere in the Infrared - A Review", (February 1962),
      esp. Fig. 6.

3.6   M. Gutnick, "An Estimate of Precipitable Water along High Altitude
      Ray Paths", AFCRC-TN-60-452 (March 1960).

3.7   G. N. Plass, V. R. Stull, P. J. Wyatt, "The Infrared Absorption of
      Water Vapor", Aeronutronic Report U-1717, and "The Infrared
      Absorption of $CO_2$", Aeronutronic Report U-1718, Contract AF 04(695)-96.

3.8   G. N. Plass, "Spectral Band Absorptance for Atmospheric Slant Paths",
      Aeronutronic Report U-1786, Technical Report 3, Contract AF 04(695)-96,
      (August 1962).

3.9   J. B. Zirker, F. L. Whipple, & R. J. Davis, "Time Available for
      Optical Observation of an Earth Satellite, p. 23 ff. in "Scientific
      Uses of Earth Satellites", J. A. van Allen, Editor, University
      of Michigan, Ann Arbor, 2nd Edition (1958).

3.10  cf. F. S. Johnson, "Satellite Environment Handbook", p. 79,
      Stanford (1961).

3.11  cf. A. H. Gordon, "Cloud Physics", Nature, p. 647 (August 18, 1962).

3.12  R. K. McDonald et al, "Infrared Reflection Measurements of Cirrus
      Clouds", Boeing Report D2-20981 (June 30, 1962).

3.13  D. Deirmendjian, "Scattering and Polarization of Polydispersed
      Suspensions with Partial Absorption", Rand Corporation, RM-3228-PR
      (June 1962).

REFERENCE LIST FOR SECTION 3 (continued)

3.14  R. D. Cadle, Stanford Research Institute, private communication.

3.15  cf. "Handbook of Geophysics for Air Force Designers", AFCRL, second edition, pp. 5-40 and 5-77 (1959).

3.16  T. von Karman & M. Biot, "Mathematical Methods in Engineering", p. 146 ff, McGraw-Hill (1940).

3.17  P. Dupleich, Rotation in Free Fall of Rectangular Wings of Elongated Shape", NACA TM-1201 (April 1949).

3.18  A. M. O. Smith, "On the Motion of a Tumbling Body", I.A.S. Journal 20, 73 (1953).

SECTION 4

DETECTION AND DECISION SYSTEMS FOR NON-GAUSSIAN BACKGROUNDS

## 4.1  INTRODUCTION

A central question encountered in the design of IR surveillance detection and decision systems is the discrimination between a target and a severe background.  There are really two related problems, namely:

(1)  How to find the optimum detection system.

(2)  How to best describe the background and target radiances.

For our purposes discrimination between a target and a severe background means that the detection system will be required to decide whether a particular alarm signal received is due to a target or a back-ground condition, that is, the system must be able to distinguish between targets and severe backgrounds occurring separately rather than simul-taneously.  The occurrence of a target together with a severe background will be a very rare event (and therefore relatively unimportant) since each individual event in itself is rare.  It is the events which produce false target indications which cause the main difficulty in IR surveillance.

For example, consider an infrared detection system operating from an Earth satellite whose purpose is to detect a missile launch from plume radiation.  If it is accepted that there exist occasional severe backgrounds due to high-altitude, infrared-reflecting clouds, then the

next question is how to make a detection system work despite the severe background. Numerous discrimination schemes have been suggested which take advantage of background and target signal characteristic differences. Each scheme may be examined in terms of the background model(s) which may be developed to decide which appear most promising. Statistical methods are generally involved, and such methods will be used for selection of background descriptions and comparison of various alternate detection systems.

An optimum detection system is defined for our purposes as one which is capable of extracting a target signal from a background and of deciding for or against alarm activation with a minimum of incurred errors or "cost." There are two kinds of possible errors which may be made in deciding for or against an alarm with associated probabilities of error. These are:

(1) Mistaking a target for a cloud.

(2) Mistaking a cloud for a target.

The second type of error becomes serious if the cloud radiance probability density distribution overlaps the target radiance distribution and if the threshold for alarm decision is determined so that a warning will be sounded for the majority of possible target radiances. False alarm then becomes a nuisance, and it is imperative that the detection system be designed with an optimum capability for discrimination against background radiances in the high radiance tail of the probability density distribution.

A general criterion for system performance based upon statistical decision theory is formulated in Section 4.2. This provides a fundamental basis for examining various discrimination schemes. The general approach has been to minimize the expected costs for the various possible detection outcomes. This approach, however, requires a knowledge of the a priori probability of target presence and the assignment of costs to the possible detection outcomes.*

---

*See Section 4.2 b for specification of the four possible detection outcomes.

4-2

It is shown in Section 4.2 that the Neyman-Pearson criterion[4] of minimizing the conditional probability of target miss for a given conditional probability of false alarm represents a partial minimization of the expected cost. The virtue of this criterion is that it does not require a knowledge of a priori probabilities and costs. Furthermore, in most of the situations encountered in the present study, this criterion reduces to the single signal threshold criterion for deciding for or against target presence.

In Section 4.3 the properties of probability density functions representing the background radiance patterns under the various imposed conditions (sun angle, elevation angle of azimuthal scan, etc.) are investigated and typical non-Gaussian models are presented. Finally, since the physical model developed permits only the derivation of probability density functions for background radiance and not for the signal input to the decision device, the conditions under which these two probability density functions are identical are examined, and possible approximate methods for transforming the radiance probability density function to signal density function are considered.

It may not be possible to discover the optimum detection system design. In fact, one would probably be content with a system which works despite severe background without too much regard for whether the system is optimum or not. A variety of design approaches are possible if optimization is not required but, instead, simply a workable system.

A performance criterion developed in Section 4.2 e is applied in Sections 4.4 and 4.5 to the cases of the single sensor and the multiple sensor with correlation of output signals. The criterion permits the comparison of the relative performance of these two types of systems. The result of the comparison indicates that correlation can enhance system performance considerably if sunlit clouds are indeed several times larger than the target.

4-3

In Section 4.6, the optimum linear filter is considered. In this connection, the best representation of background information has become controversial. As Robinson[1] has pointed out, many of the possible representations of background radiance information do not retain enough of the background information to permit the design of an optimum detection system. The problem of representing the background adequately becomes more severe when sophisticated discrimination methods are considered. Some of the possible representations of background which may often be found inadequate are:

(1) One dimensional Wiener transform and autocorrelation function.
(2) Two dimensional Wiener transform and autocorrelation function.[2]
(3) Radiance probability density function.
(4) Radiance joint probability density function.[3]
(5) Rough radiance maps using limited gray scale.

The problem with the use of the first two descriptions which Robinson[1] has pointed out, arises because of two factors. First, the background probability density function is generally non-Gaussian. In this case the methods applied to the selection of an optimum linear signal processing do not permit the selection of the best possible processing which may actually be a non-linear filter rather than linear. Secondly, the requirement of decision for or against alarm of the basis of signal level relative to a threshold introduces an inherent non-linearity in the system. Any design approach which does not account for the non-Gaussian nature of the background and the non-linearity of the decision processes cannot be expected to succeed.

It is clear that it is not essential to retain all background information for design purposes, since, depending upon the detection and discrimination method selected, much information will be irrelevant to system performance. A complete background description would consist of

an enormous quantity of high resolution, large radiance-ranges, radiance maps with geographical location, time (including season and sun angle), weather conditions, detector position, wavelength region, and other conditions assigned to each map. Fortunately, the complete description will probably never be required for the design of any particular system. The problem is, then, reduced to one of selecting the appropriate background description for the design of a detection system employing the selected discrimination method.

The comparison criterion developed and applied in the later sections specifies the best way to express the background in the appropriate form with regard to the particular discrimination method which it is desired to use. Thus, the problem of the appropriate form of the background representation disappears. However, the great practical difficulty of obtaining the numerical values for parameters appearing in the background expression still remains. The solution to this particular problem lies in improving methods of data gathering, processing, and reduction and in performing additional background measurements of sufficient extent.

## 4.2  PERFORMANCE CRITERIA

Various performance criteria will be discussed and compared in this section. The general approach to the design of optimum detection systems has been to formulate the expected cost in terms of the decision outcomes. This approach is one suggested by statistical decision theory.[6,7] The criterion for this general approach is that the best system is one which minimizes the expected cost of the system outcomes. Here cost is used in a very broad sense of damage or hurt of any sort incurred. However, the practical feasibility of this decision theory approach is limited by the knowledge of certain doubtfully obtainable a priori probabilities and by the necessity of assigning cost values to particular detection system outcomes. We will see that a partial minimization of costs

is possible even though the numerical values of the a priori probabilities and costs of system outcomes are not known. This partial minimization is adopted in the subsequent applications.

The minimization problem is outlined as follows: A sample function is observed over a finite time interval. This sample function consists of background signal having known statistics and may or may not contain a target signal. The observed sample function is suitably pro-cessed and then a decision is made as to whether a target signal is present or not. For each of the four possible combinations* of target signal presence and decision a cost is assigned. The system is then optimized by finding the decision rule which leads to a minimum value of the expected cost.

a. Probability Density Functions

It is convenient to formulate the detection problem on a discrete basis. The background is described by a set of numbers which give the radiance in each resolution cell of a finite area. Since these numbers are obtained by sampling the outputs of sensors, they also include all of the noise components arising from the background signal and the system. A convenient method of representing these background samples is a row matrix of n elements, where n is the number of resolution cells in the area being considered. The components of this matrix may be assigned in any known manner to the resolution cells. It is assumed that the time sequence in which the cells are observed precludes the possibility of a particular moving target appearing in more than one cell. Let the back-ground matrix be designated as

$$\bar{B} = \left\{ b_1, \ b_2, \ \cdots \cdots, \ b_n \right\} \qquad (4.1)$$

---

*See Section 4.2 b

The background has associated with it a probability density function designated as $w_o(\overline{B})$ and normalized such that

$$\int w_o(\overline{B}) \ d\overline{B} = 1 \qquad (4.2)$$

The function $w_o(\overline{B})$ represents the probability that the background signal will be found between $\overline{B}$ and $\overline{B} + d\overline{B}$ when it is multiplied by $d\overline{B}$.

The target, or targets, may also be described by a matrix, most of whose elements are zero. It is assumed that each target is sufficiently small, so that it can occupy only one resolution cell. This matrix is designated as

$$\overline{T} = \left\{ t_1, \ t_2, \ \ldots \ldots, \ t_n \right\} \qquad (4.3)$$

It is also necessary to assign a probability of target presence and a density function for target amplitude when a target is present. Hence, let $P_o$ be the a priori probability that no target is present, and $P_1$ be the a priori probability that one or more targets are present. As will be seen later, it is often difficult to say precisely what these probabilities are. Since these probabilities are mutually exclusive

$$P_1 + P_o = 1 \qquad (4.4)$$

The probability density function for target amplitude is designated as $w_1(\overline{T})$ and normalized so that

$$\int w_1(\overline{T}) \ d\overline{T} = 1 \qquad (4.5)$$

Thus, the a priori probability density function associated with the target matrix is

$$p(\overline{T}) = P_o \ \delta(\overline{T}-0) + P_1 \ w_1 \ (\overline{T}) \qquad (4.6)$$

where

$$\delta(\bar{T}-0) = \begin{cases} 1 \text{ for } \bar{T} = 0 \\ \\ 0 \text{ for } \bar{T} \neq 0 \end{cases} \tag{4.7}$$

The observed resultant signal is in general some combination of the background signal and the target signal. The background and target signals are assumed to be statistically independent.[*] For most systems the target and background signals are combined by simple addition, but it is not necessary to make this assumption for the general derivation being considered.[**]

Let the observed resultant signal be designated by a row matrix also, so that

$$\bar{S} = \left\{ s_1, \ s_2, \ \ldots, \ s_n \right\} \tag{4.8}$$

--------

[*]There are conceivable conditions where background and target signals are not statistically independent. For example, launching might be difficult under weather conditions that produce high backgrounds.

[**]If the target is a true point source, the assumption of additivity is exact. Any real target will, however, obscure a portion of the background. Thus, a substitutive rule will be used in a later section since the target image for systems of interest will be on the order of a resolution element in size. This approximation also permits a simplification in the mathematics.

Associated with this matrix are two conditional probability density functions, $p \, (\bar{S} \, | \bar{T} \neq 0)$ and $p \, (\bar{S} \, | \bar{T} = 0)$. The first probability density function is the probability that if a target signal is present and has a particular value $\bar{T}$ then the background signal will be such as to give a resultant signal which lies between $\bar{S}$ and $\bar{S} + d\bar{S}$. The second probability density function, namely $p \, (\bar{S} \, | \bar{T} = 0)$, is the probability that if a target signal is absent then the resultant signal lies between $\bar{S}$ and $\bar{S} + d\bar{S}$. This latter density function is identical with the probability density function of the background, $w_o(\bar{S})$.

Although the probability density functions introduced in the preceding paragraph appear simple at first sight, they contain a wealth of information from the 2n random variables of background and target. The practical description of the background in terms of such probabilities may not be possible at all as will be seen in Section 4.3 where this subject is again taken up. Despite the complexity of these conditional probability density functions, they enable the definition of various kinds of averages which are practical to use. Also, restriction of the number of variables permits the practical applications of these functions. In any case, this framework, while complicated, is necessary to describe the problem carefully and does yield suitable quantities for practical use.

b. Decision Rules and Cost Functions

The decision operation, which decides for or against alarm activation, is designated by $\delta\,(\bar{S},\, \Omega\,)$. The matrix $\bar{S}$ is the measurement space and $\Omega$ is some selected subset. For a single threshold decision, the specification of $\Omega$ divides the measurement space into two regions. All $\bar{S}$ not contained in $\Omega$ lead to a decision of no target present, and $\bar{S}$ lying within $\Omega$ lead to a decision that a target signal is present. Thus

$$\delta(\bar{S},\, \Omega\,) = \begin{cases} 1 \text{ for } S \subset \Omega \\[1em] 0 \text{ for } S \cap \Omega = 0 \end{cases} \tag{4.9}$$

4-9

The sub-space over which we have elected to decide for target presence may be found by integration of $\delta(\bar{S}, \Omega)$ over all $\bar{S}$. Similarly, the sub-space over which we decide for target absence is the integral of $\{1 - \delta(\bar{S},\Omega)\}$ over all $\bar{S}$.

Finally, it is necessary to assign evaluation or cost and gain functions to the four possible outcomes which are the result of time, target condition and the applied decision rule. The possible outcomes and their associated cost functions $C(\bar{T}, \delta)$ are:

Decision for target absent when target is absent.

$$C(\bar{T} = 0, \quad \delta = 0) = C_o$$

Decision for target present when target is actually absent.

$$C(\bar{T} = 0, \quad \delta = 1) = C_f$$

Decision for target absent when target is actually present

$$C(\bar{T} \neq 0, \quad \delta = 0) = C_m$$

Decision for target present when it is present.

$$C(\bar{T} \neq 0, \quad \delta = 1) = C_d$$

(4.10)

The costs associated with the correct decisions are $C_o$ and $C_d$, where $C_o$ is the cost of deciding target absence correctly and $C_d$ is the cost of deciding for target presence correctly. It will be seen that these particular costs are actually gains and so will be negative numbers or zero. The costs associated with incorrect decisions are positive costs and are $C_f$ and $C_m$, costs of false alarm and of target miss, respectively. The costs $C_f$ and $C_m$ will usually be assigned large values relative to the magnitudes of $C_d$ and $C_o$.

4-10

Since the occurrence of various cost values is random, it is appropriate to find the expected value of the cost, $E \langle C(\bar{T}, \delta) \rangle$ .

$$\bar{C} = E \langle C(T, \delta) \rangle = E \langle C_o \rangle + E \langle C_f \rangle + E \langle C_m \rangle + E \langle C_d \rangle \quad (4.11)$$

It is readily seen that

$$E \langle C_o \rangle = C_o P_1 \int p(\bar{s} \mid \bar{T} = 0) \left\{ 1 - \delta(\bar{s}, \Omega) \right\} d\bar{s} \quad (4.12)$$

$$E \langle C_f \rangle = C_f P_o \int p(\bar{s} \mid \bar{T} = 0) \delta(\bar{s}, \Omega) d\bar{s} \quad (4.13)$$

$$E \langle C_m \rangle = C_m P_1 \int p(\bar{s} \mid \bar{T} \neq 0) \left\{ 1 - \delta(\bar{s}, \Omega) \right\} d\bar{s} \quad (4.14)$$

$$E \langle C_d \rangle = C_d P_1 \int p(\bar{s} \mid \bar{T} \neq 0) \delta(\bar{s}, \Omega) d\bar{s} \quad (4.15)$$

from which

$$\bar{C} = P_1 C_m + P_o C_o + \int \delta(\bar{s}, \Omega) \left\{ P_o p(\bar{s} \mid \bar{T} = 0)(C_f - C_o) \right. \quad (4.16)$$

$$\left. + P_1 p(\bar{s} \mid \bar{T} \neq 0)(C_d - C_m) \right\} d\bar{s}$$

In deriving Eq. (4.16) the normalizing relationships

$$\int p(\bar{s} \mid \bar{T} = 0) d\bar{s} = 1 \quad (4.17)$$

and

$$\int p(\bar{s} \mid \bar{T} = 0) d\bar{s} = 1 \quad (4.18)$$

have been used. The expected cost may also be written in terms of the conditional probability of false alarm, $P_f$. and the conditional probability of detection, $P_d$, defined respectively by

$$P_f = \int \delta(\bar{s}, \Omega) p(\bar{s} \mid \bar{T} = 0) d\bar{s} \quad (4.19)$$

and

$$P_d = \int \delta(\bar{s}, \Omega) \; p \, (\bar{s} \,|\, \bar{T} \neq 0) \; d\bar{s} \qquad (4.20)$$

In terms of $P_f$ and $P_d$ the expected cost is

$$\bar{C} = P_1 \, C_m + P_o \, C_o + P_o \, P_f \, (C_f - C_o) + P_1 \, P_d \, (C_d - C_m) \qquad (4.21)$$

The general design criterion may now be stated. The optimum system will be that system whose parameters produce a minimum for the expected cost. In other words, the decision rule $\delta(\bar{s}, \Omega)$ must be chosen so as to minimize the expected cost. The appropriate decision rule is that $\delta(\bar{s}, \Omega)$ zero when the integrand of Eq. (4.16) is positive and unity when the integrand is negative, that is

$$\delta(\bar{s}, \Omega) = \begin{cases} 0 \text{ when } \wedge \leqslant \dfrac{C_f - C_o}{C_m - C_d} \cdot \dfrac{P_o}{P_1} \\[4mm] 1 \text{ when } \wedge > \dfrac{C_f - C_o}{C_m - C_d} \cdot \dfrac{P_o}{P_1} \end{cases} \qquad (4.22)$$

where the likelihood ratio , is defined as

$$\wedge = \frac{p(\bar{s} \,|\, \bar{T} \neq 0)}{p(\bar{s} \,|\, \bar{T} = 0)} \qquad (4.23)$$

The actual application of Eqs. (4.22) and (4.23) clearly depends upon having some data with respect to cost values and a priori probabilities. Thus, this result has somewhat limited practical scope. One way to get around this is to use a partial minimization of the expected cost Eq. (4.21). This leads naturally to the Neyman-Pearson criterion if we minimize the last term on the right of Eq. (4.21) as we shall see.

4-12

According to the Neyman-Pearson criterion,[4] a decision for target presence is made when the ratio $\Lambda$ defined by Eq. (4.23) exceeds some particular value, say K, for the observed $\bar{S}$. When for some $\bar{S}$, $\Lambda$ falls below K, then a decision for target absence is made. The value of K is selected to give a preassigned false alarm rate. This amounts to a specification of $C_f$. For the Neyman-Pearson decision rule, the decision operator is then

$$\delta_{NP} \, (\bar{S}, \Omega \,) = \begin{cases} 1 \text{ when } \Lambda > K \\ \\ 0 \text{ when } \Lambda \leqslant K \end{cases} \qquad (4.24)$$

A unique decision operator is not specified since K may have any desired value.

It is of interest to compare Eqs. (4.22) and (4.23) with the Neyman-Pearson criterion for selecting the decision rule. In the previous case a definite value of $\Lambda$ is specified when the costs and a priori probabilities are known. Under the Neyman-Pearson criterion, however, the threshold is arbitrary.

The following argument indicates that the Neyman-Pearson criterion is a first step towards minimizing the expected cost. If the expected cost is expressed as in Eq. (4.21), a possible approach to minimizing the cost would be to optimize one of the four terms on the right side while holding the other three constant. The only control permitted is over the terms involving $P_f$ and $P_d$. Under the Neyman-Pearson criterion, the choice of K fixes the value of $P_f$. Since $(C_d - C_m)$ is always a negative quantity, a partially optimum system will be that for which $P_d$ is a maximum so that the cost is minimized. This procedure corresponds precisely to the Neyman-Pearson criterion.

The great virtue of the Neyman-Pearson criterion lies in the fact that it enables some control over the cost without requiring a specification of the costs or a priori probabilities. This advantage is to some extent illusory, however, since it is not possible using this criterion to know what the actual cost is. Furthermore, since costs are not evaluated, the actual gain achieved by using the optimum system rather than some compromise system cannot be determined.

c. Single Threshold Criterion

Another decision criterion often used is the single signal threshold rule. Under this rule a decision for target presence is made when $\bar{S}$ exceeds some threshold value, say $\bar{S}_\theta$. The decision operator in this case is

$$\delta(\bar{s}, \Omega) = \begin{cases} 1 \text{ when } \bar{S} > \bar{S}_\theta \\[2em] 0 \text{ when } \bar{S} \leqslant \bar{S}_\theta \end{cases} \tag{4.25}$$

This criterion is the same as the Neyman-Pearson criterion when $\bigwedge$ is a monotonic function of $\bar{S}$ in which case the Neyman-Pearson condition separates the signal space into just two regions. However, if for a given value of $\bigwedge$ there correspond several values of $\bar{S}$, then no single signal threshold can satisfy the Neyman-Pearson minimization.

An example will be discussed to demonstrate the relation between the Neyman-Pearson condition and the single threshold condition. Suppose that the background probability density function, $w_0(\bar{B})$ is bimodal with most clouds providing radiance less than the target radiance and a very few clouds producing radiances much in excess of the target radiance values. Note that these latter radiances correspond to small values of the probability density function. The Neyman-Pearson condition will require two signal thresholds: one which separates the low cloud radiances from the

4-14

range of target radiances and a second one which separates the high cloud radiances from the target range.  In this manner both low and excessively high cloud signals will be excluded from the $\Omega$ subspace.  However, the region of high radiances which is excluded by the upper signal threshold will not affect system performance significantly provided  the probability of occurrence of such clouds is very small, i.e., their contribution to $\int p \; (\bar{S} \,|\, \bar{T} = 0) \; d\bar{S}$ is small.  For all practical purposes, then, a single signal threshold would suffice.  This is expected to be the case for missile-launch detection systems.  Thus, the establishment of a single signal threshold for practical systems is equivalent to design according to the Neyman-Pearson criterion provided that the target and cloud distributions are well separated and most backgrounds are in one region of the signal space.

Other decision criteria are possible such as for systems using correlation.  For example, a decision for target presence might be made only when the threshold for a single detector is exceeded and the signals from adjacent detectors remain below the signal threshold.  In this way discrimination against large reflecting clouds can be achieved.

If the detection system is equipped with data storage capability, the possibility of reserving a decision until more data is accumulated is permitted.[*]

d. A Priori Probabilities and Costs

As already mentioned, the Neyman-Pearson approach is the only approach which is reasonably general yet independent of a priori probabilities and cost assignments.  In order to use the more general minimum cost criterion of Eq. (4.22) these probabilities and costs must be known or estimated.  It might prove instructive to examine what is involved in estimating these quantities.

---

[*]In this case, Wald's sequential criterion might be useful.[5]

Since the probability of any enemy ICBM attack varies from day to day as the international situation changes, the estimates of $P_1$ must be updated since $P_1$ is the a priori probability of target presence in the interval $t_0$ and $t_0 + dt$. Other conditions which are usually steady relative to the height of internal tension feed into the estimates of $P_1$ such as the number of enemy missiles on launch pads and their probable targets. Various governmental, military, and intelligence agencies make estimates of the probability of an enemy attack from which it might be possible to derive the probability of target presence in the field of view of the detection system, $P_1$. Since much subjectivity goes into these estimates, their reliability may be poor. So far no test cases have occurred to verify the estimates, although past experience and the absence of an attack indicate that $P_1$ is usually considerably smaller than unity. In view of the questionable reliability of estimates of $P_1$, any design criterion which is independent of a knowledge of $P_1$ is favored.

The cost functions of Eq. (4.10) are even more difficult to estimate. In any discussion of costs of errors of a surveillance system, complicated interactions of the surveillance system with other parts of the defense system have to be considered which causes difficulty in such a general discussion unless the rules of the defense game are known. What is the cost of a detection miss for one single element in an extensive surveillance system consisting of warning radars as well as satellite infrared systems? Perhaps the cost is that of not having the advantage of an earliest possible warning. Thus, it might be inversely proportional to the extent of build-up of the retaliatory forces actually achieved at the moment the attacking warheads reach their targets. Or perhaps it is a function of the warning time actually achieved by the overall system so that the cost of a miss depends upon the functioning of the rest of the surveillance system.

What is the cost of a false alarm? Does it amount to the cost
of scrambling SAC and initiating the procedure for additional retaliation?
Does it also depend upon the lack of credibility in the warning provided
by the rest of the surveillance system?

One might be permitted to say that

$$c_m > c_f$$

if the assumption that retaliation is not actually ordered until one or
more enemy hits have been experienced is allowed. In this case, a false
alarm will initiate an alert and also will be checked out by future experi-
ence, but a miss may mean the loss of the advantage of an alert and possibly
of some of the retaliatory forces as well.

So far the decision criteria for an optimum system and for other
systems have been discussed. The assumption which is made is that the
system which uses the minimum cost decision rule would be the optimum system.
Since it is difficult, if not impossible, to know $P_1$ and the costs, it
will not always be possible to discover the optimum detection system by
applying the optimum decision rule design criterion. In fact, one would
probably be satisfied with the best workable system of several possible
choices. What is needed, then, is some measure of individual system per-
formance which may be used to compare different systems and which will
permit, in practice, the selection of the best system. Such a performance
measure should be derivable from the Neyman-Pearson criterion or the
essentially equivalent single signal threshold criterion. One usable
performance criterion is discussed in the following section.

In summary of the previous subsections, a general performance
criteria has been derived in the form of a decision rule which minimizes
the expected cost. This criterion is shown to be of limited usefulness
since it is required to know the a priori probability of a target occurrence

4-17

and cost functions assigned to the various outcomes. The Neyman-Pearson criterion is shown to be free of these limitations and yet to retain much of the rigor of the more general criterion. Finally, it is argued that in most cases the Neyman-Pearson criterion corresponds to the simple decision criterion of setting a single signal threshold.

e. A Usuable Comparison Criterion

It is desired to develop an analytical measure of detection system performance which may be used to compare different systems. The various systems will differ in their decision rules since the decision rule used reflects the type of discrimination scheme of a particular system.

Methods for achieving background discrimination are briefly:

(1) Spatial discrimination by using small instantaneous fields of view. Thus, if the resolution element (an individual detector of an array) is on the order of the target size, the field of extensive backgrounds is reduced. This method has been considered in the single scanning detector.

(2) Spatial discrimination by using inherent background patterns and correlations. The fact that the spatial frequencies of cloud radiance differ from that of the target (essentially a point source) might be utilized for discrimination. Also, correlations due to regularities in cloud size and distribution may permit discrimination. An example has been considered for clouds several resolution elements wide in which signals from adjacent elements are compared and no alarm is sounded if both signals exceed the threshold.

(3) Spectral discrimination by choosing the most appropriate spectral region. It appears that the 4.3 micron band offers no great advantage over the 2.7 micron region, however.

(4) Spectral discrimination by examining spectral line shapes or by comparing fluctuations in two or more different spectral regions.

(5) Temporal discrimination by determining the time history of a potential alarm radiance. Target motion or self modulation may reveal its true identity.

(6) Discrimination accomplished by limiting the chances of observing a severe background. Thus, a reduction in coverage say by limiting the scan to large angles relative to the sun position to reduce seeing bad forward scattering or limiting the scan to regions near and above the horizon to take advantage of transmissivity losses might be useful.

(7) Polarization discrimination by recognizing that radiation reflected from clouds may be polarized differently than target emission.

A particular system may perform measurements upon both target and background signals. In general, a system may be required to:

(1) Detect the presence of a completely known signal in the presence of background noise.

(2) Detect the presence of an incompletely known signal.

(3) Detect an incompletely known signal and measure its unknown characteristics.

As a result, the decision rule may become an involved function of various system operations.

The gain functions associated with the correct decisions ($C_d$ and $C_o$) will be neglected and the system which produces fewest errors of target miss variety for a given rate of false alarm error will be considered the best

4-19

system, which is in accordance with the Neyman-Pearson criterion. It is assumed that a tolerable false alarm rate, represented by $P_f$, may be assigned. For comparison purposes, systems will be examined when their false alarm rates are identical. Then the system with the smallest conditional probability of miss is the correct choice. Since

$$P_m = \int p(\bar{S} \mid \bar{T} \neq 0 \left\{ 1 - \delta(\bar{S}, \Omega) \right\} \, d\bar{S} = 1 - P_d \qquad (4.26)$$

this is the same decision rule for the best system as selecting the system with the largest $P_d$ from all systems having equal $P_f$.

The particular system which is best for one value of $P_f$ may not be the best at all other values of $P_f$. Thus, curves of $P_d$ versus $P_f$ for various systems may cross at some point, and the order of best performance may become inverted.

It is necessary at this point to consider how the $s_n$ signals from the n sensors are combined to yield the total signal $\bar{S}$. The decision operator will be determined by this operation. For example, all $s_n$ signals might be summed and then passed through a signal threshold device, or each s could be individually passed through a threshold device before combination. Various relationships between the individual $s_n$ signals might be required as a condition for decision making. One such relationship could be a statistical correlation and certain restrictions upon the degree of correlation could make up a decision rule. The procedure whereby the $s_n$ signals are processed to give the resultant $\bar{S}$ which is involved in the decision operator will be critical and will be the feature of the various systems which may be examined.

The decision operator must be modified to permit the inclusion of the procedure for combining the $s_n$ signals which, in turn, depends upon the discrimination scheme. Call this decision operator $\delta(\bar{S}(s_i), \Omega)$.

Certain simplifications may be possible in the expansions of the conditional probabilities $p(\bar{S} \mid \bar{T} = 0)$ and $p(\bar{S} \mid \bar{T} \neq 0)$ appearing in the general equations for $P_f$ and $P_d$ (Eqs. (4.19) and (4.20)). For example, false alarms result only when an alarm is given but no target is present. However, a target may be present in the $i^{th}$ signal and be missed, yet an alarm signal sounded due to some other $s_j$ satisfying the alarm condition even though $s_j$ contains no target signal. This fortuitous alarm will be an extremely rare event since it requires both that a target be missed, which for most systems is very unlikely, together with a false alarm event, which is also rare. Thus terms in $p(\bar{S} \mid \bar{T} = 0)$ of the sort $p(s_i \notin \Omega_i, \; s_j \subset \Omega_j \mid t_i \neq 0, \; t_j = 0)$ may be neglected. Here $\Omega_i$ is the subspace of all $s_i$ for which a decision for target presence is made.

An alarm should be given when one or more targets appear. Because of the spacing of missile launches in both time and space, it is unlikely that more than one target will be detected at any one instant although the probability does increase as the spatial separation of the $i^{th}$ and $j^{th}$ sensors becomes larger. It is probably quite unlikely that two missiles will be launched simultaneously side by side so that target signals appear in adjacent sensor signals. Thus, terms in the expansion of $p(\bar{S} \mid \bar{T} \neq 0)$ of the sort $p(s_i \subset \Omega_i, \; s_{i+1} \subset \Omega_{i+1} \mid t_i \neq 0, \; t_{i+1} \neq 0)$ may be neglected.

The decision rule will determine the detailed form of Eqs. (4.19) and (4.20). For example, suppose a system of two sensors, $s_1$ and $s_2$ and a decision rule

$$\delta(\bar{s}, \Omega) = \begin{cases} 1 \text{ when } s_1 > s_\theta \\ 1 \text{ when } s_2 > s_\theta \\ 0 \text{ when } s_1 \leq s_\theta; \; s_2 \leq s_\theta \end{cases} \tag{4.27}$$

4-21

Then

$$
\left\{
\begin{array}{l}
\overline{S} = \left\{ s_1, s_2 \right\} \\[2ex]
\overline{T} = \left\{ t_1, t_2 \right\}
\end{array}
\right.
\tag{4.28}
$$

and $\overline{T} = 0$ means $t_1 = 0$ and $t_2 = 0$. No assumption about the correlation between $s_1$ and $s_2$ need be made since the result may be written for the general case. Then $P_f$ is

$$
\begin{aligned}
P_f &= \iint p(s_1, s_2 \mid t_1 = 0, t_2 = 0) \quad \delta(s_1, s_2; s_\theta) \, ds_1 \, ds_2 \\[2ex]
&= \int_{s_\theta}^{\infty} \int_{s_\theta}^{\infty} p(s_1 \mid t_1 = 0) \quad p(s_2 \mid t_2 = 0, s_1) \, ds_1 \, ds_2
\end{aligned}
\tag{4.29}
$$

Similarly we can find the detailed expression for $P_d$. $\overline{T} \neq 0$ means that $(t_1 \neq 0, t_2 = 0)$; $(t_1 = 0, t_2 \neq 0)$, or $(t_1 \neq 0, t_2 \neq 0)$.

Thus, $P_d$ becomes

$$
\begin{aligned}
P_d = \iint \Big\{ &p(s_1, s_2) \mid t_1 \neq 0, t_2 = 0) + \\[2ex]
&p(s_1, s_2 \mid t_1 = 0, t_2 \neq 0) + \\[2ex]
&p(s_1, s_2 \mid t_1 \neq 0, t_2 \neq 0) \Big\} \, \delta(s_1, s_2; s_\theta) \, ds_1 \, ds_2
\end{aligned}
\tag{4.30}
$$

where

$$
\begin{aligned}
p(s_i, s_j \mid t_i \neq 0, t_j = 0) &= \\[1ex]
p(s_i \mid t_i \neq 0) \, p(s_j \mid t_i \neq 0, t_j = 0, s_i)
\end{aligned}
\tag{4.31}
$$

and

$$
\begin{aligned}
p(s_i, s_j \mid t_i \neq 0, t_j \neq 0) &= \\[1ex]
p(s_i \mid t_i \neq 0) \, p(s_j \mid t_i \neq 0, t_j \neq 0, s_i)
\end{aligned}
\tag{4.32}
$$

4-22

Eqs. (4.29) and (4.30) above take into account correlations between background signals, $b_1$ and $b_2$, and correlations such as the probability of a double target ($t_i \neq 0$, $t_j \neq 0$).

Finally, it is necessary to specify how $b_i$ and $t_i$ components add to yield the resultant $s_i$. If

$$s_i = b_i + t_i \tag{4.33}$$

and

$$p(s_i/t_i = 0) = w_o (s_i) \tag{4.34}$$

then

$$p(s_i/t_i \neq 0) = \int w_o (b_i) w_1 (s_i - b_i) db_i$$
$$\tag{4.35}$$
$$= \int w_i (t_i) w_o (s_i - t_i) dt_i$$

Under certain conditions, the convolution integrals above may be simplified by approximation if some of the properties of $w_o(b_i)$ and $w_1 (t_i)$ are known. For example, if the probability density function of background radiances is less than some small fraction of the comparable missile radiance densities, then a good approximation is

$$\int w_o (s_i) w_1 (s_i - b_i) db_i \cong w_1 (s_i). \tag{4.36}$$

It is permissible to use this approximation for most of the background distributions considered here. Note finally that the background must be represented as an n-dimensional joint probability density function given by Eq. (4.37)

$$w_o (\overline{B}) = p (b_1) p (b_2 | b_1) p (b_3 | b_1, b_2) p (b_n | b_1, b_2 \ldots, b_{n-1})$$

It is seen, then, that the approach used here determines how the background is to be described. Unfortunately, for correlated backgrounds with n any

larger than 2 or perhaps 3 or 4, the practical measurement and determination of such joint probability density functions becomes well nigh impossible. The following section considers this problem in more detail and typical probability density functions for non-Gaussian distributions are presented.

## 4.3 PROBABILITY DENSITY FUNCTIONS

### a. Properties of Correlated Joint Density Functions

In Section 4.2 a the nomenclature for n-dimensional probability density functions was introduced for background signals, target signals, and resultant signals. It is probably not possible to obtain these complete joint density functions for n any larger than 3 or 4. If the n random variables were statistically independent, the joint density function could then be written down as

$$p(\overline{S}) = p(s_1) \, p(s_2) \, \cdots \, p(s_n) \qquad (4.38)$$

However, these individual random variables are not statistically independent and Eq. (4.38) cannot be used to represent the joint probability density with good accuracy. Eq. (4.37) might be used if corrections for random variable correlation could be incorporated.

Suppose a joint probability density function exists for two correlated random variables $s_i$ and $s_j$ designated by $p(s_i, s_j)$. Let $s_i$ and $s_j$ have individual probability density functions $p(s_i)$ and $p(s_j)$, respectively. Also, let $p(s_i \mid s_j)$ and $p(s_j \mid s_i)$ be corresponding conditional probability density functions for $s_i$ given $s_j$ and $s_j$ given $s_i$, respectively. Then

$$p(s_i, s_j) = p(s_i) \, p(s_j \mid s_i) = p(s_j) \, p(s_i \mid s_j) \qquad (4.39)$$

Suppose next that the correlation between $s_i$ and $s_j$ is perfect so that the correlation coefficient $\rho$ is unity. Then $p(s_i, s_j)$ becomes

$$p(s_i, s_j) = p(s_i) \; \delta(s_i - s_j) = p(s_j) \; \delta(s_j - s_i) \qquad (4.40)$$

where

$\delta(s_i - s_j)$ and $\delta(s_j - s_i)$ are delta functions

$$\delta(s_i - s_j) = \delta(s_j - s_i) = \begin{cases} 1 & s_i = s_j \\ \\ 0 & s_i \neq s_j \end{cases} \qquad (4.41)$$

Finally suppose the two random variables are statistically independent so $\rho = 0$. Then $p(s_i, s_j)$ is given by Eq. (4.42) as

$$p(s_i, s_j) = p(s_i) \, p(s_j) \qquad (4.42)$$

By comparison of Eqs. (4.41) and (4.42) with the general form of Eq. (4.39), it will be seen that the conditional probabilities, $p(s_i \mid s_j)$ and $p(s_j \mid s_i)$, range in functional structure from delta functions for perfect correlation to the individual density functions for no correlation. Thus, for some intermediate value of $\rho$, the delta function in Eq. (4.40) must be replaced by a function broader in $(s_i - s_j)$ whose dependence upon the conditional variable, say in this case $s_i$, becomes less as $\rho$ approaches zero. The actual function will, in most cases, be difficult to estimate, but the above considerations indicate something of its general form as a function of the degree of correlation.

The n-dimensional joint probability density function, $p(\bar{S})$, must satisfy certain properties such as

$$\int p(\bar{S}) \, d\bar{S} = 1 \qquad (4.43)$$

4-25

$$\int \ldots \int p(\overline{S}) \, ds_1 \ldots \ldots ds_{n-1} = p(s_n) \tag{4.44}$$

$$\int s_i \, p(\overline{S}) \, d\overline{S} = \mu \tag{4.45}$$

$$\int s_i^2 \, p(\overline{S}) \, d\overline{S} = \alpha_{ii} + \mu^2 \tag{4.46}$$

$$\int s_i \, s_j \, p(\overline{S}) \, d\overline{S} = \alpha_{ij} + \mu^2 \tag{4.47}$$

where

$$\alpha_{ii} = E \left\langle (s_i - \mu)^2 \right\rangle \tag{4.48}$$

and

$$\alpha_{ij} = E \left\langle (s_i - \mu)(s_j - \mu) \right\rangle \tag{4.49}$$

are expectation values. Note that $p(\overline{S})$ defined by Eq. (4.38) satisfies all these properties except Eq. (4.49) unless $\alpha_{ij} = 0$ that is, unless there is no correlation.

It may in some instances be possible to approximate $p(\overline{S})$ when correlation is involved by

$$p(\overline{S}) = p(s_1) \, p(s_2) \ldots p(s_n) + f(\overline{S}) \tag{4.50}$$

where $f(\overline{S})$ must satisfy the properties

$$\int f(\overline{S}) \, d\overline{S} = 0 \tag{4.51}$$

$$\int \ldots \int f(\overline{S}) \, ds_1 \ldots ds_{n-1} = 0 \tag{4.52}$$

$$\int s_i \, f(\overline{S}) \, d\overline{S} = 0 \tag{4.53}$$

$$\int s_i^2 \, f(\overline{S}) \, d\overline{S} = 0 \tag{4.54}$$

4-26

$$\int s_i \, s_j \, f(\bar{S}) \; d\bar{S} = \alpha_{ij} \qquad\qquad (4.55)$$

The problem reduces to finding the appropriate form for $f(\bar{S})$. In general, the approximation for $p(\bar{S})$ of Eq. (4.50) will not satisfy higher order properties of the true $p(\bar{S})$.

In summary, two approaches to approximating joint probability density functions in the case of correlation have been suggested, namely, correct successive $p(s_i)$ in Eq. (4.38) to account for the correlation or assume independence and then make an additive correction (Eq. 4.50).

b. <u>Deduction of Probability Density Function from Physical Models</u>

If physical models for the background radiance and target radiance can be derived, say from theoretical and empirical studies, how may the required probability density functions be obtained? In general, a set of particular conditions must hold for the production of a given radiance value. If $p_i$ is the probability of the occurrence of the $i^{th}$ condition, and if the conditions are statistically independent, the probability of obtaining the new radiance is

$$p(H) = \sum_k \prod_i p_{ik} \qquad\qquad (4.56)$$

where the sum of k is over all sets of i which separately produce H. Although H is a function of all i, each $p_i$ will be determined by the specification of H and the particular set k giving rise to H. Finally, if the $p_i$ are not statistically independent, a convolution of probabilities will be required.

In actual practice, $p(H)$ will probably have to be obtained from the physical model by Monte Carlo computer technique. It may also be easier to obtain an estimated cumulative distribution function, $P(H)$ and then differentiate with respect to H to obtain $p(H)$.

4-27

At this point another difficulty arises in the practical application of the method for assessing system performance. It has been shown how the probability density functions for model cloud background radiances may be obtained in principle. However, Eqs. (4.29) and (4.30) show that the probability density function of the signal as it appears to the decision operation is what is actually required. The cloud radiance is converted by the sensor to a voltage. At the same time some modification of the original radiance probability density function may occur since the sensor may not be truly linear for all radiance values or previous signals may have an effect. Also, the sensor may introduce noise of its own which definitely changes the density function. As the signal processing proceeds, the linearity, noise, and bandwidths of preamplifiers will further change the signal distribution. The signal presented to the decision operation device will represent possibly a much different probability density function. Unless these modifications of the original signal are well understood, it will not be possible to relate the background densities to system performance. We will show immediately below what simplifying assumptions may be made about the system to remove this difficulty.

Let the input irradiance to the $i^{th}$ sensor be $H_i(\theta, \phi)$. Because of the scanning law and sensor motion

$$\theta = \theta(t)$$
$$\phi = \phi(t)$$

(4.57)

so that

$$H_i(\theta, \phi) = H_i(t)$$

(4.58)

It is assumed that the probability density function $p(H_i)$ is known and that it is required to obtain $p(s_i)$.

The output signal at time t corresponding to $H_i(t)$ is $s_i(t)$. However, contributions to $s_i(t)$ result not only from the instantaneous

value of $H_i(t)$ but also from the past values of $H_i(t)$. This is due to the system response function and its inherent rise time and causes the difficulty in converting $p(H_i)$ to $p(s_i)$. Another source of difficulty is the noise introduced by the system. However, we assume that the internal system noise is sufficiently low so as to be neglected without appreciable error.

The way in which the history of $H_i$ is taken into account is to de.i.ae a system impulse response function, $k(t)$, which when convoluted with $H_i$ gives $s_i$, i.e.

$$s_i(t) = \int_0^\infty H_i(t - \lambda) \, k(\lambda) \, d\lambda .$$  (4.59)

However, this simple integral gives the correct signal only for linear systems. Higher order integral equations are required for other types of signal processing. In our case, we are interested only in the signal processing which occurs up to the input to the decision operator, and this processing is, in many cases, closely linear.

Eq. (4.59) relates individual values of $H_i$ occurring over a sampling time interval of the $i^{th}$ sensor to the output signal, $s_i$. However, what we need is some relationship between $p(s_i)$ and $p(H_i)$, not between individual values of the random variables. In general, such a relationship cannot be found analytically except for certain special or simple cases such as Gaussian background distributions or for sensors with sufficiently rapid rise times.

Suppose the impulse response function delays the signal by an amount $t_o$ but otherwise doesn't change the signal. Such a function is represented by the delta function

$$\delta(t - t_o)$$

For this case

$$s_i(t) = H_i(t_o) \qquad (4.60)$$

and the probability density functions are identical, i.e.,

$$p(H_i) = p(s_i) \qquad (4.61)$$

Finally, if $H_i(t)$ is a slowly varying function of time relative to the time constant of the detection system, i.e., $H_i(t)$ does not change appreciably over a time interval from $t - T$ to $t + T$ where $T$ is the time constant of the system, then

$$s_i(t) \approx H_i(t) \int_o^\infty k(\lambda)\, d\lambda \qquad (4.62)$$

The problem of obtaining $p(s_i)$ vanishes for this special case. Actually, all that is required is that the relationship between $s_i(t)$ and $H_i(t)$ be monotonic so that a single value of $s_i(t)$ exists for a given $H_i(t)$. Then, again, Eq. (4.61) is valid.

For a high frequency cutoff filter, the transfer function is

$$K(\omega) = \frac{K}{1 + j\omega T} \qquad (4.63)$$

where $T$ is the characteristic response time of the system. The Fourier transform

$$k(t) = \frac{1}{\pi} \int_o^\infty K(\omega)\, e^{j\omega t}\, d\omega \qquad (4.64)$$

of this function generates the impulse response function

$$k(t) = \begin{cases} \dfrac{Ke^{-t/T}}{T} & t \geqslant 0 \\ \\ 0 & t < 0 \end{cases} \qquad (4.65)$$

4-30

Let us Fourier analyze what happens to the signal as it is processed. The Fourier transform of the input signal is

$$H(t) = \frac{1}{\pi} \int_0^\infty \mathcal{H}(\omega) e^{j\omega t}\, d\omega \qquad (4.66)$$

$$\mathcal{H}(\omega) = \int_0^\infty H(t) e^{-j\omega t}\, d\omega \qquad (4.67)$$

Eq. (4.59) becomes upon substitution

$$s_i(t) = \frac{1}{\pi} \int_0^\infty H(t-\lambda) \int_0^\infty K(\omega) e^{j\omega\lambda}\, d\omega\, d\lambda$$

$$= \frac{1}{\pi} \int_0^\infty K(\omega)\, d\omega \int_0^\infty H(t-\lambda) e^{j\omega\lambda}\, d\lambda \qquad (4.68)$$

$$= \frac{1}{\pi} \int_0^\infty K(\omega) e^{j\omega t}\, d\omega \int_0^\infty H(t-\lambda) e^{-j\omega(t-\lambda)}\, d\lambda$$

$$= \frac{1}{\pi} \int_0^\infty K(\omega)\, \mathcal{H}(\omega) e^{i\omega t}\, d\omega$$

For $K(\omega)$ given by Eq. (4.63) the product $K(\omega)\, \mathcal{H}(\omega)$ which is effectively the Fourier transform of $s_i(t)$ will be small for high frequencies (large values of $\omega$). To see this, expand $\mathcal{H}(\omega)$

$$\mathcal{H}(\omega) = \mathcal{H}(0) + \omega h'(0) + \frac{\omega^2}{2!}\, \mathcal{H}''(0) \qquad (4.69)$$

$$+ \ldots \ldots + \frac{\omega^n}{n!}\, \mathcal{H}^{(n)}(0)$$

For large $\omega$ , multiplication by $K(\omega)$ effectively reduces the power of $\omega$ in each term and the new series converges more rapidly as $\omega$ increases in size than the original.

If the loss of high frequency components of $H_i(t)$ is small compared to the mean value of $H_i(t)$, then the radiance probability density function will closely approximate the signal density function. If, however, the high frequency losses are high, the probability density function will be appreciably altered.

If $k(t)$ is not an extremely narrow function of $t$, but, on the other hand, is not excessively broad either, then an approximation may be used with good results. Thus for each $s_i(t)$ given by Eq. (4.59) there will correspond an interval of input signals $(H_i, H_i + \delta H_i)$. The width of this interval, $\delta H_i$, depends upon the width of the weighting function, $k(t)$. An average probability density, $p_{ave}$, is assigned over this interval. Then, approximately

$$ p(s_i) \, ds_i \approx p_{ave} \, \delta H_i \qquad\qquad (4.70) $$

The wider $k(t)$ the poorer will be the approximation of Eq. (4.70).

Another point of view with regard to the problem of relating input and output probability density functions is simply that, when the input is a random variable rather than a time variable of known analytic form, no Fourier transform exists for such a variable. As a consequence, the modification of the input density by the system cannot be evaluated unless the modification is negligible or slight so that the transformation of the random variable reduces to a simple algebraic operation. In order to handle this problem when the optimum linear filter is considered in Section 4.6, the random functions are converted to autocorrelation functions (with consequent loss of phase information) for which transformations are possible.

c. **Typical Background Distributions**

Next, consider some typical examples of non-Gaussian background distributions. Such distributions are required in order to account for radiance from several different sources. For example, partial cloud cover gives rise to a bimodal distribution of radiance; one mode is centered around the clear sky mean and the other around the cloud mean. Clouds at two different levels may be responsible for a bimodal distribution because of the differing transmissivity of the paths to and from the clouds.

Some properties of bimodal noise, each mode being represented by a Gaussian function, are examined below. The underlying assumptions are:

(1)  Noise and signal are uncorrelated from one resolution element to the next.

(2)  Noise and signal are additive.

(3)  A decision is made that signal is present if $t + b > s_\theta$ or absent if $t + b \leq s_\theta$ where t and b are signal and noise voltages at the output of the radiation detector and $s_\theta$ is a threshold voltage.

(4)  The noise probability density function is

$$p(b)db = \left[ \frac{a_1}{\sqrt{2\pi}\ \sigma_1} \exp\left\{ -(b-\mu_1)^2/2\ \sigma_1^2 \right\} \right.$$

$$\left. + \frac{a_2}{\sqrt{2\pi}\ \sigma_2} \left\{ \exp\ -(b-\mu_2)^2/2\ \sigma_2^2 \right\} \right] db$$

(4.71)

where the $a_1$ and $2_2$ are called weights of the distribution. They might physically represent the probabilities of the presence of high or low

4-33

clouds. $\mu_1$ and $\mu_2$ are called modes of the distribution and $\mu_2 - \mu_1$ is called the spacing of the distribution. Physically $\mu_1$ and $\mu_2$ might represent the mean radiance of high and low clouds multiplied by the responsivity of the sensor, the size of the aperture stop and the subtend of the field stop. $\sigma_1^2$ and $\sigma_2^2$ are called the variances of the distribution. Physically they might represent the variance in radiance of high and low clouds multiplied by the same factors as $\mu_1$ and $\mu_2$.

The false alarm probability and signal detection probability have been evaluated under the five assumptions by integrating numerically the noise density function and the signal plus noise density function. Some results for the false alarm probability are shown in Figures 4.1 through 4.5. These figures show false alarm probability plotted horizontally from right to left against threshold voltage plotted vertically. The graphs are on "probability paper" on which a Gaussian distribution plots as a straight line.

Figure 4.1 shows the effect of varying the weights of the distribution from $a_2$ = 0.5 to $a_2$ = 0.01. Figure 4.6 shows a graph of the probability density function for the extreme case $a_1$ = 0.99, $a_2$ = 0.01. Figure 4.1 also shows the false alarm probability characteristics for equivalent Gaussian distributions -- that is, the false alarm characteristics that would be anticipated by a system designer who had measured the mean and variance of the background noise and had fitted it with a Gaussian distribution. These characteristics are, of course, straight lines.

The signal detection probability characteristics under these simple assumptions are obtained by displacing the false alarm curves of Figures 4.1 through 4.5 vertically by the signal amplitude in the same units as the threshold scale. In Figures 4.2 through 4.4, the weights are $a_1$ = 0.9 and $a_2$ = 0.1.

Figure 4.2 shows the effect of varying the spacing of the two modes by holding $\mu_1$ fixed and progressively decreasing $\mu_2$. As the spacing decreases the characteristic approaches Gaussian behavior.
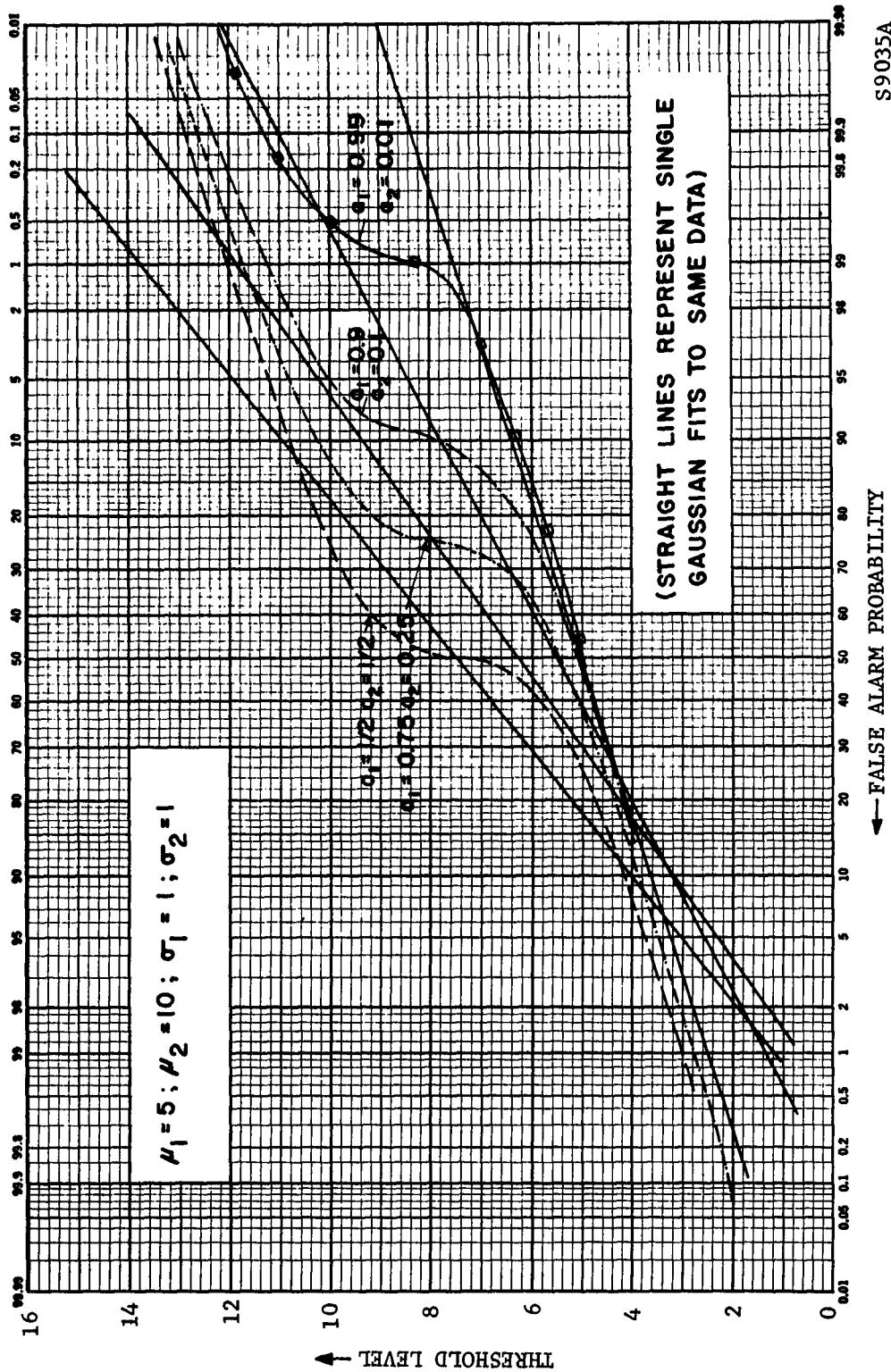
FIGURE 4-1.  EFFECT OF VARYING WEIGHTS

4-35
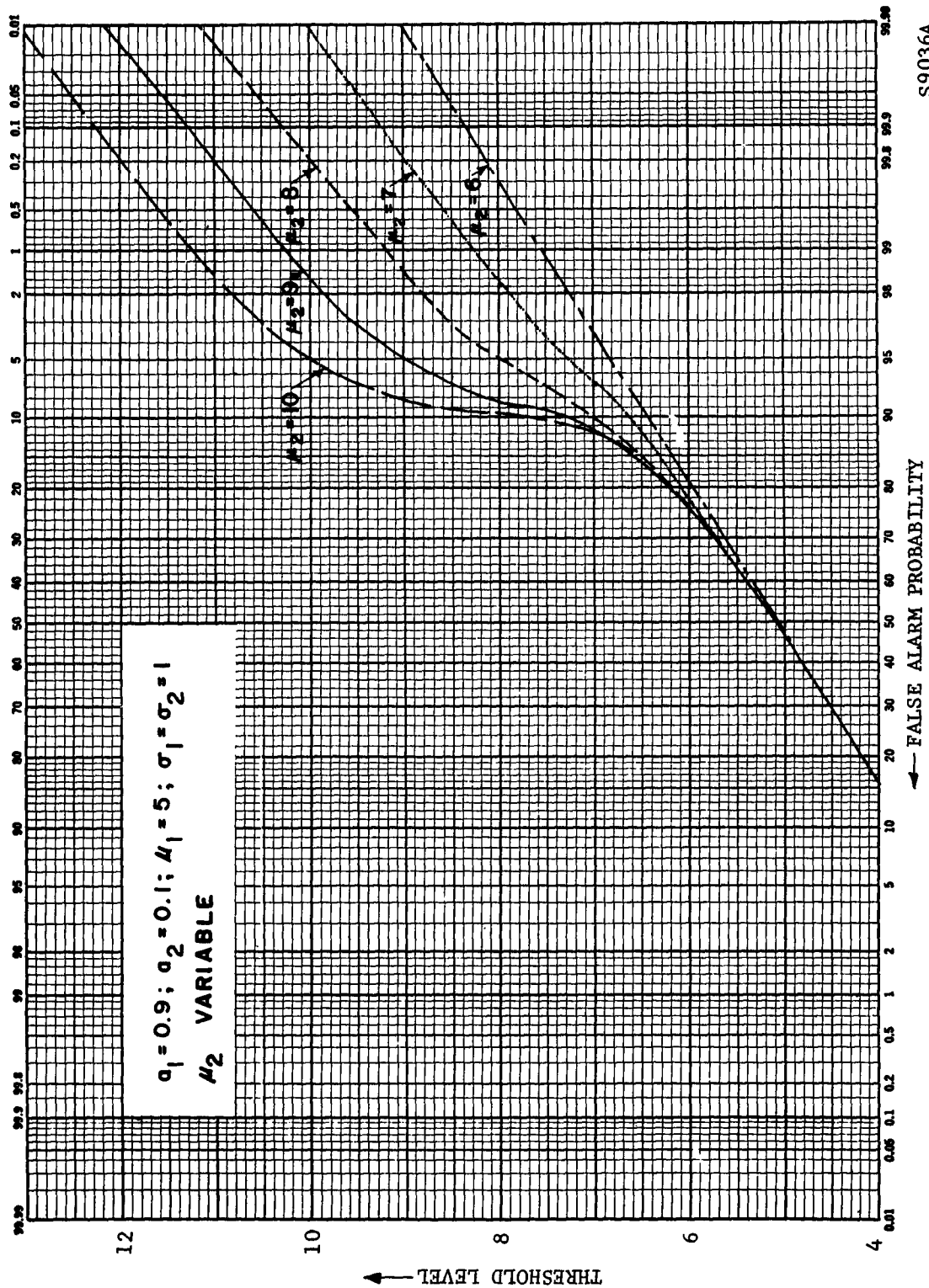
FIGURE 4-2. EFFECT OF VARYING SPACING

4-36
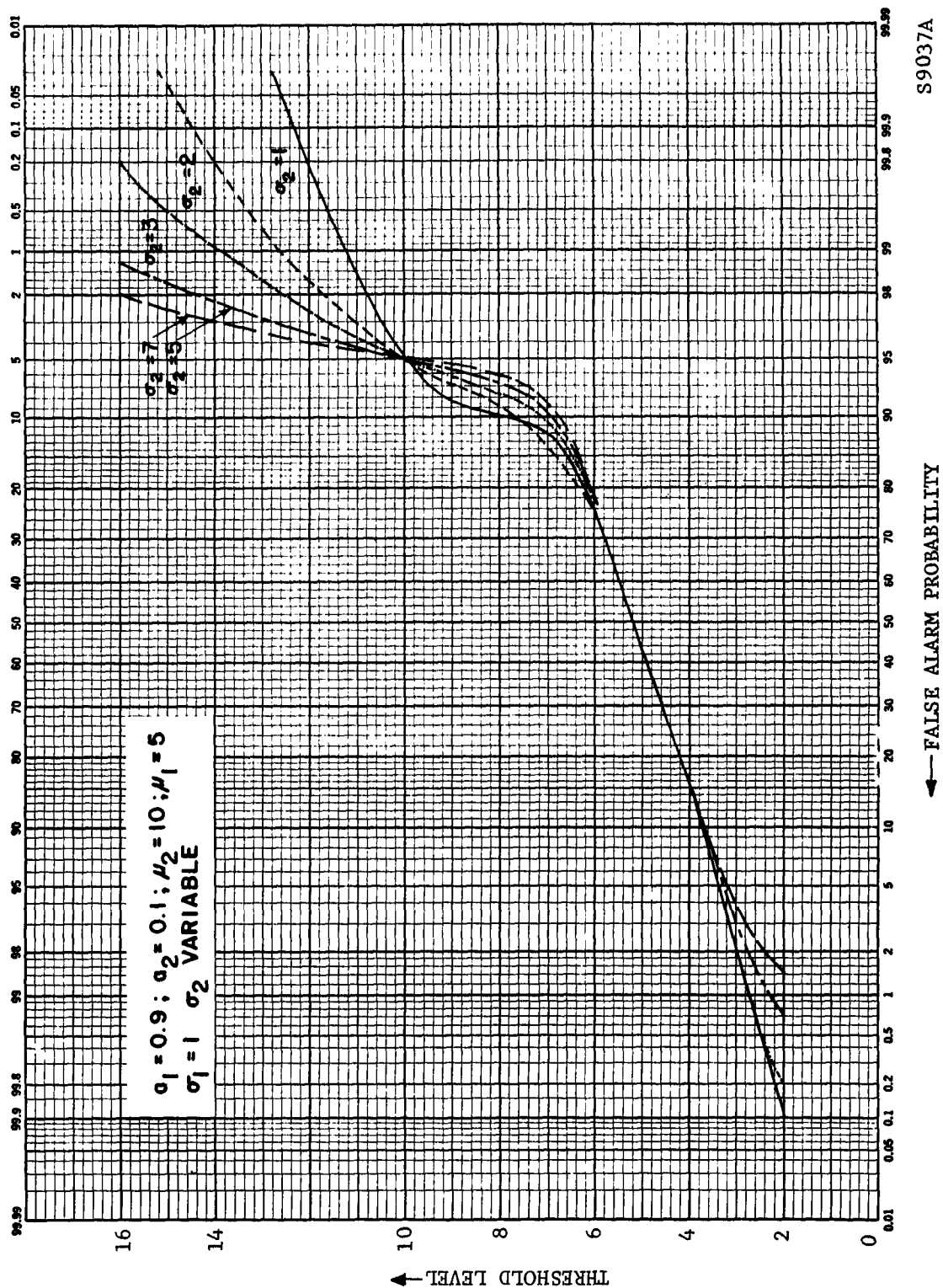
FIGURE 4-3. EFFECT OF VARYING WIDTH - $\sigma_2$ VARIABLE

S9037A

$a_1 = 0.9$ ; $a_2 = 0.1$ ; $\mu_2 = 10$ ; $\mu_1 = 5$
$\sigma_1 = 1$   $\sigma_2$ VARIABLE

◄—FALSE ALARM PROBABILITY

◄—THRESHOLD LEVEL

$\sigma_2 = 7$
$\sigma_2 = 5$
$\sigma_2 = 3$
$\sigma_2 = 2$
$\sigma_2 = 1$

$a_1 = 0.9$; $a_2 = 0.1$; $\mu_1 = 5$; $\mu_2 = 10$; $\sigma_2 = 1$ $\sigma_1$ VARIABLE
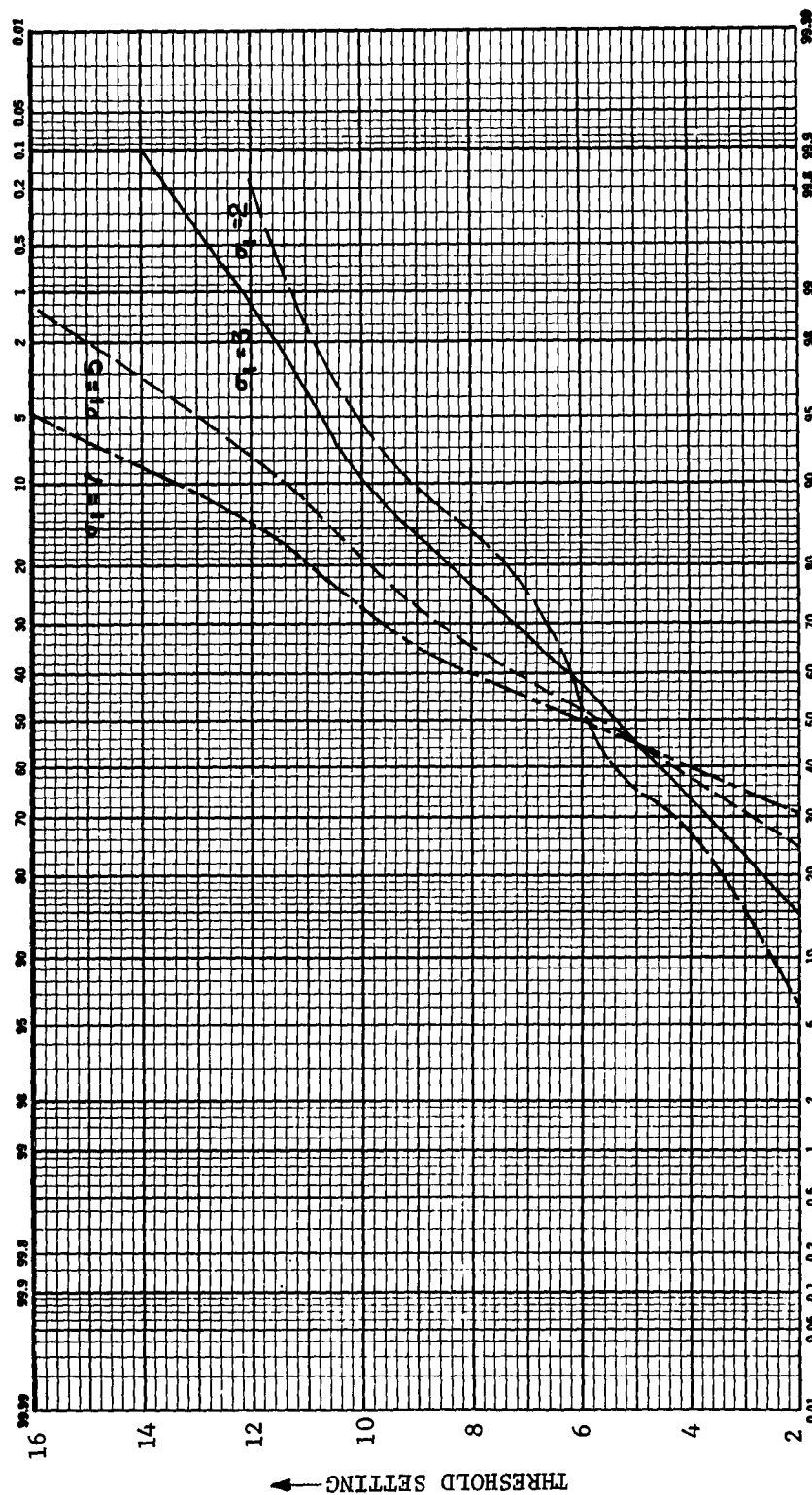
FIGURE 4-4. EFFECT OF VARYING WIDTH - $\sigma_1$ VARIABLE

S9038A

THRESHOLD SETTING

4-38
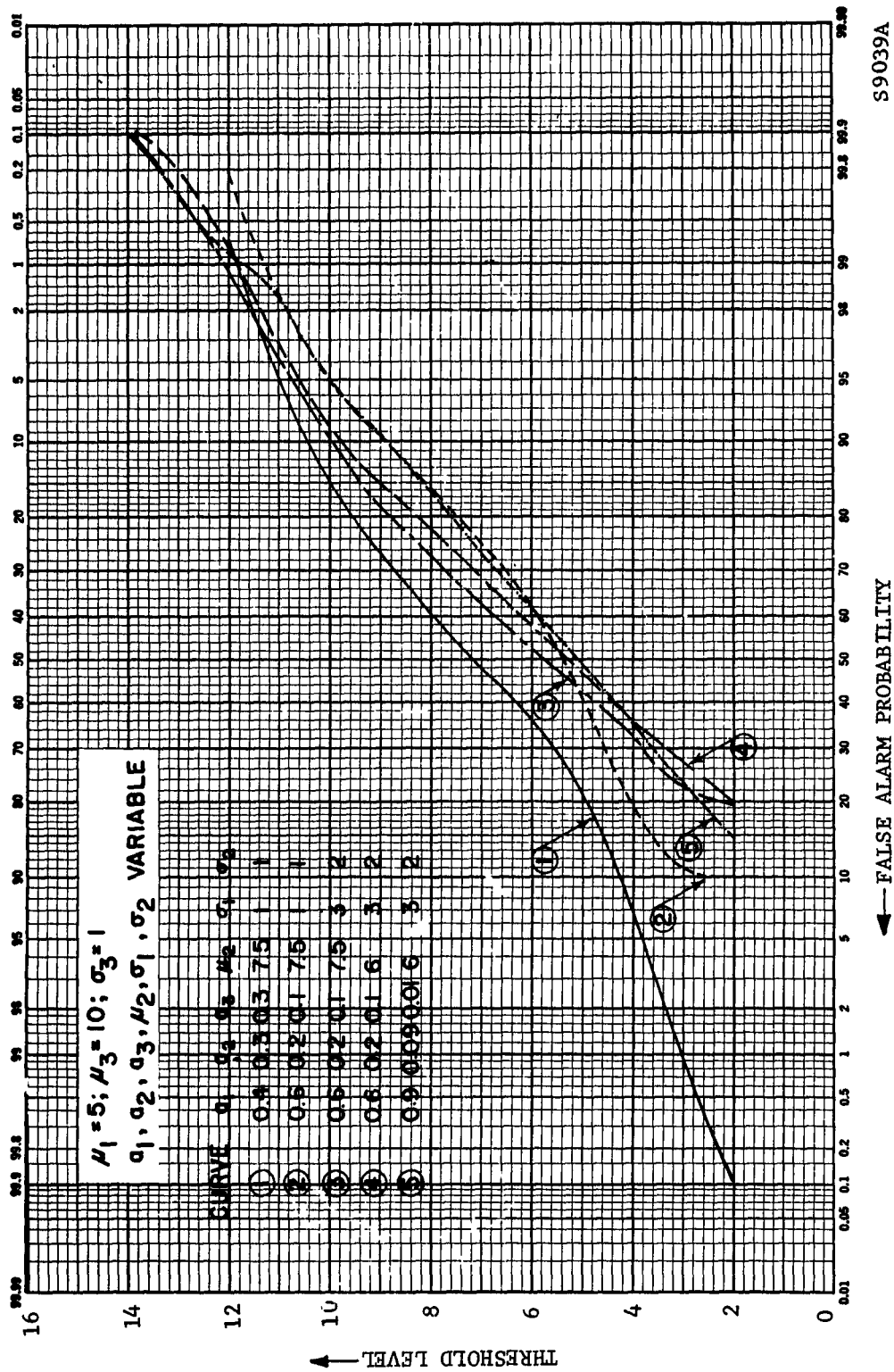
FIGURE 4-5. TRIMODAL GAUSSIAN

4-39

DENSITY FUNCTION

PRIMARY PEAK 0.99

SECONDARY PEAK
0.01

RADIANCE (n) ——▶

PROBABILITY DENSITY
OF RADIANCE

S9040A
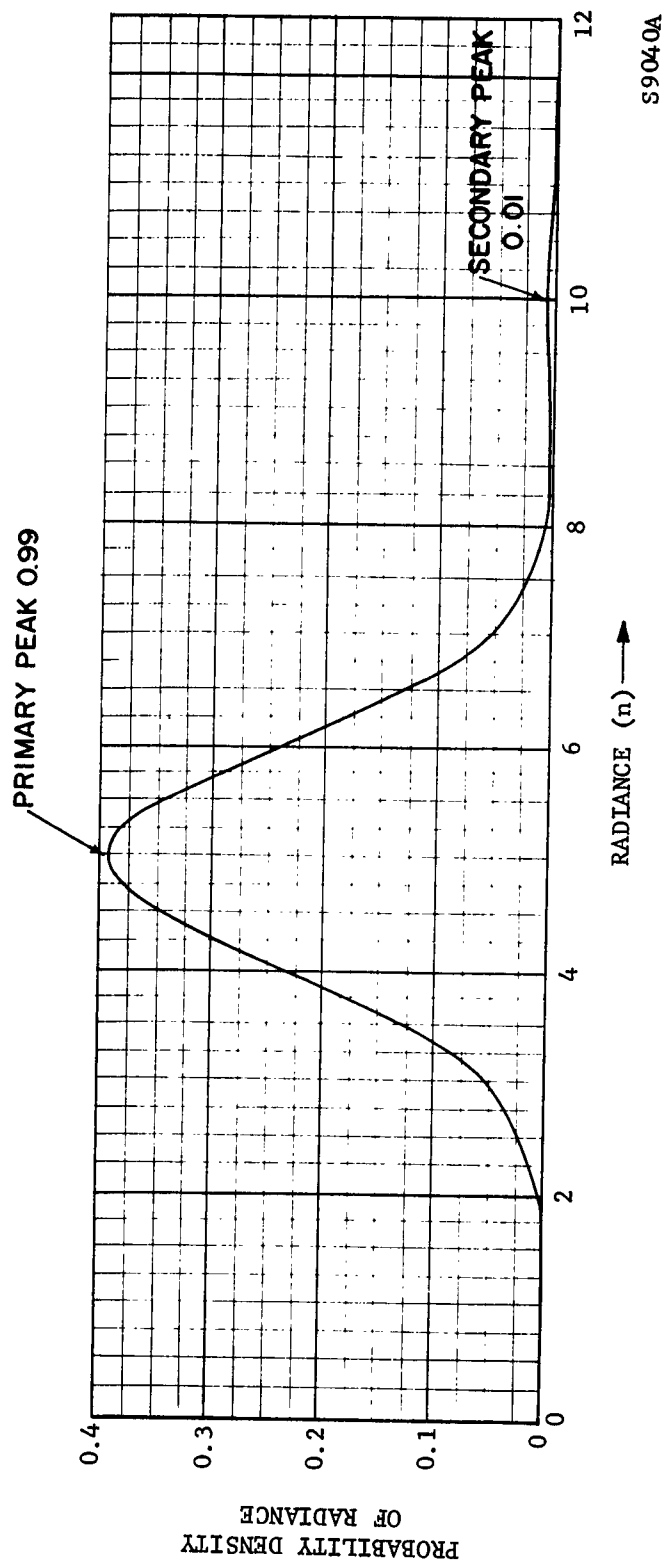
FIGURE 4-6.   BI-GAUSSIAN PROBABILITY - DENSITY FUNCTION

4-40

Figure 4.3 shows the effect of increasing the width of variances of the second term. Figure 4.4 shows the effect of increasing the variance of the first term. Figure 4.5 shows the false alarm characteristics of five cases of rather closely spaced trimodal noise.

In general, it is seen that the false alarm characteristic of a simple "independent look" system operating against bimodal noise can be substantially different from the characteristic expected from a similar system operating against noise which has been assumed to be Gaussian even in the case that the second peak is small enough that it might well be missed in a background measurement. The bimodal characteristics approach the characteristic of the high mode at very high thresholds and the low mode at very low thresholds. Between these two extremes is a transition hump. The magnitude of the hump decreases as the weight of either mode is decreased or as the spacing of the modes is decreased.

Figure 4.7 shows another multimodal background radiance probability density function. The low radiance, due to atmospheric scattering, blackbody radiation, and reflection from very low clouds, is represented by a delta function centered at or near the origin. The medium radiance, due to possible cloud cover at the tropopause, and the high radiance, due to occasional very high altitude clouds, are represented by two Gaussian functions. This distribution differs from the above bimodal cases in that the Gaussian functions have much larger variances relative to the mean and in that the bulk of the background radiance is contained at low radiance levels (the delta function). The two Gaussian functions then represent the structure of the high radiance tail of the total background probability density function. This is the important region of the total density function since it is the high background radiances which must be distinguished from targets. The equation plotted in Figure 4.7 is
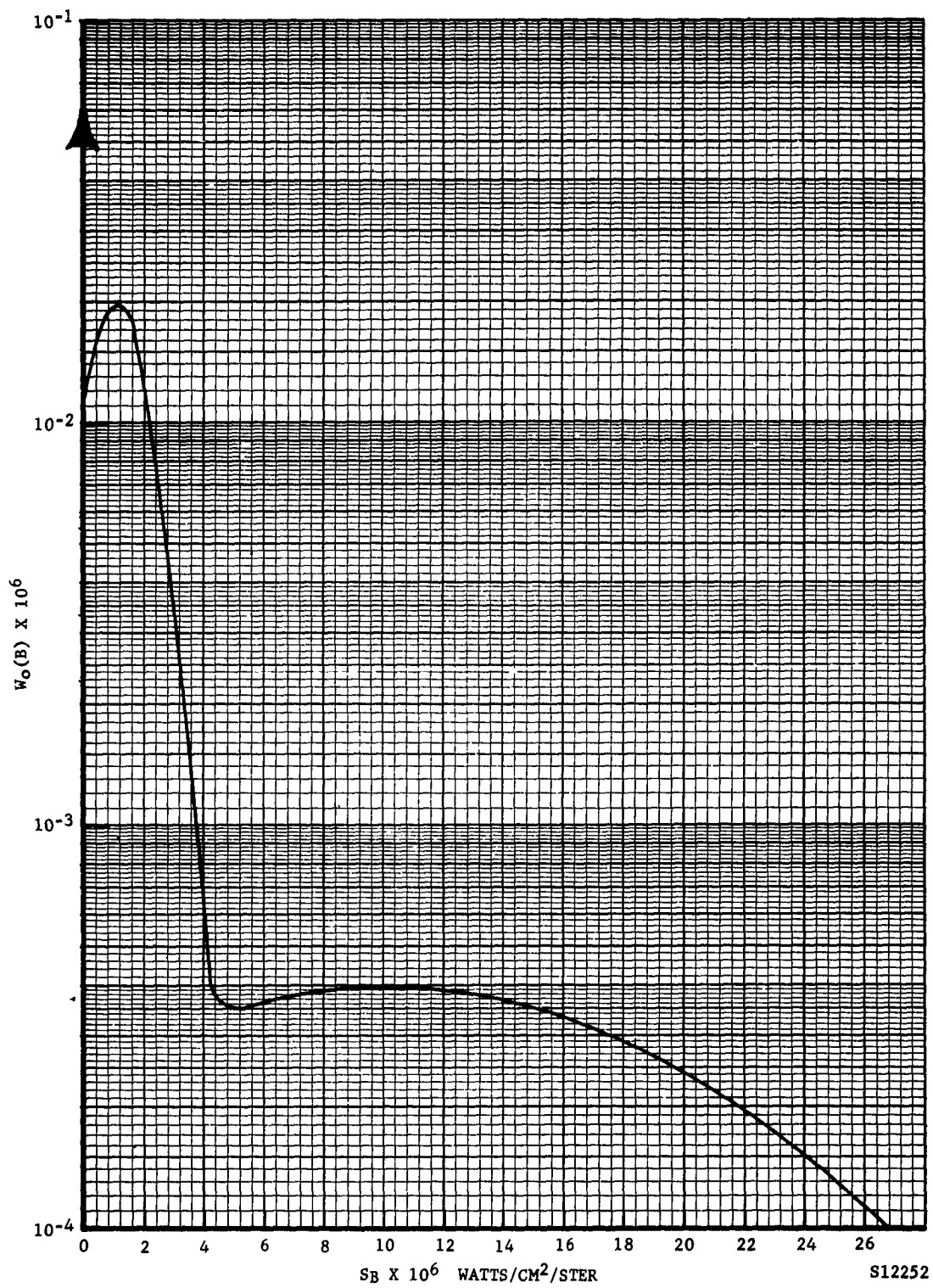
FIGURE 4.7  BACKGROUND RADIANCE PROBABILITY DENSITY FUNCTION

4-42

$$w_o(b) = a_o\, \delta(b{=}0) + \frac{a_1}{\sqrt{2\pi}\,\sigma_1}\; e^{-(b-\mu_1)^2/2\,\sigma_1^2}$$

$$+ \frac{a_2}{\sqrt{2\pi}\,\sigma_2}\; e^{-(b-\mu_2)^2/2\,\sigma_2^2} \tag{4.72}$$

where

$$a_o = 0.94$$

$$a_1 = 0.05$$

$$a_2 = 0.01$$

$$\mu_1 = \sigma_1 = 10^{-6}\ \text{watt/cm}^2\ \text{ster}$$

$$\mu_2 = \sigma_2 = 10^{-5}\ \text{watt/cm}^2\ \text{ster}$$

Such a background radiance distribution may be related to a distribution of cloud heights since

$$p(h) = w_o(b)\, \frac{db}{dh} = w_o(b)\, \frac{bf_o}{t}\, \frac{dt}{dh} \tag{4.73}$$

where $p(h)$ is the probability of a cloud at an altitude between $h$ and $h + dh$, $f_o = 1/\cos i + 1/\cos e$, $t$ is the transmissivity, and $dt/dh$ is obtained from Table 3.2.

Under the assumption of a coplanar case ($f_o$ = const.), a maximum overall radiance of $2.6 \times 10^{-5}$ watt/cm$^2$ ster (see Section 2, Fig. 2.5), ($i = 75°$, and $\theta = 37°$, Fig. 4.8) is obtained for the cloud height distribution. The two peaks shown correspond to altitudes of 16 km and 28 km. The probability density function, $p(h)$, has been normalized to unity. The low altitude distribution is not shown in detail, but there is a 95% probability of having no cloud above 12 km altitude (26 kft).
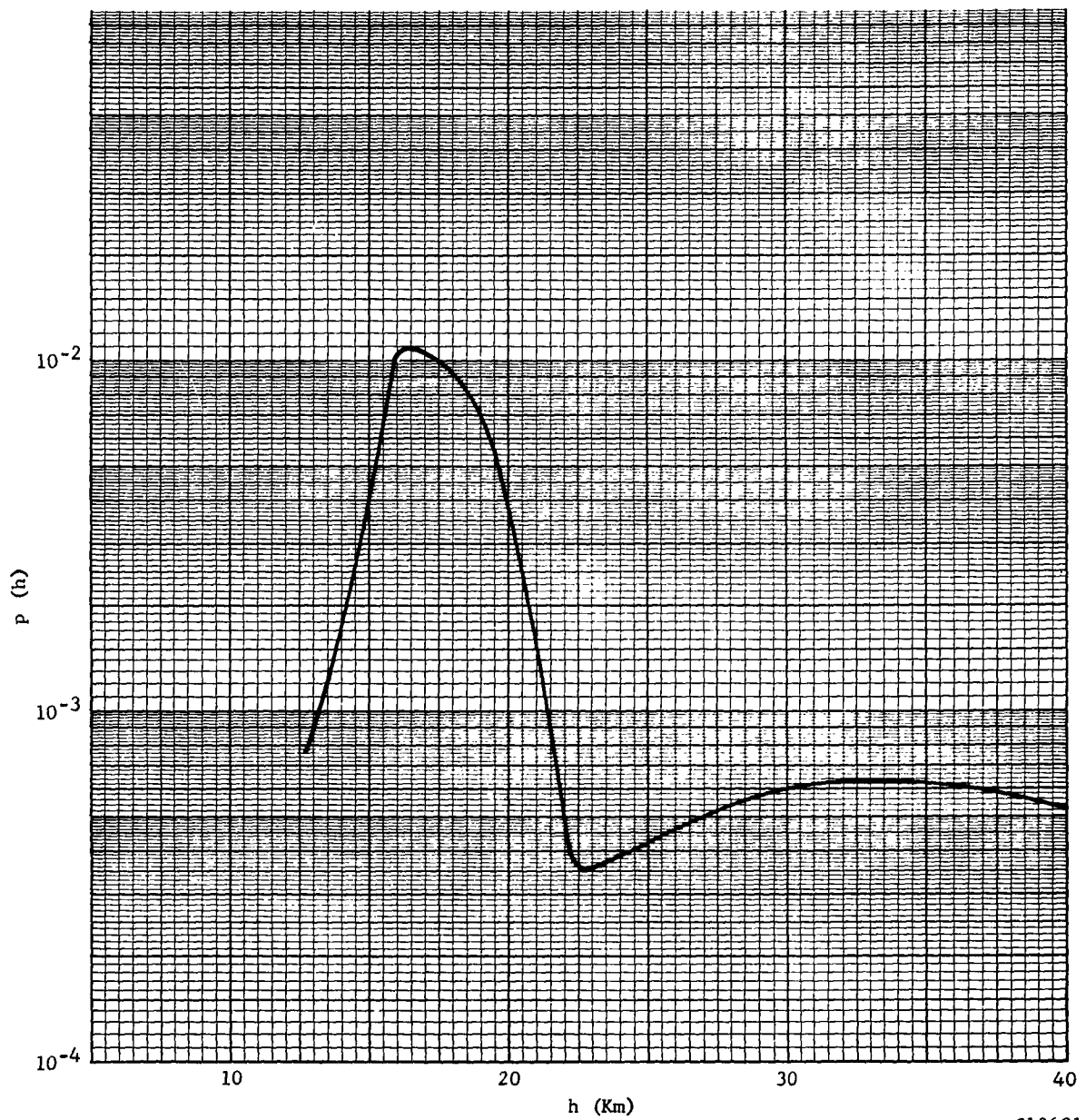
FIGURE 4.8.  CLOUD DISTRIBUTION

4-44

## 4.4  SINGLE SENSOR

Consider, now, a detection system consisting of a single detector element and having no memory or correlator.  The response function will be assumed to be narrow so that for all practical purposes the probability density functions of the background or target radiances are also good approximations of $w_o(b)$ and $w_1(t)$, respectively.  Let the decision for alarm be the condition that the total received signal, s, exceed a threshold level, $s_\theta$.  In this simple case, $P_f$ is given by Eq. (4.19) in which

$$\begin{cases} \overline{S} = \left\{ s \right\} , \\ \overline{T} = \left\{ t \right\} \end{cases} \qquad (4.74)$$

$$\overline{T} = 0 \text{ means } t = 0, \text{ and}$$

$\mathcal{S}(\overline{S}, \Omega)$ is given by Eq. (4.25) so that Eq. (4.19) reduces to

$$P_f = \int_{s_\theta}^{\infty} p(s \mid t = 0) \, ds \qquad (4.75)$$

Similarly, $P_d$ is

$$P_d = \int_{s_\theta}^{\infty} p(s \mid t \neq 0) \, ds \qquad (4.76)$$

Using Eqs. (4.34), (4.35)  and (4.36)  results in

$$P_f = \int_{s_\theta}^{\infty} w_o(s) \, ds \qquad (4.77)$$

$$P_d = \int_{s_\theta}^{\infty} w_1(s) \, ds \qquad (4.78)$$

4-45

The specification of $P_f$ and $w_o(s)$ determines $s_\theta$ according to Eq. (4.77). This value together with $w_1(s)$ then determines $P_d$ for the case of the single sensor (Eq. (4.78)). Figure 4.9 shows $P_f$ for $w_o(s)$ given by Figure 4.7. $P_d$ may be obtained for any desired value of $s_\theta$ if the target probability density function is available.

If we now compare the result of our performance prediction ($P_d$ for a given $P_f$) with the prediction which would have resulted from an assumption of a purely Gaussian radiance distribution matched to the actual distribution (or simply use a minimum root-mean-square noise criterion), it is readily apparent that the structure of the high radiance tail of an actual distribution has a pronounced affect. (See also the discussion of Section 4.3 c and Fig. 4.1). The structure of the high radiance tail does have an affect upon the calculated $P_f$ which is essentially ignored under the r.m.s. approach.

If $w_o(s)$ and $w_1(s)$ are known, another way to find the best $s_\theta$ for the single sensor is to choose it such that the ratio of $P_d/P_f$ obtained from Eqs. (4.77) and (4.78) is a maximum. This value of $s_\theta$, $s_{\theta,m}$, is found by solving

$$\frac{d}{ds_\theta} \left\{ \frac{\int_{s_\theta} w_1(s)\, ds}{\int_{s_\theta} w_o(s)\, ds} \right\} = 0 \qquad (4.79)$$

or

$$\frac{w_1(s_{\theta,m})}{w_o(s_{\theta,m})} = \frac{P_d(s_{\theta,m})}{P_f(s_{\theta,m})} \qquad (4.80)$$
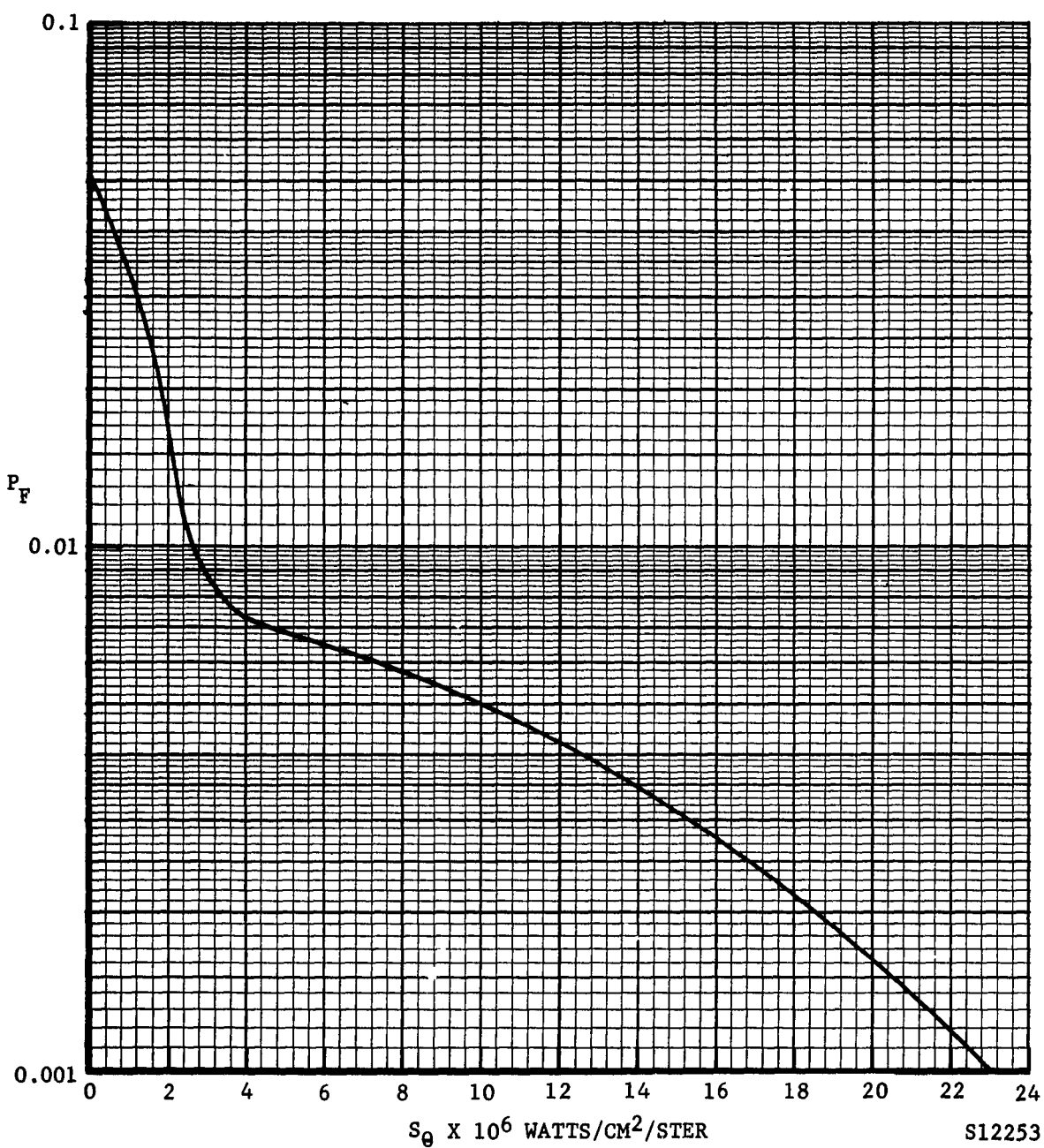
FIGURE 4.9. CONDITIONAL FALSE ALARM PROBABILITY

4-47

## 4.5 CORRELATED SENSOR OUTPUTS

Substantial gains in system performance are achieved when the outputs of individual sensors are correlated. Suppose a detection system consisting of two adjacent sensors. The decision rule is: signals from each of the sensors are compared. No alarm is given if the signals from each one exceed a threshold. An alarm is sounded if the signal from either one exceeds the threshold while the signal from the adjacent sensor doⱼ not. Finally, no alarm is given if the signals from each sensor individually are below the threshold.

A false alarm may well be the result of two erroneous outcomes. The signal from sensor #1 may exceed the threshold while #2 remains below, or vice versa. Since the cloud image will almost always be much larger than a single sensor resolution element, it is unlikely that one sensor will view an infrared reflecting cloud while the other does not. Thus, the probability of false alarm is reduced. Note finally, that the occurrence of the two targets in adjacent resolution elements is assumed to be extremely rare and so is neglected.

The decision rule is

$$\delta(\bar{s}, \Omega) = \begin{cases} 1 \text{ when} & s_1 > s_\theta; \ s_2 \leqslant s_\theta \\ 1 \text{ when} & s_2 > s_\theta; \ s_1 \leqslant s_\theta \\ 0 \text{ when} & s_1 > s_\theta; \ s_2 > s_\theta \\ 0 \text{ when} & s_1 \leqslant s_\theta; \ s_2 \leqslant s_\theta \end{cases} \qquad (4.81)$$

The assumptions made so far may be summarized as follows:

$$
\left\{
\begin{array}{l}
\bar{S} = \left\{ s_1 = b_1 + t_1, \quad s_2 = b_2 + t_2 \right\} \\[2ex]
(s_i \mid t_i = 0) = b_i \\[2ex]
(s_i \mid t_i \neq 0) \approx t_i \\[2ex]
\bar{T} = 0 \Longleftrightarrow (t_i = 0, \ t_2 = 0) \\[2ex]
\bar{T} \neq 0 \Longleftrightarrow (t_i \neq 0, \ t_j = 0) \text{ or } (t_i \neq 0, \ t_j \neq 0) \\[2ex]
P (t_i \neq 0, \ t_j \neq 0) \approx 0
\end{array}
\right.
\tag{4.82}
$$

Then

$$
\begin{aligned}
p(\bar{S} \mid \bar{T} = 0) &= p(s_1, \ s_2 \mid t_1 = 0, \ t_2 = 0) \\[1ex]
&= p(s_1 \mid t_1 = 0) \ p(s_2 \mid t_1 = 0, \ t_2 = 0, \ s_1)
\end{aligned}
\tag{4.83}
$$

Also

$$
\begin{aligned}
p(\bar{S} \mid \bar{T} \neq 0) &= p(s_1, \ s_2 \mid t_1 \neq 0, \ t_2 = 0) \\[1ex]
&\quad + p(s_1, \ s_2 \mid t_1 = 0, \ t_2 \neq 0) + p(s_1, s_2 \mid t_1 \neq 0, \ t_2 \neq 0)
\end{aligned}
\tag{4.84}
$$

But it is assumed that the condition represented by the last term on
the right of Eq. (4.84) is impossible so that this term must be excluded.
Also, because of symmetry

$$
\begin{aligned}
p(\bar{S} \mid \bar{T} \neq 0) &= 2 \ p(s_1, \ s_2 \mid t_1 \neq 0, \ t_2 = 0) \\[1ex]
&= 2 \ p(s_1 \mid t_1 \neq 0) \ p(s_2 \mid t_1 \neq 0, \ t_2 = 0, \ s_1)
\end{aligned}
\tag{4.85}
$$

The following additional assumptions are made:

$$p(s_2 \mid t_1 \neq 0, \ t_2 = 0, \ s_1) = p(s_2 \mid t_2 = 0) \tag{4.86}$$

i.e., $p(s_2 \mid t_2 = 0)$ is independent of the fact that $t_1 \neq 0$,

and

$$p(s_2 \mid t_2 = 0) = w_o \ (s_2)$$

$$\tag{4.87}$$

$$p(s_1 \mid t_1 \neq 0) = w_1 \ (s_1)$$

Using the above information and Eqs. (4.19) and (4.20) gives, finally,

$$P_f = 2 \int_{s_\theta}^{\infty} \int_{s_2 = 0}^{s_\theta} w_o(s_1) \ p(s_2 \mid t_2 = 0, \ s_1 = b_1) \ ds_1 \ ds_2 \tag{4.88}$$

$$P_d = 2 \int_{s_\theta}^{\infty} \int_{s_2 = 0}^{s_\theta} w_1(s_1) w_o \ (s_2) \ ds_1 \ ds_2 \tag{4.89}$$

Eqs. (4.88) and (4.89) should be compared with Eqs. (4.77) and (4.78) for the single sensor. The modification due to correlation will be apparent.

The ratio of $P_d/P_f$ is

$$\frac{P_d}{P_f} = \frac{\displaystyle\int_{s_\theta}^{\infty} w_1(s_1) \ ds_1 \ \int_{0}^{s_\theta} w_o \ (s_2) \ ds_2}{\displaystyle\int_{s_\theta}^{\infty} \int_{0}^{s_\theta} w_o \ (s_1) \ p \ (s_2 \mid t_2 = 0, \ s_1 = b_1) \ ds_1 \ ds_2} \tag{4.90}$$

The term $p(s_2 \mid t_2 = 0, s_1 = b_1)$ cannot be simplified since it represents the probability of finding $s_2$ knowing that the adjacent background signal was $b_1$ and, therefore, it contains the background correlation information.

A comparison of Eq. (4.90) with the $P_d/P_f$ ratio for the single sensor discussed in the previous section indicates the possibilities for improvement of system performance using correlation techniques.

a.  Improvement due to Correlation

It should be readily apparent that the evaluation of Eq. (4.90) for any but exceptionally simple cases would be extremely difficult. However, let us restate Eq. (4.90) in simplified terms and introduce some indicative numbers to see what degree of improvement is possible. For the single sensor

$$\left(\frac{P_d}{P_f}\right)_{single} = \frac{P\ (s > s_\theta \mid t \neq 0)}{P\ (s > s_\theta \mid t = 0)} \tag{4.91}$$

and for two sensors with correlation

$$\left(\frac{P_d}{P_f}\right)_{two} = \frac{P\ (s_1 > s_\theta, t_1 \neq 0)\ P\ (s_2 \leqslant s_\theta \mid t_1 \neq 0, t_2 = 0, s_1)}{P\ (s_1 > s_\theta, t_1 = 0)\ P\ (s_2 \leqslant s_\theta \mid t_1 = 0, t_2 = 0, s_1)} \tag{4.92}$$

The improvement is represented by the factor

$$I = \frac{P\ (s_2 \leqslant s_\theta \mid t_1 \neq 0, t_2 = 0, s_1)}{P\ (s_2 \leqslant s_\theta \mid t_1 = 0, t_2 = 0, s_1)} \tag{4.93}$$

If the correlation of the background is strong, then this factor will be appreciably greater than one. Suppose, for example, that if $s_1$ is found to exceed $s_\theta$ and if $t_1 = 0$ and $t_2 = 0$ then $s_2$ has a probability of exceeding $s_\theta$ of 0.9. Also, suppose that if $s_1$ is found to exceed $s_\theta$ but $t_1 \neq 0$ that the probability that $s_2$ will exceed $s_\theta$ given $t_2 = 0$ is a very small number, $\epsilon$. Then the improvement is

$$I = \frac{1 - \varepsilon}{1 - 0.9} \approx 10$$

An example of the relationship between a simple cloud model and the improvement will be examined. Suppose that a severe background is represented by a cloud 10 detector elements wide. We then ask, what is the probability that if the $i^{th}$ detector sees the cloud the $i + 1$ detector will not see the cloud. If the cloud is uniform in radiance, then the $i^{th}$ detector must be viewing near an edge in order that the $i + 1$ element not view the cloud also. We estimate the chances of this as two in ten or a probability of 0.2. In this case, the system performance would be increased by a factor of 5 because of correlation. A cloud 20 elements wide would give the improvement factor of 10 obtained above for the conditions assumed.

b. Correlation Coefficient

A useful measure of correlation is the correlation coefficient which has been mentioned before. The correlation coefficient for the simple cloud model introduced in the preceding section is derived immediately below.

The correlation coefficient is the ratio of the covariance of two random variables to the product of the square roots of their variances.

$$\rho_{xy} = \frac{C \text{ ov } (x,y)}{\sqrt{\text{Var } (X) \text{ Var } (y)}} \qquad (4.95)$$

In terms of the joint probability density function of x, y, p (x,y) the correlation coefficient is

$$\rho_{xy} = \frac{\displaystyle\int\int (x - \mu_x)(y - \mu_y) \, dxdy \, p \, (x,y)}{\displaystyle\int\int (x - \mu_x)^2 \, p(x,y) \, dxdy \int\int (y - \mu_y)^2 \, p \, (x,y) \, dxdy} \qquad (4.96)$$

What is the correlation coefficient corresponding to the example of a cloud ten elements wide? We have

$$\rho = \frac{E(b_i - \mu)(b_{i+1} - \mu)}{E(b_i - \mu)^2 E(b_{i+1} - \mu)^2} \qquad (4.97)$$

where E represents the expectation operator. We take for our model a discrete distribution of $b_i$.

$$P(b_i) = 0.005 \qquad (4.98)$$

$$E(b_i) = E(b_{i+1}) = \sum_i r_i P(b_i) \qquad (4.99)$$

and assume that when the cloud is observed, $b_i = 10^{-5}$ which exceeds $s_\theta$ and $b_i = 0$ when the cloud is not in view. Since there are ten positions where this value of $b_i$ will be received

$$E(b_i) = \mu = 10 \times 10^{-5} \times .005 = 5 \times 10^{-7} \qquad (4.100)$$

now

$$E(b_i - \mu)^2 = E(b_i^2) - \mu^2 = \sum_i b_i^2 P(b_i) - \mu^2 \qquad (4.101)$$

and

$$\sum_i b_i^2 P(b_i) = 10 \times 10^{-10} \times .005 = 5 \times 10^{-12} \qquad (4.102)$$

Also,

$$E(b_i - \mu)(b_{i+1} - \mu) = E(b_{i+1}) - \mu^2 \qquad (4.103)$$

and since there are nine positions for both $b_i$ and $b_{i+1}$ to exceed $s_\theta$

$$E(b_i b_{i+1}) = \sum_i b_i b_{i+1} P(b_i) = 9 \times 10^{-5} \times 10^{-5} \times .005 = 4.5 \times 10^{-2} \qquad (4.104)$$

Finally, the correlation coefficient is

$$\rho = \frac{4.5 \times 10^{-12} - 2.5 \times 10^{-13}}{5 \times 10^{-12} - 2.5 \times 10^{-13}} = 0.9 \tag{4.105}$$

For a cloud five resolution elements wide, a similar calculation yields a correlation coefficient of 0.8.

## 4.6 OPTIMUM LINEAR FILTER

In this section the validity of using optimum linear filters in detection systems based on threshold decision criteria is examined. Some simple arguments demonstrate that the criteria used in the design of optimum linear filters do not usually produce optimum system performance for threshold systems. Also, the fact that the exact form of the target signal as a function of time is not known (the target signal is a random variable) is demonstrated to require a completely statistical approach to linear filter design.

The ideal filter would be one with no attenuation over the frequency band occupied by the target signal and infinite attenuation over the rest of the frequency spectra. The current problem is to decide on the best signal treatment when the background and target spectra overlap. Internally generated noise will be neglected since noise due to the background signal levels and their fluctuations will exceed any internally generated noise.

There exist several possible criteria for the design of linear filters such as:

(1) Minimize the mean square error at the output of the filter (maximize the fidelity of target signal reproduction).

(2) Maximize the ratio of signal power to average background power at the output.

For the purposes of target detection, the latter criterion is used since this would be expected to optimize the detection sensitivity. When it is required to retain the form of the input signal with the best possible fidelity of reproduction in the output, the criterion of minimizing the mean square error in the signal at the output is applied. The actual output signal usually consists of the modified input signal together with some passed background signal. The criterion states that the mean square of the difference between the actual output signal and the modified ideal signal output is to be minimized. The ideal output is obtained from a knowledge of the pure input signal or its spectral density and the system transfer function.

An optimum linear filter may be found using either criterion regardless of the background probability density distribution function. The procedure invariably results in an optimum linear filter but no assurance is given that a more optimum non-linear filter does not exist. Indeed, for non-Gaussian distributions of background with weighted high radiance tails, a better non-linear filter may generally be found.

Let us find a matched linear filter for a non-Gaussian background distribution and a target signal of known time dependence. The matched filter is one where the spectral density (power per unit bandwidth) of the background is constant for all wavelengths so that the filter is "matched" to the target signal. The spectral density of background is not generally constant so the matched filter must be preceded by a filter which converts the background input to white noise. At the same time, the target signal input will become modified. Figure 4.10 shows the hypothetical system being considered. The input background noise is b(t) with a spectral density of $S_b(\omega)$ given by

$$S_b(\omega) = \int_{-\infty}^{\infty} e^{-j\omega\tau} R_b(\tau) \, d\tau \tag{4.106}$$

where $R_b(\tau)$ is the autocorrelation function of the background.

4-55
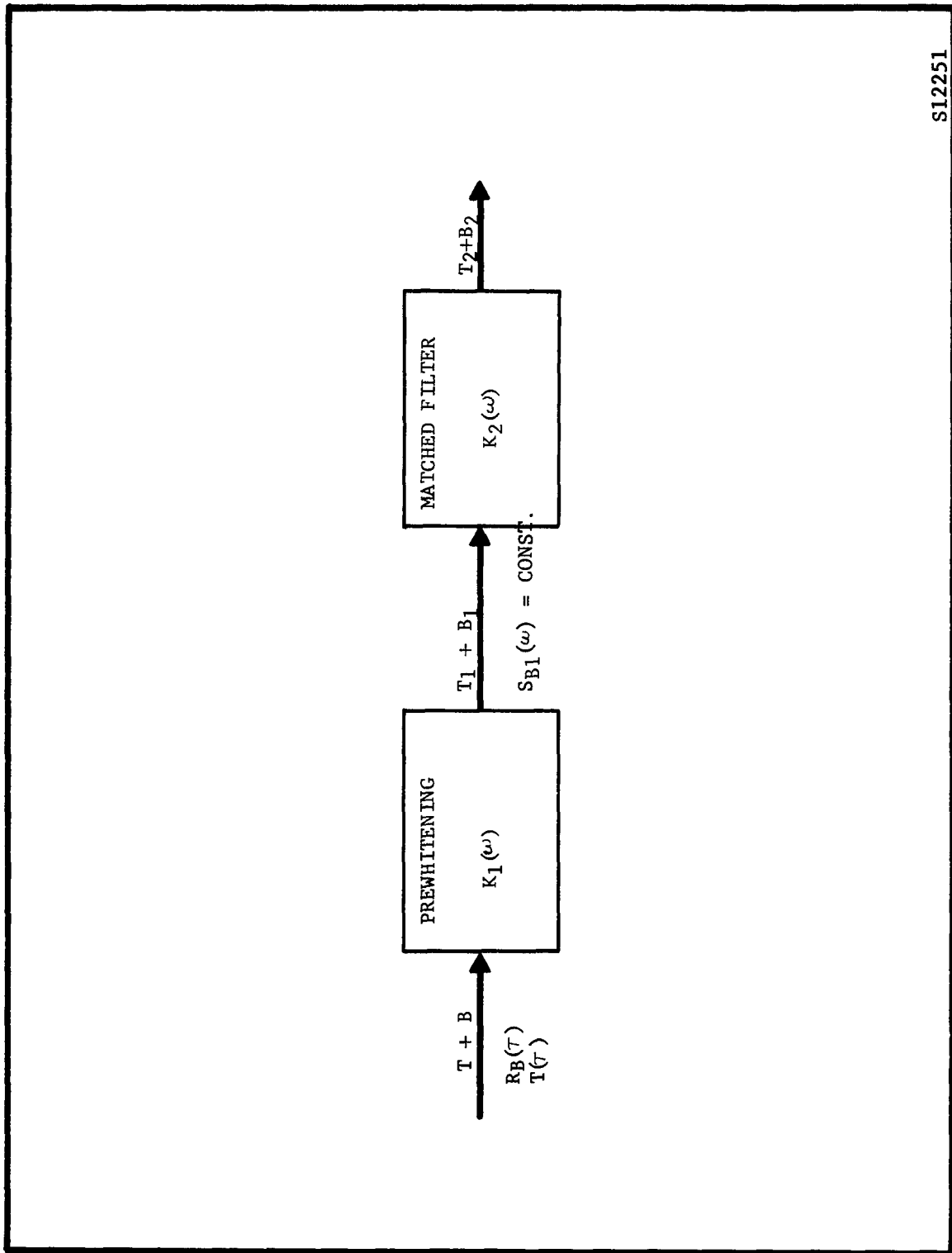
FIGURE 4.10.  MATCHED FILTER

The autocorrelation function of the background input signal is required in order to obtain the spectral density of the background (these two functions are related by the Wiener theorem). If the background irradiance is observed for a period of time, T the autocorrelation function is

$$R_b\ (\mathcal{T}) = \lim_{T \to \infty} \frac{1}{T} \int_0^T b\ (\lambda)\ b(\lambda + \mathcal{T})\ d \qquad (4.107)$$

In actual practice, since the period of observation does not approach infinity, $R_b(\mathcal{T})$ can be estimated for a stationary background by

$$R_b^e\ (\mathcal{T}) = \frac{1}{T - \mathcal{T}} \int_0^{T - \mathcal{T}} b(\lambda)\ b(\lambda + \mathcal{T})\ d\lambda \qquad (4.108)$$

The radiance from clouds is probably best described as a random function of position coordinations with some provision made for rough positional correlations which may exist. For such a case, the determination of the autocorrelation function becomes a statistical problem. The autocorrelation function is defined in Eq. (4.107) as a time average. There exists a theorem which states that the autocorrelation function may be expressed as an ensemble average (average over a large collection of possible background patterns) as well.

Because of the practical equivalence of the time average and the ensemble average, the autocorrelation function can also be expressed as

(4.109)

$$R_b\ (\mathcal{T}) = \int_0^\infty \int_0^\infty s_1\ s_2\ p(s_1, s_2 | \mathcal{T})\ ds_1\ ds_2 = \int_0^\infty \int_0^\infty s_1 s_2 p(s_1) p(s_2 | s_1) \ ds, ds_2$$

where $p(s_1,\ s_2 | \mathcal{T})$ is the probability that $s_1$ and $s_2$ will be found when the time separation in their respective measurements is $\mathcal{T}$. The signals $s_1$ and $s_2$ may be considered to be the outputs of a sensor at time $t_o$ and

$t_o + \mathcal{T}$ respectively. If the background radiance pattern is a weak function of time, $s_1$ and $s_2$ may also be considered as signals from separate identical sensors separated in the object space by the distance $\mathcal{T}$ times the scanning rate.

The average background power out of the prewhitening filter will be

$$\overline{b_1 (\mathcal{T})^2} = \frac{1}{\pi} \int_0^\infty K_1 (\omega) \, K_1 (\omega)^* \, S_b (\omega) \, d\omega \qquad (4.110)$$

where $K_1 (\omega)$ is the transfer function of the prewhitening filter and, in general, is complex. $K_1 (\omega)^*$ is its complex conjugate. $K_1$ must be chosen so that

$$S_{b1} (\omega) = S_{b1} \qquad (4.111)$$

where $S_{b1} (\omega)$ is the spectral density of the background signal at the output of the prewhitening filter and $S_{b1}$ is a constant determined by practical limitations of real sensors and preamplifiers.

$$S_{b1} (\omega) = K_1 (\omega) \, K_1 (\omega)^* \, S_b (\omega) = S_{b1} \qquad (4.112)$$

Thus, with a knowledge of $S_b (\omega)$ and the choice of $S_{b1}$, it is possible to solve for the $K_1 (\omega)$ required to whiten the background.

Since the autocorrelation function is an even function, i.e.,

$$R_b (\mathcal{T}) = R_b (-\mathcal{T}) \qquad (4.113)$$

the spectral density $S_b (\omega)$ defined by Eq. (4.106) will be real, and it will always be possible to find an appropriate $K_1 (\omega)$ which will in general be complex.

The input target signal, $t(\mathcal{T})$, will also have been modified by the prewhitening filter to a new target signal, $t_1(\mathcal{T})$. If $M(\omega)$ is defined as

$$M(\omega) = \int_{-\infty}^{\infty} e^{-j\omega\mathcal{T}} \, t(\mathcal{T}) \, d\mathcal{T} \tag{4.114}$$

and

$$t(\mathcal{T}) = \frac{1}{\pi} \int_{0}^{\infty} e^{j\omega t} \, M(\omega) \, d\omega \tag{4.115}$$

then it may be shown that

$$t_1(\mathcal{T}) = \frac{1}{\pi} \int_{0}^{\infty} e^{j\omega\mathcal{T}} \, M(\omega) \, K_1(\omega) \, d\omega \tag{4.116}$$

The criterion of maximum signal power to background power ratio requires that $K_2(\omega)$, the transfer function of the second filter, be chosen to make a maximum of

$$\frac{\left[ \, t_2(\mathcal{T}_o) \, \right]^2}{\left[ \, b_2(\mathcal{T}) \, \right]^2} \tag{4.117}$$

$$= \frac{1}{\pi \, S_{b1}} \cdot \frac{\left| \int_{0}^{\infty} e^{j\omega\mathcal{T}_o} \, M(\omega) \, K_1(\omega) \, K_2(\omega) \, d\omega \right|}{\int_{0}^{\infty} K_2(\omega) \, K_2(\omega)^* \, d\omega}$$

It is possible to show that the appropriate filter transfer function is

$$K_2(\omega) = e^{-j\omega\mathcal{T}_o} \, M^*(\omega). \tag{4.118}$$

To summarize, what has been done above is to apply optimum linear filter theory to a non-Gaussian background which was described

appropriately for this approach in terms of the autocorrelation function. The autocorrelation function, spectral density (Wiener spectrum), and joint probability density functions are related background descriptions and their use in deriving the optimum linear filter was illustrated. The particular approach chosen applied the criterion of maximum signal to background signal ratio.

The assumptions which were made were that the target signal w· a known function of time and that the autocorrelation function of the random background signal was given. If the target signal is also a random variable then a matched filter cannot be obtained by application of Eq. (4.118). Missile targets will generate signals with a random distribution of amplitudes although the time variation of the signal may actually be determined by the scanning mode and scan rate parameters.

In the case where the target signal is a random variable its autocorrelation function must be obtained (Eq. (4.109)) since the actual form of the signal is not known with certainty but only predictively. If, then, the target Wiener spectrum (Fourier transform of the target autocorrelation function) overlaps the Wiener spectrum of the background, the proper choice of a filter is not immediately obvious (Fig. 4.11). However, a criterion requiring the filter to generate a maximum root-mean-square target signal to root-mean-square background signal is evidently applicable. Thus, we are to find the linear filter (or transfer function, $K(\omega)$) which maximizes the ratio of Eq. (4.119).

$$\frac{\overline{t_{out}}^2}{\overline{b_{out}}^2} = \frac{\int_0^\infty S_t(\omega) K(\omega) d\omega}{\int_0^\infty S_b(\omega) K(\omega) d\omega} \tag{4.119}$$

where $S_t(\omega)$ is the target spectral density.
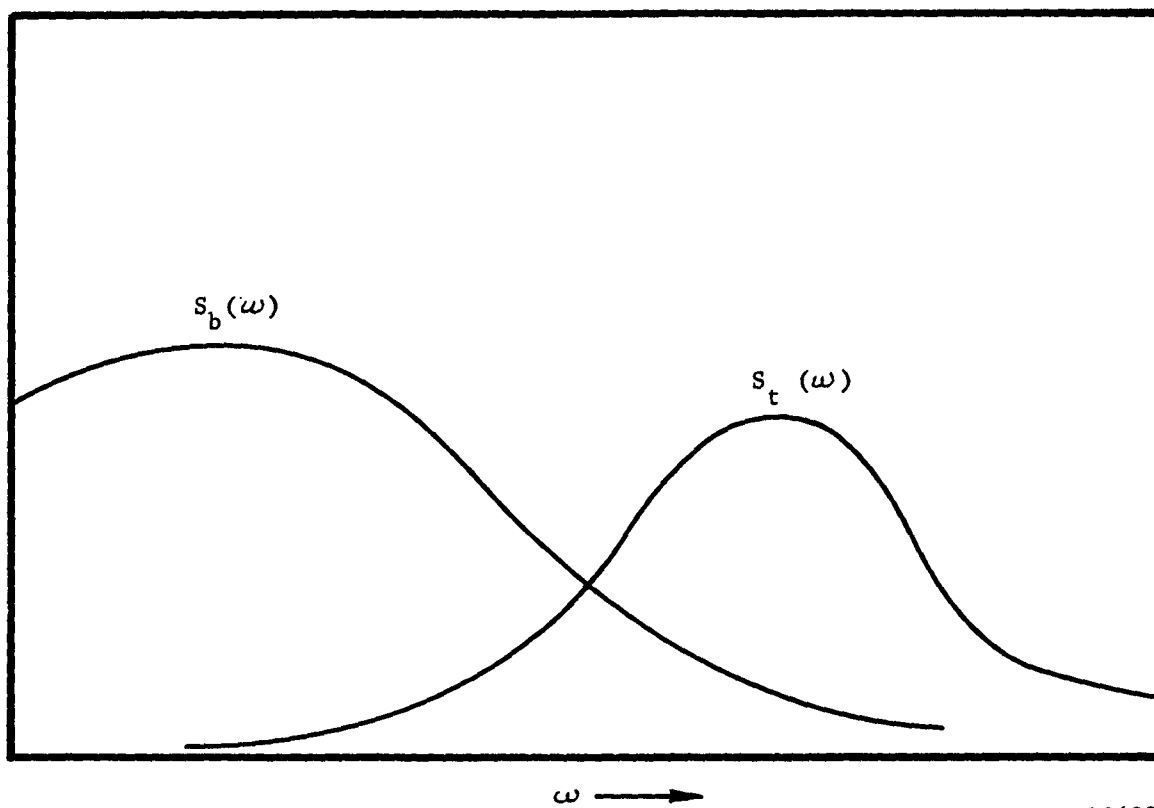
4-60

FIGURE 4.11. POWER SPECTRA

Actually, more will be required of $K(\omega)$ than that it lead
to a maximum value for Eq. (4.119). For example, the condition of a
maximum of average target to average background power could be satis-
fied if $K(\omega)$ is infinite over that range of $\omega$ where $S_b(\omega)$ is zero
but $S_t(\omega)$ remains finite. Such a filter cannot be realized in practice
since an infinite filter gain is implied. It should be possible to
find some compromise $K(\omega)$ which is practically realizable and yet
permits good signal processing and presentation to a decision operator.
This particular problem of random target signals will not be pursued
further.

The system depicted in Fig. 4.10 is completely linear and produces
the best peak target signal power to root mean square background signal
possible. However, a complete alarm system also contains a threshold
decision filter which is inherently non-linear. An alarm is sounded
if a signal is found to exceed a given threshold value or some other
condition is fulfilled. There is usually some finite probability that
the background alone will exceed the threshold, and it is just the peak
background signals that really concern us. One cannot, therefore, expect
the linear system which maximizes the peak target signal to the root-mean-
square background signal to be the best for discrimination purposes.
Considerations of other decision criteria and discrimination schemes
lead to similar conclusions. An example of another criterion is developed
in the following paragraph.

The total system transfer function of a matched linear filter
is

$$K(\omega) = K_1(\omega)\, K_2(\omega) \tag{4.120}$$

where we have seen that $K_1(\omega)$ is related to the reciprocal of the
input background spectral density and $K_2(\omega)$ is related to the input

signal Fourier transform. Suppose then, that a detection system having such a transfer function is required to distinguish missile targets from severe cloud backgrounds using a signal gradient criterion. The target is associated with high radiance gradients whereas a cloud is considered to produce much smaller gradients. However, the transfer function of the prewhitening filter raises the spectral density of the background at high frequencies, making discrimination at this end of the spectrum more difficult. The advantage of the point source resemblance of the target is at least partially compromised.

A system providing the maximum ratio of target signal power to root-mean-square background power may not be best for purposes of discrimination of target signal presence from severe backgrounds. Indeed, we have considered likely cases of background which have increased probability density above the value of a Gaussian prediction at high radiance levels. Thus, the performance of the optimum linear filter could be exceeded by a system specifically designed to discriminate on the basis of some characteristic possessed by the high level background signals.

Since the infrared sensors and preamplifiers are inherent parts of infrared detection systems, it will be germane to consider the requirements placed on these elements by the nature of the decision operator. For a discrimination scheme which requires that some characteristic of the signal be preserved the minimum mean-square error criterion is applicable. For systems utilizing correlation as discussed in the previous section, sensitivity may be the most important factor* which suggests the

---

*Actually, the requirement that the probability density functions of target and background inputs remain essentially unchanged may be a more stringent requirement than high sensitivity. This would require a linear system with a minimum system time constant.

use of the maximum signal to noise criterion.  Thus, such a criterion is
by no means inapplicable to our problem but must be restricted to those
subsystems where its application is appropriate.

REFERENCE LIST FOR SECTION 4

1. D. Z. Robinson, Proc. IRE, $\underline{47}$, No. 9, 1554 (1959).

2. P. Elias, D. S. Grey and D. Z. Robinson, J. Opt. Soc. Am., $\underline{42}$, 127 (1952).

3. H. J. Eldering, Proc. IRIS, $\underline{6}$, No. 3, 189 (1961).

4. J. Neyman and E. S. Pearson, Phil. Trans. Roy. Soc. London, $\underline{231A}$, 289 (1933).

5. A. Wald, "Sequential Analysis", John Wiley, New York, (1947).

6. D. Middleton, "An Introduction to Statistical Communication Theory", McGraw-Hill, Chap. 18-20, New York, (1960).

7. L. A. Wainstein and V. D. Zubakov, "Extraction of Signals from Noise", Prentice-Hall (1962).

# APPENDIX 4A

## WIENER SPECTRA ON THE SURFACE OF A SPHERE

This appendix is concerned with the description of the
correlations between individual random variables representing the
radiance of particular resolvable points. The usual method of
description by autocorrelation functions or Wiener spectra defined
on a plane is very arbitrary. A flat plane is a poor representation
of the earth outside a very limited area and is similarly poor for an
apparent object surface of a particular equipment. The arbitrary
choice of a finite plane approximation allows representation of a
random pattern by a two-dimensional Fourier series. This repre-
sentation is adequate to reconstruct the pattern on the plane. It
does not allow correct matching of two partially non-overlapping
patterns and the plane approximation itself can only be used over
a small area where the difference between spherical and plane
trigonometry is comparable to a desired spatial resolution.

Consequently, it was decided to investigate the correlation
properties of radiance patterns on a sphere representing the earth
itself. The distortions involved in viewing these patterns would then
be considered to be part of the information processing in the observing
system.

It was first shown that the radiance patterns observed with
any arbitrary resolution could be represented (in the sense of recon-
struction) by a series of Laplace spherical harmonics. The asymptotic
properties and correlation-power spectral properties of these series
were investigated. It was found that the Wiener-Khintchine theorem is

not valid in spherical geometry. The principal virtue of Fourier representation is therefore nullified.

It is suggested that this observation has serious consequences for Wiener spectral analyses of background in general. Two-dimensional plane spectra are often used with the explicit or implicit justification that a plane is an adequate approximation to a sphere over a small region. It is assumed that the properties of the plane Wi.·.,er spectra could be extended to spherical spectra at the expense only of labor if the extra accuracy were ever required.

Suppose that the near infrared radiance pattern of the earth is observed with a finite angular resolution $\alpha$ from a series of satellites at altitude h. Then the linear resolution of the measurements at the earth surface is never less than $\alpha$h. The radiance is also bounded in magnitude to a value at least less than a specular reflection of the sun. Consequently, the observed pattern is continuous and absolutely integrable. It may be represented by a function $g(\theta,\emptyset)$ where the coordinates $\theta$ and $\emptyset$ are spherical angular coordinates. Absolute integrability implies that the function g will have a Fourier transform. The assumption of finite resolution implies that the transform of the observable process will be band limited.

It would also be possible to have a sufficient number of satellites spaced around the earth so that the entire surface would be observed simultaneously. In this case, the complete function $g(\theta,\emptyset)$ must obey the periodicity constraints

$$g(\theta,\emptyset) = g(\theta, \emptyset + 2\pi)$$

$$g(\theta,\emptyset) = g(\theta + \pi, \emptyset)$$

Because of these constraints and band limited Fourier transform ability, the function $g(\theta, \emptyset)$ can be represented in all the detail

4-67

that it can be observed by a Fourier series with a finite number of terms.  The number of terms will be of the order of $2 \left\{ 4\pi R^2/(\alpha h)^2 \right\}$ .  A particular form of Fourier series which can be used to represent a function in spherical coordinates is the series of Laplace spherical harmonics which consist of products between a series of complex exponentials in $h\emptyset$ and associated Legendre polynomials in the n, h and $\theta$.  In this series the harmonic of order h,n has h periods around the $\theta = \pi/2$ (equator) circumference and n periods around a $\emptyset = 0$ (meridian) circumference.  The series expansion is set out explicitly in the analysis section below.

Conceptually a class of background radiance processes is selected as generated by a weather condition, a point of observation and a sun location.  A number of sample functions of this process are observed on different occasions from an array of satellites.  Each sample function is broken down into its representation as a series of Laplace spherical harmonics.  The coefficients $c_{nh}$ of this series together contain enough information to reconstruct each sample function.  Application of this technique to a number of sample functions will yield a set of values for each $c_{nh}$.  The distribution of this set of values is an estimate of the probability distribution of the coefficient.

4A.2  SPHERICAL HARMONICS

Any particular radiance pattern on the sphere can be represented by the series

$$g(\theta,\emptyset) = \sum_{n=0}^{\infty} \left[ a_{no} \, P_n(\cos\theta) + \sum_{h=1}^{n} (a_{nh} \cos h \, \emptyset + b_{nh} \sin h \, \emptyset) \, P_n^{h} (\cos \theta) \right]$$

where the $a_{nh}$ and $b_{nh}$ are a series of Fourier coefficients, the $P_n^h$ are associated Legendre polynomials of the first kind. The series can be put in a more compact form as

$$g\,(\theta,\emptyset) = \sum_{n=0}^{\infty} \sum_{h-n}^{n} c_{nh}\,e^{ih\emptyset}\,P_n^h\,(\cos\,\theta)$$

because

$$\sum_{h=0}^{n} a_{nh}\,\cos\,h\,\emptyset + b_{nh}\,\sin\,h\,\emptyset = \sum_{h=0}^{n} \frac{a_{nh}}{2}\,(e^{ih\emptyset} + e^{-ih\emptyset})$$

$$+ \frac{b_{nh}}{2i}\,(e^{ih\emptyset} - e^{-ih\emptyset})$$

$$= \sum_{h=0}^{n} \frac{e^{ih\emptyset}}{2}\,(a_{nh} - ib_{nh}) + \frac{e^{-ih\emptyset}}{2}\,(a_{nh} + ib_{nh})$$

$$= \sum_{h=-n}^{n} c_{nh}\,e^{ih\emptyset}$$

where $c_{nh} = \dfrac{a_{nh} - ib_{nh}}{2}$ for $h > 0$

$c_{nh} = a_{n0}$ for $h = 0$

$c_{nh} = \dfrac{a_{nh} + ib_{nh}}{2}$ for $h < 0$

4-69

$$\therefore \quad c_{n-h} = c_{nh}^{*}$$

The coefficients are found from the integrals

$$a_{no} = \frac{2n+1}{4\pi} \int_{-\pi}^{\pi} d\phi \int_{0}^{\pi} \sin\theta \, d\theta \, g(\theta, \phi) \, P_n(\cos\theta)$$

$$a_{nh} = \frac{2n+1}{4\pi} \frac{(n-h)!}{(n+h)!} \int_{-\pi}^{\pi} d\phi \int_{0}^{\pi} \sin\theta \, d\theta \, g(\theta,\phi) \, P_n^{h}(\cos\theta) \cos h\phi$$

$$b_{nh} = \frac{2n+1}{4\pi} \frac{(n-h)!}{(n+h)!} \int_{-\pi}^{\pi} d\phi \int_{0}^{\pi} \sin\theta \, d\theta \, g(\theta,\phi) \, P_n^{h}(\cos\theta) \sin h\phi$$

$$a_{nh} - i b_{nh} = \frac{2n+1}{2\pi} \frac{(n-h)!}{(n+h)!} \int_{-\pi}^{\pi} d\phi \int_{0}^{\pi} \sin\theta \, d\theta \, g(\theta,\phi) \, P_n^{h}(\cos\theta) \, e^{-h\phi}$$

## 4A.3 CHANGING COORDINATES

In order to investigate the description of correlation by these series it will be necessary to transform coordinates $\theta, \phi$ to others $\theta^1, \phi^1$ through what amounts to a rotation of the sphere. The angle of rotation $\alpha$ is given by

$$\cos\alpha = \cos\theta \cos\theta^1 + \sin\theta \sin\theta^1 \cos(\phi-\phi^1)$$

because the scalar product of the vectors $(1,\theta,\phi)$ and $(1,\theta^1,\phi^1)$

$$A.A^1 = xx^1 + yy^1 + zz^1$$

4-70

$$= \cos \phi \cos \phi^1 \sin \theta \sin \theta^1 + \sin \phi \sin \phi^1 \sin \theta \sin \theta^1 + \cos \theta \cos \theta^1$$

$$= \cos \theta \cos \theta^1 + \sin \theta \sin \theta^1 (\cos \phi \cos \phi^1 + \sin \phi \sin \phi^1)$$

$$= \cos \theta \cos \theta^1 + \sin \theta \sin \theta^1 \cos (\phi - \phi^1)$$

But $A.A^1 = \cos \alpha$

It can then be shown that $P_n^h (\cos \theta^1) e^{ih\phi^1}$ can be expressed in terms

of $\theta$ and $\phi$ and the rotation required to carry $\theta, \phi$ into $\theta^1, \phi^1$ by

$$P_n^h (\cos \theta^1) e^{ih\phi^1} = \sum_{r=-n}^{n} \frac{(n-r)!}{(n-h)!} S_{2n}^{hr} P_n^r (\cos \theta) e^{ir\phi}$$

where

$$S_{2n}^{hr} = \frac{1}{(n+r)!} e^{-i(h+r)\rho} e^{-i(r-h)\sigma} (\cos \tau)^{h+r} (\sin \tau)^{r-h}$$

$$\frac{d^{n+r}}{d(\cos^2 \tau)^{n+r}} (\cos^2 \tau)^{n-h} (\cos^2 \tau - 1)^{n+h}$$

and the $\rho$, $\sigma$ and $\tau$ are defined in terms of the direction cosines

of the axis of rotation from $\theta, \phi$ to $\theta^1 \phi^1$ and the magnitude of the

rotation as follows

Direction cosines of axis of rotation are

w.r.t. x    $q_1/\omega = \frac{-v}{\omega} \sin \sigma \sin \tau$        $\sigma = \tan^{-1} (-q_1/q_2)$

"  y    $q_2/\omega = \frac{v}{\omega} \cos \sigma \sin \tau$        $\rho = \tan^{-1} (q_3/q_4)$

"  z    $q_3/\omega = \frac{v}{\omega} \sin \rho \cos \tau$        $\tau = \sin^{-1} \sqrt{\frac{q_1^2 + q_2^2}{v^2}}$

4-71

Magnitude of rotation $\alpha$ is related to $q_4$

$$\cos \frac{\alpha}{2} = q_4 = v \cos \rho \cos \gamma \qquad \gamma = \cos^{-1}\sqrt{\frac{q_3^2 + q_4^2}{v^2}}$$

and

$$\sin \frac{\alpha}{2} = \frac{\omega}{v} \quad ; \omega = \sqrt{q_1^2 + q_1^2 + q_3^2} \quad ; \quad v = q_1^2 + \sqrt{q_2^2 + q_3^2 + q_4^2}$$

specifically if $v = 1$, $\omega = \sin \alpha/2$.

The direction cosines of the axis of rotation may be determined as follows:

Let an initial vector A be $(1,\theta,\phi)$

a lagged vector B be $(1,\theta^1, \phi^1)$

A = $\cos \phi \sin \theta$, $\sin \phi \sin \theta$, $\cos \theta$

B = $\cos \phi^1 \sin \theta^1$, $\sin \phi^1 \sin \theta^1$, $\cos \theta^1$

A x B = $(A_y B_z - A_z B_y), (A_z B_x - A_x B_z) , (A_x B_y - A_y B_x)$

The axis of rotation unit vector is (A x B). (i, j, k)/$\sin \alpha$

$$(q_1, q_2, q_3)/\sin \frac{\alpha}{2} = \left\{ (\sin \phi \sin \theta \cos \theta^1 - \cos \theta \sin \phi^1 \sin \theta^1), \right.$$

$$(\cos \theta \cos \phi^1 \sin \theta^1 - \cos \phi \sin \theta \cos \theta^1),$$

$$\left. (\cos \phi \sin \theta \sin \phi^1 \sin \theta^1 - \cos \phi^1 \sin \theta^1 \sin \phi \sin \theta) \right\} / \sin \alpha$$

Solving $\sigma$, $\rho$, $\tau$

$$\tan\sigma = -\frac{q_1}{q_2} = -\frac{\sin\phi\,\sin\theta\,\cos\theta^1 - \cos\theta\,\sin\phi^1\,\sin\theta^1}{\cos\theta\,\cos\phi^1\,\sin\theta^1 - \cos\phi\,\sin\theta\,\cos\theta^1}$$

$$\tan\rho = \frac{q_3}{q_4} = (\cos\phi\,\sin\theta\,\sin\phi^1\,\sin\theta^1 - \cos\phi^1\,\sin\theta^1\,\sin\phi\,\sin\theta)$$

$$\frac{\sin\alpha/2}{\sin\alpha\,\cos\alpha/2}$$

$$\sin^2\tau = (\sin\phi\,\sin\theta\,\cos\theta^1 - \cos\theta\,\sin\phi^1\,\sin\theta^1)^2 +$$

$$(\cos\theta\,\cos\phi^1\,\sin\theta^1 - \cos\phi\,\sin\theta\,\cos\theta^1)^2$$

$$\cos^2\tau = (\cos\phi\,\sin\theta\,\sin\phi^1\,\sin\theta^1 - \cos\phi^1\,\sin\theta^1\,\sin\phi\,\sin\theta)^2 + \cos^2\frac{\alpha}{2}$$

$$= (\cos\phi\,\sin\theta\,\sin\phi^1\,\sin\theta^1 - \cos\phi^1\,\sin\theta^1\,\sin\phi\,\sin\theta)^2$$

$$\frac{(\cos\phi\,\sin\theta\,\cos\phi^1\,\sin\theta^1 + \sin\phi\,\sin\theta\,\sin\phi^1\,\sin\theta^1 + \cos\theta\cos\theta^1)^2 - 1}{2}$$

$$\sin^2\tau = \sin^2\phi\,\sin^2\theta\,\cos^2\theta^1 - 2\sin\phi\,\sin\theta\,\cos\theta^1\,\cos\theta\,\sin\phi^1\,\sin\theta^1 +$$

$$\cos^2\theta\,\sin^2\phi^1\,\sin^2\theta^1 + \cos^2\phi\,\sin^2\theta\,\cos^2\theta^1 -$$

$$2\cos\phi\,\sin\theta\,\sin\theta^1\,\cos\theta\,\cos\phi^1\,\cos\theta^1 + \cos^2\theta\,\cos^2\phi^1\,\sin^2\theta^1$$

$$= \sin^2\theta\,\cos^2\theta^1$$

$$- 2\sin\theta\,\cos\theta\,(\sin\phi\,\cos\theta^1\,\sin\phi^1\,\sin\theta^1 + \cos\phi\,\sin\theta^1\,\cos\phi^1\,\cos\theta^1)$$

$$+ \cos^2\theta\,\sin^2\theta^1$$

$$= \sin^2\theta \, \cos^2\theta^1 + \cos^2\theta \, \sin^2\theta^1 - 2 \sin\theta \, \cos\theta \, \sin\theta^1 \, \cos\theta^1$$

$$(\sin\emptyset \, \sin\emptyset^1 + \cos\emptyset \, \cos\emptyset^1)$$

$$= \sin^2\theta \, \cos^2\theta^1 + \cos^2\theta \, \sin^2\theta^1 - 2 \sin\theta \, \cos\theta \, \sin\theta^1 \, \cos\theta^1 \, \cos(\emptyset - \emptyset^1)$$

Note if $\emptyset = \emptyset^1$

$$\sin^2\tau = (\sin\theta \, \cos\theta^1 - \cos\theta \, \sin\theta^1)^2$$

$$= \sin^2(\theta - \theta^1).$$

$$\tau = \pm(\theta - \theta^1 + 2\ell\pi)$$

$$\tan\sigma = -\frac{\sin\emptyset \, (\sin\theta \, \cos\theta^1 - \cos\theta \, \sin\theta^1)}{\cos\emptyset \, (\cos\theta \, \sin\theta^1 - \sin\theta \, \cos\theta^1)} = \tan\emptyset \qquad \sigma = \emptyset + 2m\pi$$

$$\tan\rho = \frac{\cos\emptyset \, \sin\emptyset \, (\sin\theta \, \sin\theta^1 - \sin\theta \, \sin\theta^1)}{2 \cos^2\frac{\alpha}{2}} = 0 \qquad \rho = 0 + n\pi$$

Also note that if $\theta^1 = \theta + \xi$

$$\emptyset^1 = \emptyset + \eta$$

$$\sin^2\tau = \sin^2\theta \left\{ \cos^2\theta \, \cos^2\xi + \sin^2\theta \, \sin^2\xi - 2 \cos\theta \, \sin\theta \, \cos\xi \, \sin\xi \right\}$$

$$+ \cos^2\theta \left\{ \sin^2\theta \, \cos^2\xi + \cos^2\theta \, \sin^2\xi + 2 \cos\theta \, \sin\theta \, \cos\xi \, \sin\xi \right.$$

$$- 2 \sin\theta \, \cos\theta \left\{ \cos\theta \, \sin\theta \, \cos^2\xi - \sin^2\theta \, \cos\xi \, \sin\xi + \right.$$

$$\left. \cos^2\theta \, \cos\xi \, \sin\xi - \cos\theta \, \sin\theta \, \sin^2\xi \right\} \cos\eta$$

$$\cos^2\tau = 1 - \sin^2\tau$$

## 4A.4 AUTOCORRELATION AND POWER SPECTRA

For a one-dimensional Fourier series representation on an interval $(-T,T)$

$$g(x) = \sum_{n=-\infty}^{\infty} G_n \, e^{\frac{i \, 2\pi n x}{2T}}$$

$$G_n = \int_{-T}^{T} g(x) \, e^{\frac{-2\pi n x}{2T}} \, dx$$

the two quantities

$$R(\xi) = \lim_{T \to \infty} \frac{1}{2T} \int_{-T}^{T} g(x) \, g(x+\xi) \, dx$$

and

$$W_n = \lim_{T \to \infty} \frac{G_n G_n^*}{2T}$$

may be defined. They are called the autocorrelation function and power spectral density of the random process $g(x)$. They have far reaching statistical implication if the process is stationary. Substituting the series for $g(x)$ into the integral for $R(\xi)$

$$R(\xi) = \lim_{T \to \infty} \frac{1}{2T} \int_{-T}^{T} g(x+\xi) \sum_n G_n \, e^{\frac{i 2\pi n x}{2T}} \, dx$$

Interchanging the orders of limiting processes (which is permissible if $g(x)$ is absolutely integrable)and changing variables to $y = x + \xi$

4-75

$$R(\xi) = \sum_n G_n \, e^{-\frac{i2\pi n\xi}{2T}} \quad \underset{T\to\infty}{\text{Lim}} \; \frac{1}{2T} \int_{-T+\xi}^{T+\xi} g(y) \, e^{\frac{i2\pi ny}{2T}} \, dy$$

since the process $g(x)$ is stationary this is

$$R(\xi) = \underset{T\to 0}{\text{Lim}} \; \frac{1}{2T} \sum_n G_n \, G_n{}^{*} \, e^{\frac{+i2\pi n\xi}{2T}}$$

which also implies

$$W_n = \underset{T\to\infty}{\text{Lim}} \int_{-T}^{T} R(\xi) \, e^{-\frac{i2\pi n\xi}{2T}} \, d\xi$$

This Fourier transform relationship between $R(\xi)$ and $W_n$ is called the Wiener-Khintchine theorem. It is the purpose of this analysis to see whether a similar relationship holds for the Laplace spherical harmonics.

4A.5  CORRELATION ON A GREAT CIRCLE

Consider first two special cases

(a)    $g(\theta, \emptyset) = g(\emptyset)$

and

(b)    $g(\theta, \emptyset) = g(\theta)$

In case (a) we have    $g(\theta, \emptyset) = \sum_{h=-\infty}^{\infty} C_n \, e^{ih\emptyset}$

and clearly x has been replaced by $\emptyset$ with no other change but that the range of $\emptyset$ is restricted to lie in $(-\pi, \pi)$. The limiting process specified

above is meaningless but the other identities carry through formally.
Case (b) may be written as

$$g(\theta,\emptyset) = g(\cos\,\theta) = \sum_{n=0}^{\infty} C_n\,P_n\,(\cos\,\theta)$$

$$C_n = \frac{2n+1}{2} \int_0^\pi g(\cos\,\theta)\,P_n\,(\cos\,\theta)\,\sin\,\theta\,d\theta$$

Now define $R(\zeta) = \int_0^\pi \sin\,\theta\,d\theta\,g(\cos\,\theta)\,g\left\{\cos(\theta - \zeta)\right\}$

and substitute for $g\left\{\cos(\theta - \zeta)\right\}$

$$R(\zeta) = \int_0^\pi \sin\,\theta\,d\theta\,g(\cos\,\theta) \sum_{n=0}^{\infty} C_n\,P_n\,\left\{\cos(\theta-\zeta)\right\}$$

$$P_n\left\{\cos(\theta-\zeta)\right\} = P_n\,(\cos\,\theta)\,P_n\,(\cos\zeta) + 2\sum_{m=1}^{n} \frac{(n-m)!}{(n+m)!}\,P_n^{\,m}\,(\cos\,\theta)\,P_n^{\,n}\,(\cos\zeta)$$
$$\cos\,m\,(\emptyset-\emptyset^1)$$

taking $\emptyset = \emptyset^1$ and $m = 0$ which amounts to assuming that $g(\theta,\emptyset)$ is constant
around lines of latitude

$$P_n\left\{\cos(\theta - \zeta)\right\} = P_n\,(\cos\,\theta)\,P_n\,(\cos\zeta)$$

$$R(\zeta) = \sum_n C_n\,P_n\,(\cos\zeta) \int_0^\pi \sin\,\theta\,d\theta\,g\,(\cos\,\theta)\,P_n\,(\cos\,\theta)$$

$$= \sum_n P_n\,(\cos\zeta)\,C_n^{\,2}$$

which is a form of the required theorem.

4-77

## 4A.6  CORRELATION IN SPHERICAL HARMONICS

In the general case define

$$R(\xi,\eta) = \int_{-\pi}^{\pi} d\phi \int_{0}^{\pi} \sin\theta \, d\theta \, g(\theta,\phi) \, g(\theta^1,\phi^1)$$

with the intention of showing that this is equivalent to

$$R(\xi,\eta) = \text{constant} \sum_{n=0}^{\infty} \sum_{h=-n}^{n} C_{nh}^{2} \, e^{ih(\phi-\phi^1)} \, P_n^{h} \cos(\theta-\theta^1)$$

$$= \text{constant} \sum_{n=0}^{\infty} \sum_{h-n}^{n} C_{nh}^{2} \, e^{ih\eta} \, P_n^{h}(\cos\xi)$$

then

$$R(\xi,\eta) = \int_{-\pi}^{\pi} d\phi \int_{0}^{\pi} \sin\theta \, d\theta \, g(\theta,\phi) \sum_{n=0}^{\infty} \sum_{h=-n}^{n} Cnhe^{ih\phi^1} P_n^{h}(\cos\theta^1)$$

$$= \int_{-\pi}^{\pi} d\phi \int_{0}^{\pi} \sin\theta \, d0 \, g(\theta,\phi) \sum_{n} \sum_{h} C_{nh} \sum_{r=-n}^{n} \frac{(n-\lambda)!}{(n-h)!} \, S_{2n}^{hr} \, P_n^{\lambda}(\cos\theta) \, e^{ir\phi}$$

$$= \sum_{n=0}^{\infty} \sum_{h=-n}^{n} C_{nh} \sum_{\lambda=-n}^{n} \frac{(n-r)!}{(n-h)!} \int d\phi \, e^{ir\phi} S_{2n}^{hr} \int \sin\theta d\theta g(\theta,\phi) \, P_n^{r}(\cos\theta)$$

The algebra required to perform this integration and compare with the
desired result is very tedious in general.  It is therefore worthwhile
to test a special case in order that the labor may not be wasted.
Therefore, try a simple case where n = 2 and $\phi = \phi^1$.  (Note that $\phi = \phi^1$

does not imply a great circle correlation necessarily).

$$g(\theta,\emptyset) = \sum_{h=-2}^{2} C_{2h}\, e^{ih\emptyset}\, P_2{}^h (\cos\theta)$$

all other coefficients are zero.

Also $\sin^2\mathcal{T} = \sin^2(\theta-\theta^1) = \sin^2\xi$

$\tan\sigma = \tan\emptyset$

$\tan\rho = 0$

Taking the principal solutions

$$S_4{}^{hr} = \frac{1}{(2+r)!}\, e^{-i(r-h)\emptyset}(\cos\mathcal{T})^{h+r}(\sin\mathcal{T})^{r-h}\,\frac{d^{2+r}}{d(\cos^2\mathcal{T})^{2+r}}(\cos^2\mathcal{T})^{2-h}$$

$$(\sin^2\mathcal{T})^{2+h}$$

so that

$$\int d\emptyset\, e^{ir\emptyset}\, S_{2n}{}^{hr}\int \sin\theta\, d\theta\, g(\theta,\emptyset)\, P_n{}^r(\cos\theta)$$

$$= \frac{S_{2n}{}^{hr}}{e^{-i(r-h)\emptyset}}\,\frac{2\pi}{2n+1}\,\frac{(n+h)!}{(n-h)!}\, C_{nh} \qquad \text{in this case}$$

and

$$R(\xi,\eta) = \sum_{n=2}^{2}\ \sum_{h=-2}^{2} C_{2h} \sum_{r=-2}^{2} \frac{2\pi}{5}\,\frac{(2+h)!\,(2-r)!}{(2-h)!^2}\,\frac{S_4{}^{hr}}{e^{-i(r-h)\emptyset}}\, C_{2h}$$

and it is to be seen whether this is equal to

$$\sum_{n=2}^{2}\ \sum_{h=-2}^{2} C_{2h}{}^2\, P_2{}^h(\cos\xi)$$

We shall proceed to tabulate and compute these summations taking the simpler second one first.

TABLE 1

$$\text{TABULATION OF } \sum_{h=-2}^{2} (C_{2h})^2 P_2^h(y) = \sum_{h=-2}^{2} (C_{2h})^2 \frac{(1-y^2)^{\frac{h}{2}}}{2^2 2} \frac{d^{2+h}}{dy^{2+h}}(y^2-1)^2$$

| Term | Coefficient | $(1-y^2)^{\frac{h}{2}}$ | $\frac{d^{2+h}}{dy^{2+h}}(y^2-1)^2$ | Value of Derivative | Total Coefficient |
|---|---|---|---|---|---|
| $c_{22}^2$ | 1/8 | $(1-y^2)$ | $\frac{d^4}{dy^4}(y^2-1)^2$ | 24 | $3(1-y^2)$ |
| $c_{21}^2$ | 1/8 | $(1-y^2)^{\frac{1}{2}}$ | $\frac{d^3}{dy^3}(y^2-1)^2$ | $24y$ | $3y\sqrt{1-y^2}$ |
| $c_{20}^2$ | 1/8 | $(1-y^2)^0$ | $\frac{d^2}{dy^2}(y^1-1)^2$ | $4(3y^2-1)$ | $\frac{1}{2}(3y^2-1)$ |
| $c_{2-1}^2$ | 1/8 | $(1-y^2)^{-\frac{1}{2}}$ | $\frac{d}{dy}(y^2-1)^2$ | $4y(y^2-1)$ | $-\tfrac{1}{2}y\sqrt{1-y^2}$ |
| $c_{2-2}^2$ | 1/8 | $(1-y^2)^{-1}$ | $(y^2-1)^2$ | $(1-y^2)^2$ | $+\frac{1}{8}(1-y^2)$ |

Consequently the entire series should be

$$3(1-y^2)c_{22}^2 + 3y\sqrt{1-y^2}\,c_{21}^2 + \tfrac{1}{2}(3y^2-1)\,c_{20}^2 - \tfrac{1}{2}y\sqrt{1-y^2}\,c_{2-1}^2 + \tfrac{1}{8}(1-y^2)\,c_{2-2}^2$$

$$= 3\sin^2\zeta\, c_{22}^2 + 3\cos\zeta\sin\zeta\, c_{21}^2 + \tfrac{1}{2}(3\cos^2\zeta - 1)c_{20}^2 - \tfrac{1}{2}\cos\zeta\sin\zeta\, c_{2-1}^2 + \tfrac{1}{8}\sin^2\zeta\, c_{2-2}^2$$

TABLE 2

$$\sum_{h=-2}^{2} c_{2h}^2 \sum_{r=-2}^{2} \frac{2\pi}{5} \frac{(2+h)!(2-r)!}{(2-h)!^2} \frac{8}{z^{-1}(r-h)} \frac{hr}{4}(\cos\xi)$$

$$= \sum_{h=-2}^{2} c_{2h}^2 \frac{(2+h)!}{(2-h)!^2} \frac{2\pi}{5} \sum_{r=-2}^{2} \frac{(2-r)!}{(2+r)!} z^{\frac{h+r}{2}}(1-z)^{\frac{r-h}{2}} \frac{d^{2+r}}{dz^{2+r}} z^{2-h}(z-1)^{2+h}$$

Putting $z = \cos^2\xi$

| h | r | h coeff | r coeff | $z^{\frac{h+r}{2}}(1-z)^{\frac{r-h}{2}}$ | Derivative | Value of Derivative | Product |
|---|---|---------|---------|------------------|------------|---------------------|---------|
| -2 | -2 | $2\pi/4!5$ | 4! | $z^{-2}(1-z)^0$ | $\frac{d^0}{dz^0}$ | $z^4(z-1)^0$ | $2\pi/5z^2$ |
| -2 | -1 | $2\pi/4!5$ | 3! | $z^{-3/2}(1-z)^{\frac{1}{2}}$ | $\frac{d}{dz}$ | $4z^3$ | $\frac{2\pi}{5}z^{3/2}(1-z)^{\frac{1}{2}}$ |
| -2 | 0 | $2\pi/4!5$ | 2!/2! | $z^{-1}(1-z)^1$ | $\frac{d^2}{dz^2}$ | $12z^2$ | $\frac{2\pi}{10}z(1-z)^1$ |
| -2 | 1 | $2\pi/4!5$ | 1/3! | $z^{-\frac{1}{2}}(1-z)^{3/2}$ | $\frac{d^3}{dz^3}$ | $24z$ | $\frac{2\pi}{30}z^{\frac{1}{2}}(1-z)^{3/2}$ |
| -2 | 2 | $2\pi/4!5$ | 1/4! | $z^0(1-z)^2$ | $\frac{d^4}{dz^4}$ | 24 | $\frac{2\pi}{120}(1-z)^2$ |

Total term in $C_{2-2}^2$ is $\frac{2\pi}{5}\left(\cos^4\xi + \cos^3\xi\sin\xi + \frac{1}{2}\cos^2\xi\sin^2\xi\right.$

$$\left. + \frac{1}{6}\cos\xi\sin^3\xi + \frac{1}{24}\sin^4\xi\right)$$

| h | r | h coeff | r coeff | $z^{\frac{h+r}{2}}(1-z)^{\frac{r-h}{2}}$ | Derivative | Value of Derivative | Product |
|---|---|---------|---------|------------------|------------|---------------------|---------|
| -1 | -2 | $\frac{2\pi}{5}\frac{1}{3!}$ | 4! | $z^{-3/2}(1-z)^{-\frac{1}{2}}$ | $\frac{d^0}{dz^0}$ | $z^3(z-1)$ | $-\frac{2\pi}{5}\cdot4\, z^{3/2}(1-z)^{\frac{1}{2}}$ |
| -1 | -1 | $\frac{2\pi}{5}\frac{1}{3!}$ | 3! | $z^{-1}(1-z)^0$ | $\frac{d}{dz}$ | $z^2(4z-3)$ | $\frac{2\pi}{5}z(4z-3)$ |
| -1 | 0 | $\frac{2\pi}{5}\frac{1}{3!}$ | 1 | $z^{-\frac{1}{2}}(1-z)^{\frac{1}{2}}$ | $\frac{d^2}{dz^2}$ | $6z(2z-1)$ | $\frac{2\pi}{5}z^{\frac{1}{2}}(1-z)^{\frac{1}{2}}(2z-1)$ |
| -1 | 1 | $\frac{2\pi}{5}\frac{1}{3!}$ | 1/3! | $z^0(1-z)^1$ | $\frac{d^3}{dz^3}$ | $6(4z-1)$ | $\frac{2\pi}{5}\frac{1}{3!}(1-z)(4z-1)$ |
| -1 | 2 | $\frac{2\pi}{5}\frac{1}{3!}$ | 1/4! | $z^{\frac{1}{2}}(1-z)^{3/2}$ | $\frac{d^4}{dz^4}$ | 24 | $\frac{2\pi}{5}\frac{1}{3!}z^{\frac{1}{2}}(1-z)^{3/2}$ |

so that the total term in $C_{2-1}$ is

$$\frac{2\pi}{5}c_{2-1}^2\left[-4\cos^3\xi\sin\xi + \cos^2\xi(4\cos^2\xi-3) + \cos\xi\sin\xi(2\cos^2\xi-1)\right.$$

$$\left. + \frac{1}{6}\sin\xi(4\cos^2\xi-1) + \frac{1}{6}\cos\xi\sin^3\xi\right]$$

$$= \frac{2\pi}{5}c_{2-1}^2\left[4\cos^4\xi - 2\cos^3\xi\sin\xi + \cos^2\xi(\frac{2}{3}\sin\xi-3) + \cos\xi\sin\xi(\frac{1}{6}\sin^2\xi-1) - \frac{1}{6}\sin\xi\right]$$

It is now clear that the terms in $C_{2-2}$ and $C_{2-1}$ obtained on Table 2 have different values than those obtained on Table 1. For example, when $\zeta \longrightarrow 0$ the term in $C_{2-1}$ goes to zero on Table 1 but to $2\pi/5$ on Table 2.

The values of the $C_{nh}$ describe the radiance pattern. They can be chosen arbitrarily from any set which keeps the pattern positive, bounded and continuous. Consequently, the discrepancies in the function of $\cos \zeta$ are not to be corrected by relations between the $C_{nh}$.

Thus the Wiener-Khintchine theorem does not hold for the particular spherical harmonic series

$$g(\theta,\phi) = \sum_{h=-2}^{2} C_{2h} \, e^{ih\phi} \, P_2^{\,h}(\cos\theta)$$

when the lag $\theta-\theta^1$ is arbitrary but $\phi-\phi^1$ is zero. Consequently, the theorem does not hold in general for spherical harmonics.

DISTRIBUTION

Advanced Research Projects Agency                    2
Washington 25, D. C.

Institute for Defense Analyses                       1
1666 Connecticut Avenue, N. W.
Washington 9, D. C.
Attn:  RESD Library

University of Chicago                                1
Laboratories for Applied Sciences
Museum of Science and Industry
Chicago 37, Illinois
Attn:  L. Biberman

University of Michigan                               2
Institute for Science & Technology
P. O. Box 618
Ann Arbor, Michigan

Stanford Research Institute                          1
Menlo Park, California

Massachusetts Institute of Technology                1
Lincoln Laboratories
Lexington, Massachusetts
Attn:  WS461 Office

General Dynamics/Astronautics 2
P.O. Box 1128
San Diego 12, California
Attn:  F. Michael
        Dr. A. E. Green

Bendix Systems Division 1
3300 Plymouth Road
Ann Arbor, Michigan
Attn:  D. Lowe

Hughes Aircraft Co. 1
11940 W. Jefferson Blvd.
Culver City, California
Attn:  S. Dorfman

Space Technology Laboratories 1
Space Park
Redondo Beach, California
Attn:  A. Fulton

ASTIA 10
Arlington Hall Station
Arlington 1, Virginia

Arthur D. Little, Inc. 1
500 Sansome Street
San Francisco, California
Attn:  H. Blau

Boeing Aircraft Co. 1
Aerospace Division
P.O. Box 3707
Seattle 24, Washington
Attn: R. McDonald

Lockheed Missile & Space Company 1
Sunnyvale, California
Attn:  H. Batten

Baird-Atomic, Inc. 1
33 University Road
Cambridge 38, Massachusetts

Aerojet-General Corporation 1
Azusa, California
Attn: Dr. J. A. Jamieson

National Bureau of Standards                                               1
Boulder Laboratories
Boulder, Colorado
Attn: Dr. D. M. Gates

Commanding Officer                                                      1
Naval Ordnance Test Station
Weapons Development Department
China Lake, California
Attn: D. K. Moore

National Aeronautics and Space Administration        1
Goodard Space Flight Center
Greenbelt, Maryland        (Unclassified Reports Only)

U.S. Weather Bureau                                          1
National Weather Satellite Center
Washington 25, D. C.
Attn: Dr. S. F. Singer    (Unclassified Reports Only)

Chief Superintendent                                         1
Canadian Armament Research & Development
  Establishment
P.O. Box 1427
Quebec, Canada
Attn: Dr. C. Cumming

Aerospace Corporation                                      3
2400 El Segundo Boulevard
El Segundo, California
Attn: Dr. C. Sherwin
      H. Wesseley
      I. Spiro

The Rand Corporation                                       2
1700 Main Street
Santa Monica, California
Attn: Dr. S. Passman
      Dr. D. Deirmendjian

Denver Research Institute                               1
University of Denver
Denver, Colorado
Attn: D. Murcray

Commander
Air Force Cambridge Research Center                    1
Geophysics Research Directorate
L. G. Hanscom Field
Bedford, Massachusetts
Attn:  CRZC

Commander
Aeronautical Systems Division                          2
Air Force Systems Command
Wright-Patterson AFB, Ohio
Attn:  ASRNS

Commander
Air Force Space Systems Division                       2
Air Force Unit Post Office
Los Angeles 45, California
Attn:  Major J. Wallace
       Colonel Norman (461 Office)